The development of advanced creep constitutive equations for high chromium alloy steel (P91) at transition stress range

Lili An

Ph.D.

2015

Department of computing and engineering

A thesis submitted to the University of Huddersfield

in partial fulfilment of the requirements for

the degree of doctor of philosophy

Copyright statement

I. The author of this thesis (including any appendices and/or schedules to this thesis) owns any copyright in it (the "Copyright") and she has given The University of Huddersfield the right to use such copyright for any administrative, promotional, educational and/or teaching purposes.

II. Copies of this thesis, either in full or in extracts, may be made only in accordance with the regulations of the University Library. Details of these regulations may be obtained from the Librarian. This page must form part of any such copies made.

III. The ownership of any patents, designs, trademarks and any and all other intellectual property rights except for the Copyright (the "Intellectual Property Rights") and any reproductions of copyright works, for example graphs and tables ("Reproductions"), which may be described in this thesis, may not be owned by the author and may be owned by third parties. Such Intellectual Property Rights and Reproductions cannot and must not be made available for use without the prior written permission of the owner(s) of the relevant Intellectual Property Rights and/or Reproduction

Abstract

Creep damage is a time-dependent deformation in metals under a constant stress at high temperature condition. Since the 1980s, high chromium alloy steel P91 (9%Cr-1%Mo-0.25%V) is highly demanded in high temperature industries (Saha, 2003). Continuum damage mechanism is becoming a generic life assessment tool to predict the lifetime of materials at creep condition. The consitutive equations were proposed to predict the lifetime and creep behaviours of materials. The most widely used constitutive equations are simply called Kachanov-Rabotnov-Hayhurst (KRH) in the current research.

The lifetime of high chromium alloy steel P91 has been overestimated by the extrapolation method from short-term creep tests (high stress) to long-term creep tests (lower stress). The definition of stress ranges depends on different materials and temperatures. The current researcher classifies the stress ranges into high stress range, transition stress range and low stress range with stress exponent $n \approx 1$, $n \approx 4$, and $n > 10$ resepctively for high chromium alloy steel P91 under 600℃. The aim of the current research is improving the constitutive equations for high chromium alloy steel P91 at the transition stress range under 600℃.

The qualitative research method is used in the current project. The small but focused case study is used to validate the proposed constitutive equations for high chromium alloy steel P91 at the stresses of 80MPa and 70MPa under 600℃. Compared with the experimental lifetime of high chromium alloy steel P91

at the stress of 80MPa under 600℃, the predicted lifetime error is about 9.4%. However, at the boundary critical stress of 70MPa, the proposed constitutive equations are invalid. The current researcher argues that the both diffusion and dislocation creep deformation might control the creep deformation mechanism for high chromium alloy steel P91 at the critical stress of 70MPa under 600℃. A higher cavities nucleation rate and a higher coarsening rate might lead to the premature failure for high chromium alloy steel P91 at the critical stress of 70MPa under 600℃.

The proposed constitutive equations are only valid at the stress of 80MPa for high chromium alloy steel P91 under 600℃. The further work needs to be taken if more experimental data are available.

Table of content

List of Tables

List of Figures

Nomenclature

CDM: Continuum damage mechanism

EDT: European Technology Development

ECCC: European Creep Collaborative Committee

KRH: Kachanov-Rabotnov-Hayhurst

EBSD: Electron Back Scattered Diffraction

HAZ: Heat-Affected Zone

BEAR: Barkeley Engineering And Research

ASME: American Society of Mechanical Engineers

ASTM: American Society for Testing and Materials

D: Dame parameter, subscripts indicate specific mechanism

ρ: dislocation density, subscript i denotes initial value

P: particle spacing, i denotes initial value

K_p: Rate constant for particle coarsening

$\overline{C_t}$: Mean concentration of W/Mo in matrix at time t

C_0: Concentration of W/Mo in matrix at $t = 0$

K_s: Rate constant for precipitated particles

X: Thickness of oxidising/corroding phase

K_c: Rate constant for surface corrosion product

ε^*: Strain required to fracture corrosion product

K_{ox}: Rate constant for internal oxidation

N: Number density of cavitated grain boundary facets

R: Radius of test piece or component

r_{sg}: Subgrain radius; subscript i denotes initial value

K_N: Cavitation constant ≤1/3

$\varepsilon_{f,u}$: Uni-axial strain at fracture

l: Intercavity spacing

r: Cavity radius

T: Temperature

σ: Uni-axial stress

n: stress exponent

p: time exponent

Q: Activation energy for creep

R: Universal gas constant

$R_{u/t/T}$, $R_{u/t/T}$: Creep strength and rupture strength for a given time and temperature

t: time

t_u, $t_{u,max}$: observed time to rupture, maximum observed time to rupture

ω,$\dot{\omega}$: damage, rate of damage accumulation

ε, $\dot{\varepsilon}$, $\dot{\varepsilon}_{f,min}$: creep strain, creep strain rate, minimum creep strain rate

θ_1, θ_2, θ_3, θ_4: constants in Theta equation

θ_m: additional constant in modified Theta equation

σ, σ_0: stress, initial stress

A_0: initial undamaged area

A: damaged area

σ: nominal stress

σ_a: actual stress

m,n, p, q, A, B: constants

σ_e: effective stress

A_1, A_2, α, β, γ: constants

$\dot{N}$: cavity nucleation rate per unit grain boundary

α': an empirical factor of proportionality (m^{-2})

$\dot{\varepsilon}$: strain rate

D_{gb}: diffusion coefficient at grain boundary

Ω: atomic volume

σ_{loc}: local normal stress on the grain boundary

α: cavity radius

σ: remote or the applied stress to the grain boundary

$\chi(ij)$: damage stress criterion for creep rupture

λ_s: cavity separation

δ: grain boundary width

γ_m: surface energy terms of metal

k: Boltzmann constant ($k = 1.38 \times 10^{-23}\ J/K$)

T: temperature

ω: cavitated area fraction of the boundary, $\omega = (\frac{2R}{\lambda})^2$

σ_0: sintering stress of an isolated cavity

d: grain size

σ_I: initial stress

σ_b: back stress

ε_{fu}: uniaxial strain at fracture

$\dot{\varepsilon}_0$: a temperature creep parameter at the arbitrary normalizing stress σ_0

σ_1, σ_{EQ}: maximum stress and equivalent stress

A', B', n, m, x, $\emptyset$ and α: material constants

A, B, h, H^*, K_c and D and ν are material constants

H: strain hardening

φ: particle coarsening

α_v: dimensionless numerical factor whose magnitude depends on the shape of the grains

Acknowledgements

I would like to convey my feelings of my PhD research to the world. The PhD research has provided me the opportunities to meet people who come from all over the world. People whom I have met during my PhD research are all deserved to be appreciated sincerely.

Initially, I would like to express my sincere gratitude and appreciation to my supervisor Dr. Qiang Xu for his continued support and guidance throughout the period of my study.

I would also like to express my thankfulness to my internal and external examiners for the feedback of my first year and second year progression report. During the first year progression report, Dr Donglai Xu (internal) and Prof Xun (external) Chen had given me excellent feedbacks for supporting and continuing my second year study. During the second year progression report, Dr Fengshou Gu had also supported me strongly by giving the valuable feedback. I appreciate for their support and feedbacks.

I am also sincerely grateful to the support from Teesside University for the first two years of my research, such as the staff and facilities from school of science and engineering, financial department, career service, student service and library. In additional, I appreciate the partial financial support from Teesside University and University of Huddersfield.

I also appreciate for the manager of Interlink society Oliver Sagnier who helps me improve my English skills; solve problems; go travelling and gain working experience. I would also like to express my thanks to all my friends and colleagues I have made in Teesside University and University of Huddersfield for their supports and helps in my life.

Finally, I am indeed grateful to my parents for their great and selfless love, support and care, especially for the huge financial support for my studies in England; I am eternally indebted for this. And also thank you for the love from my family.

Publications

1) Lili An, Qiang Xu, Donglai Xu, Zhongyu Lu. (2012): Journal of Advanced Materials Research, "Review on the current state of developing of advanced creep damage constitutive equations for high Chromium alloy", Vol.510, p.776-780

2) Lili An, Qiang Xu, Donglai Xu, Zhongyu Lu. (2012), "Preliminary analysing of experimental data for the development of high Cr alloy creep damage constitutive equations", Proceedings of the 18th International Conference on Automation and Computing (ICAC), Loughborough University, Leicestershire, UK, 8 September 2012

3) Lili An, Qiang Xu, Donglai Xu, Zhongyu Lu. (2013): "Review of creep deformation and rupture mechanism of P91 alloy for the development of creep damage constitutive equations under low stress level", Proceedings of the 10th International Conference on Scientific Computing, Las Vegas, USA, 22-25 July 2013

4) Lili An, Qiang Xu, Donglai Xu, Zhongyu Lu. (2013): Journal of Advanced Materials Research,: "Analyzing the characteristics of cavity nucleation, growth and coalescence mechanism of P91 steels" , Vol.744, pp. 412-416

5) Lili An, Qiang Xu, Zhongyu Lu. (2013): "Development of advanced creep damage constitutive equations for high chromium steel P91", 6th International "HIDA" Conference on Life/Defect Assessment & Failures in High Temperature Plant, poster (2-4 December 2013, Japan)

Chapter 1

Introduction

1.1 Origin and Background

Creep damage is a time-dependent progressive deformation and damage under an applied stress and elevated temperatures condition (Naumenko & Altenbach, 2007). Stress and temperature are both main factors which affect the rate of creep. Generally speaking, creep damage occurs in metals and alloys under a constant stress at elevated temperatures; the high temperature is around 0.3~0.7 Tm (Tm indicates the absolute melting temperature of materials). A standard creep curve includes primary, secondary and tertiary creep damage stages. The creep strain rate decreases at primary creep stage; stays at a stable value at secondary stage which is also called as steady-state creep; and then the creep strain rate increases at tertiary stage until the fracture of materials (Betten, 2005; Naumenko & Altenbach, 2007).

There are two ways of creep deformation process—diffusion and dislocation creep deformation. Dislocation creep mechanism is a movement of dislocation. The dislocation movement requires a small amount of thermal activation by gliding in a slip plane. Diffusion creep is identified as vacancies diffusion through the crystal lattice within a grain. Depending on the path of vacanies' diffusion, there are two types of diffusion creep deformation. If the vacanies move through the crystal lattice, this is called Nabarro-Herring creep deformation; if the

vacanies move along the grain boundary, this is called Coble creep (Gao, 2014; University of Cambridge, 2014).

Continuum Damage Mechanics (CDM) is one branch of damage mechanics. It was initiated by Kachanov in 1958 for the case of creep damage (Kachanov, 1986; Krajcinovic, 1996, p. 476). A damage variable ω was proposed in order to describe the creep damage process as homogenerous. Continuum damage mechanism theory considers the descriotion of state variables in the framework of thermodynamics of irreverisble process. Constitutive equations combined with computational techniques is used to predict the creep behaviours of materials within the continuum damage mechanism (Kachanov, 1986; Krajcinovic, 1996, p. 476).

Constitutive equations have been established to accurately predict the creep damage behaviours of materials within the framework of continuum damage mechanics. The most popular used constitutive equations based on the homogeneous hypothesis is Kachanov-Rabotnov-Hayhurst (KRH) model. The constitutive equations were initially proposed by Kachanov (1958) and Rabotnov (1969), and improved by Leckie and Hayhurst (1974, 1977) which is applied into multi-axial state of stress condition (Liu & Murakami, 1998). The recently researcher also proved that KRH constitutive equations combined with Dyson's cavitation damage theory is the best model to predict the cavitation damage for materials (Rouse, Sun, Hyde, & Morris, 2013).

1.2 Importance of investigating creep damage

Life assessment is increasingly becoming significant for materials. Life assessment not only provides a method of an effective and reliable material design, but also provides the way to expand the lifetime of material. Continuum damage mechanism is becoming a generic life assessment tool to predict the lifetime of materials at creep condition.

The creep damage topic has been argued more than 40 years. Creep damage has caused the attention of many researchers and industries. The European Creep Collaborative Committee (ECCC) is one of the organisations to collect information and data from 16 countries involving over 40 European organisations. ECCC provides a platform for co-operation of European industry and research to exchange and update of information and data for materials in the creep regime from different projects. ECCC also frequently produces guidelines for the generation, treatments and assessement of large creep datasets for industry (European Creep Collaborative Committee, 2001-2005). The development of the ECCC organistion is summarised as, for instance, from 1992—1996, the ECCC organistaion reported the rules of uni-axial rupture strength for European products and design standards; from 1997—2000, the ECCC organistaion reported the assessment of weldment materials; and then recently the ECCC organistaion has reported the analysis and application of creep deformation and multi-axial features (Holdsworth & Merckling, 2003). In addition, the European Technology Development (ETD) company and many other international conferences (such as the 6th international conference on

"defect assessment & failures in high temperature plant"-with special reference to new steels (P91, P92, P93, P94) in 2014) also dedicated to the investigation of creep damage of materials under the creep conditions (European Technology Development, 2014).

The consequence of the creep damage accidents is not only just the great loss for industries, but also the personal safety for the employees. The accidents that caused by the creep damage (explosions of steam pipes, steam boilers, nuclear reactors and engines) are a serious issue across the world. This is an example which happened in 1985, California thermal power plant, United States. The steam line was operating at 900psi, 1000degF. The creep deformation and high temperature led to the failure after 10 years operation (Berkeley Engineering And Research, 2008). Moreover, another accident happened in 1992 in the US, as shown in Figure 1.1 (Fumitoshi, Nobuhiko, Masahiro, Masashi, & Akira, 2009).
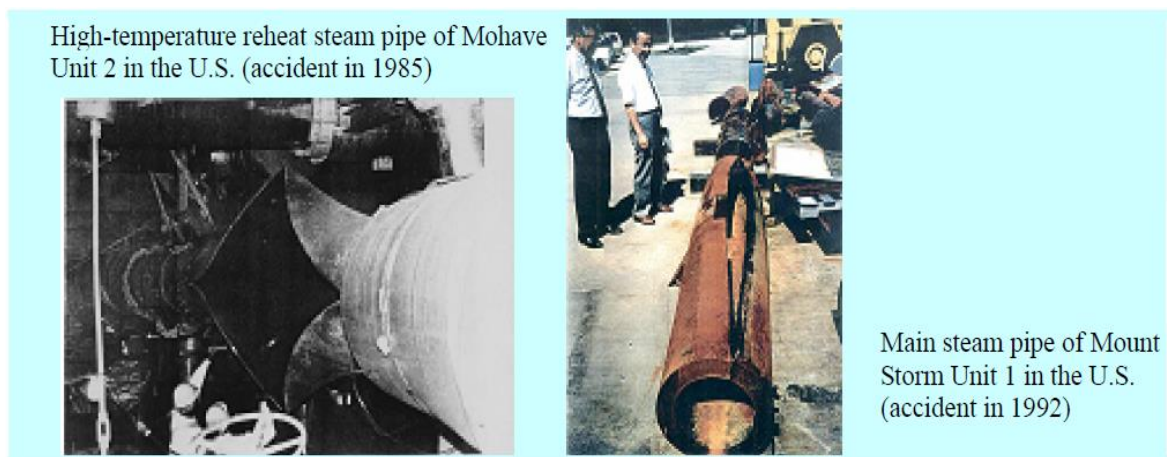
Figure 1. 1: Creep damage accidents (Fumitoshi et al., 2009)

1.3 Gap between the previous work and current research

As a candidate structural material, high chromium alloy steel 9Cr-1Mo-V-Nb (P91) has advantages of low oxidation speed, high creep strength, high resistance of corrosion ability and high thermal conductivity. It has been widely used as a component of steam pipes, headers, boilers, engine blade of aeromagnetic, turbine rotor, jet engine and others in power plant (IFM, 2009; Shibli & Starr, 2007). At high stress range, the life span and creep behaviours of P91 have been investigated by many researchers nowadays (Abe, 2012; Bendick, Cipolla, Gabrel, & Hald, 2010; Chen, Yan, Hu, Shan, & Yang, 2011; Eggeler et al., 1994; Gaffard, Besson, & Gourgues-Lorenzon, 2004; Gaffard, Gourgues-Lorenzon, & Besson, 2005; Pétry & Lindet, 2009; Shrestha, Basirat, Charit, Potirniche, & Rink, 2013; Shrestha et al., 2012; Vivier, Gourgues-Lorenzon, & Besson, 2010; Vivier, Panait, Gourgues-Lorenzon, & Besson, 2008).

The stress ranges are divied into high stress range, transtion stress range and low stress range in the current project according to the stress exponent n. Stress exponent n is derived from the ratio between changing of strain rate and stress. Firstly, the stress range varies for different materials at different temperatures. The reasons of choosing temperature 600 ℃ in the current project for high chromium alloy steel P91 are 1) temperature 600 ℃ is most common used temperature in industry; 2) the experimental data under 600℃ is more than the data at the other temperatures. Secondary, at a certain temperature, the stress range varies based on the stress exponent. For example, under 600℃ for high chromium alloy steel P91, when the stress exponent $n > 13$ with stress higher

than 130MPa, it is defined as high stress range. When the stress exponent $n \approx 4$ with stress between 70MPa and 110MPa, it is defined as transition stress range. When the stress exponent $n = 1$ with stress less than 50MPa, it is defined as low stress range. The creep deformation and damage mechanism between stress 50MPa and 70MPa, stress 110MPa and 130MPa are more complicted (Chen et al., 2011).

In industries, the pratical temperature range is between 550℃ and 650℃ for high chromium alloy steels. In reality, the high stress with a lower temperature is more important. In order to investigate the creep damage process, the applied stress is relatively high to decrease the experimental duration. It is difficult to obtain the creep data of materials at lower stress range. For example, the life span of high chromium alloy steel P91 at a lower stress of 80MPa under 600℃ is more than 13 years.

The extrapolation method combined with the constitutive equations from high stress data to low stress region is widely used by researchers for high chromium alloy steels. Within continuum damage mechanics, constitutive equations are used to predict the complex creep behaviours of materials and to estimate the life span of materials. The previous researches show that the KRH constitutive equations could accurately predict the life span or the creep behaviours of materials at the high stress range for high chromium alloy steel P91 at different temperatures (Hyde, Becker, Sun, & Williams, 2006a).

In terms of the high chromium alloy steels, the lifetime of materials at lower stress range has been estimated by the extrapolation method by using high

stress data to lower stress region. However, the accurate extrapolation method using high stress data to low stress region is critically important. This point of view has been supported by researchers (Abe, 2012; Chen et al., 2011; Chen, Yan, Wang, Shan, & Yang, 2012; Haney et al., 2009; Hyde et al., 2006a; Hyde et al., 2006b; Lim et al., 2011; Sawada, Kushima, Tabuchi, & Kimura, 2011; Xu, 2000, 2004).

In summary, the majority of the previous researches reported that the over-estimation of life span of materials by the extrapoltion method from high stress data to lower stress data. The overestimated life span of materials at lower stress range is argued by the changing of creep deformation and damage mechanisms at different stress ranges and the microstructural degradation process might lead to a premature failure of materials. This point of view has been supported by many researchers, such as (Bendick et al., 2010; Chen et al., 2012; Kimura, Kushima, & Abe, 2002; Kloc & Sklenička, 2004; Massé & Lejeail, 2012, 2013; Panait, Bendick, Fuchsmann, Gourgues-Lorenzon, & Besson, 2010a; Panait et al., 2010b; Parker, 2013; Petry & Gariboldi, 2010; Pétry & Lindet, 2009; Sawada et al., 2011; Shrestha et al., 2012; Spigarelli, 2013). Some of the previous researches reported that the microstructural degradation might lead a premature failure of materials at lower stress range (Abd El-Azim, Ibrahim, & El-Desoky, 2013; Panait et al., 2010a; Sklenicka, 2003; Spigarelli, 2013; Vivier et al., 2008). Only few of the previous research investigated the microstructure degradation procress combined with the constitutive equations to accurate the creep behaviours of materials and the life span of materials (Chen et al., 2011; Yin & Faulkner, 2006).

Based on the stress regions for high chromium alloy steel P91 under 600℃, at the low stress range (less than 70MPa under 625℃-(Gaffard et al., 2005); less than 50MPa under 600 ℃-(Chen et al., 2011)), it is difficult to conduct the creep test in reality. The current project also found that there is no experimental data at the low stress range for high chromium alloy steel P91 under 600℃ (updated until September 2014).

However, the transition stress range is also significant to investigate in order to improve the extrapolation method or improve the constitutive equations. According to the reports from Chen et al. (2011) and Yin & Faulkner (2006) the applied stresses were relatively high than the transtion stress for high chromium alloy steels P92 and P91 under 600℃, respectively. Therefore, the gap between previous research and the current research is to investigate the creep damage process combined with the constitutive equations for high chromium alloy steel P91 at transtion stress range under 600℃ to accurate predict the lifetime of materials.

1.4 Aim and Objectives

The aim of the current project is improving the constitutive equations for high chromium alloy steel P91 under 600℃, especially at the transition stress range. The considered aspects to improve the constitutive equations are creep deformation and damage mechanism, microstructural degradtion evolution process, and failure criterion at the transition stress range.

The objectives of the current research are listed as below:

1. To critically evaluate and understand the creep deformation and damage theories combine with constitutive equations in phenomenological approach
2. To devise the constitutive equations that is capable of depicting the influence of stress and the coupling between creep damage and creep deformation for high chromium alloy steel at transition stress range.

   In order to achieve that, it is essential to understand the coupling of the creep deformation and damage mechanism for high chromium alloy steel P91 at the transition stress range; moreover, to understand the characteristics of constitutive equations in terms of depicting the creep deformation and damage process, microstructural degradation evolution.
3. To validate the creep damage constitutive equations for high chromium alloy steel P91 by case study research method.

1.5 Limitations and contributions of the current research

The comparison of KRH constitutive equations and the constitutive equations in the current project is summarized as below. The formation of the current consititutive equations are similar with the KRH constitutive equations. The creep strain rate and stress is presented by the power law function rather than the hyperbolic function in the KRH constitutive equations. The diffusional creep deformation is considered in the current constitutive equations rather than the dislocation creep deformation. The brittle fracture is identified at the transition stress range rather than the ductile fracture at high stress range. The microsturctural degradation covers the strain hardening, particle coarsening and

cavitation damage in the current constitutive equations and KRH constitutive equations. The cavitation damage mechanism at the transition stress range is dominated by the diffusional cavity growth with the cavity continuous nucelation. However, based on the experimental data on cavity density and cavity size, the current researcher points out that the cavity nucelation rate (in density) has significant influence on the failure of materials than the cavity growth (in size). Thus, Dyson's cavitation damage theory caused by the cavity nucelation is adopted in the current constitutive equations model, as it is used in the KRH constitutive equations.

The limitations of the current project include three aspects. Firstly, the required experimental data for high chormium alloy steel P91 under 600℃ at the transition stress range is inadquate. Secondly, the selection of material parameters for chormium alloy steel P91 under 625℃ are used in the current constitutive equatins model. The influenece of temperature should be considered in the further work. Thirdly, the applications and validations of the proposed constitutive equations in the current research should be expanded in the further work.

The contributions of the current research project are concluded. Firstly, the current research represents a theoretical approach to improve the constitutive equations for materials at creep condition. Secondary, the current research represents the improvement of life assessment method in order to assure a safe and economical operation for industry. Accurately predicting the long-term behaviours of materials will also provide an effective and reliable design of materials. In addition, the current researcher points out the essential requirement

of the experimental data on the microstructure degradation and cavitation damage evolution process in the future. The current researcher suggests that the X-ray tomography technique could be considered in the further research.

1.6 Structure of the thesis

The structure of this thesis contains 7 chapters.

Chapter 1 introduces the background of creep damage, the importance of investigating the creep damage in industries and the gap between previous work and the current project. Chapter 1 includes the aim and objectives of the current research, and the structure of the whole thesis. Chapter 1 also includes the limitations and contributions of the current research.

Chapter 2 contains an adequate general literature reiview of creep deformation and damage mechanism and creep fracture mechanism. In terms of the materials, chapter 2 introduces the development of the high chromium alloy steel P91 in high temperature industries; some specific experimental data for high chromium steels and its weldment. Afterwords, chapter 2 introduces the cavitation damage mechanism theory, and consitutuive equations models within continuum damage mechanism. Espcecially for KRH constitutive equations, chapter 2 introduces the development of KRH constitutive equations. For high chromium P91 steels, chapter 2—collects the constitutive equations models and methods which were used in the previous researches. At last, chapter 2 includes the deficiencies of the KRH constitutive equations and the improvements which is considered in the current research.

Chapter 3 presents the current reseach method and the validation method of the proposed constitutive equations model.

Chapter 4 presents the main work in the current research. Based on the objectives of the current research, chapter 4 represents the step of improving the constitutive equations for high chromium alloy steel P91.

Chapter 5 summarizes the main conclusions and findings for the propsed constitutive equations and the formation of the proposed constitutive equations based on chapter 4.

Chapter 6 includes the case studies for high chromium alloy steel P91 under 600℃ at stresses of 80MPa and 70MPa.

Chapter 7 includes the key conclusions of the current project and the future work.

Chapter 2

Literature Review

2.1 Creep damage and deformation

2.1.1 Creep damage

The creep damage is an inevitable issue when metals and alloys are exposed at a constant stress and at elevated temperature condition. The research of creep damage has been continuously in progress more than 40 years. A number of conferences and symposiums were organized by researchers or organizations, such as the European Creep Collaborative Committee (ECCC) organisation and European Technology Development (ETD) company, in order to solve the creep damage problems in industries (European Creep Collaborative Committee, 2001-2005).

Creep damage is a time-dependent inelastic deformation process in metals under an applied stress and an elevated temperature condition. Creep damage usually occurs in metals and alloys at a constant stress and high temperature condition ($0.3\mathrm{T}_m < \mathrm{T} < 0.7T_m$, T_m is the materials' absolute melting temperature). The defination of creep damage has also been defined by many researchers, such as (Betten, 2005; Kassner & Perez-Prado, 2004; Krajcinovic, 1996; Merckling, 2005; Naumenko & Altenbach, 2007). This critical melting temperature is significant because of the atomic rearrangements by the diffusion at around $0.4T_m$ and above. Beside, for many different crystalline materials, it has been

found that the creep strain increases as a logarithm function against time (Betten, 2005).

2.1.2 Creep deformation

There are two ways of creep deformation process—diffusion and dislocation creep respectively (Betten, 2005). Diffusion creep deformation is the diffusion of vacancies through the crystal lattice of materials within a grain. Diffusion is the movement of atoms between sites. The diffusion creep deformation includes two ways—Nabarro-Herring creep (N-H creep) and Coble creep.

The difference between N-H creep and Coble creep is the path of atoms (vacancies) diffusion. In N-H creep deformation, atoms diffuse through lattice; in Coble creep deformation, atoms diffuse along the grain boundary. N-H creep deformation prefers a relative higher stress and temperature than the Coble creep deformation. Coble creep is a more grain size dependent deformation. Coble creep dominates at lower stresses and temperatures.

The rate of creep diffuison deformation depends on the grain size. The rate of the diffusion is inversely proportional to the grain size. So, increasing the grain size could reduce the rate of diffusion. The rate of creep diffusion deformation has exponential dependence on temperature. The applied stress starts the dislocation movement and the diffusion of atoms. The deformation will increase if the applied stress is increased.

Atomic diffusion creep (diffusion creep process) is a kind of defect under an high homologous temperature and lower stress (Zhang & Zhou, 2009). The creep

strain rate is proportional to the applied stress at diffusion creep, which is also reported by other researchers (Academic Resource Center; Betten, 2005; Kassner & Perez-Prado, 2004; Krajcinovic, 1996; Merckling, 2005; Naumenko & Altenbach, 2007; Riedel, 1987; University of Cambridge, 2014).
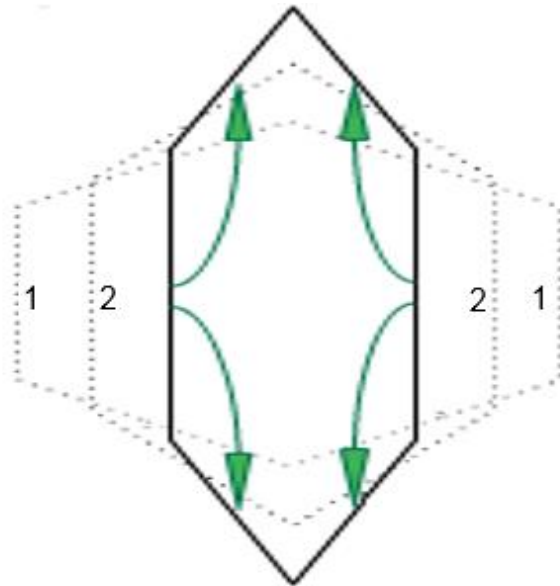
Figure 2. 1: Nabarro-Herring diffusion creep (University of Cambridge, 2014)
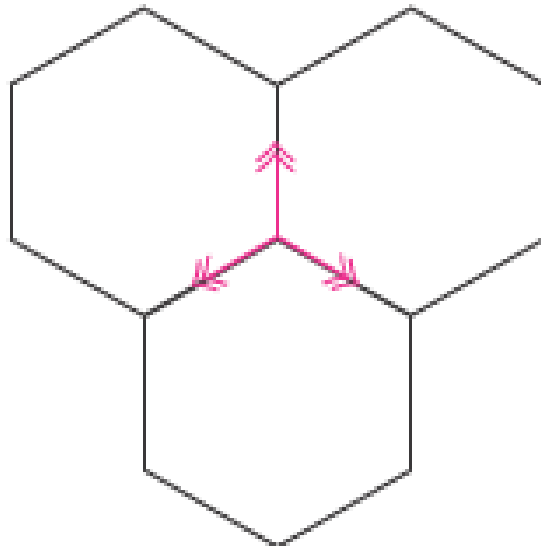
Figure 2. 2: Coble diffusion creep (University of Cambridge, 2014)

The N-H diffusion creep deformation and the coble diffusion creep deformation are shown in Figures 2.1 and 2.2 respectively. The arrows in the figures indicate the movements of atom (University of Cambridge, 2014). Figure 2.1 clearly shows the N-H diffusion creep deformation through the main body of grains. The dashed lines indicate the deformation from original state (dashed line 1) to deformation state (dashed line 2), then to the inner solid line. The arrows in Figure 2.1 shows that the grain deforms in a vertical direction. Figure 2.2 describes the Coble diffusion deformation. The arrows in Figure 2.2 indicate the atoms move along the grain boundaries.
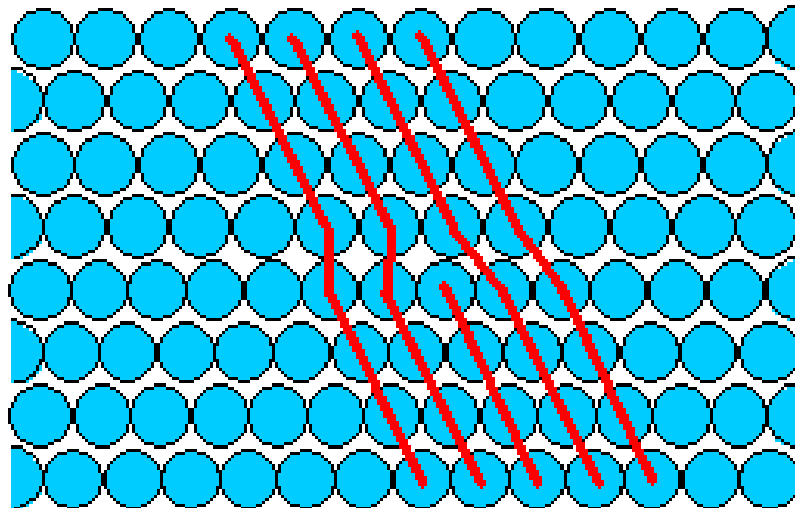
Figure 2. 3: A dislocation in 2D (University of Cambridge, 2014)

From literature review on the general creep damage theory (Riedel, 1987; Tu, 2005; Zhang & Zhou, 2009), as it is concluded that the dislocation creep deformation is described as the movement of dislocations. The dislocations are line infects initially, as it is shown in Figure 2.3 (University of Cambridge, 2014). The dislocation creep deformation is strongly dependent on the stress. The dislocation creep deformation involves the dislocation movement through the

crystal lattice of materials and causes a plastic deformation of individual crystals and in the end of the material itself. Slip motion (dislocation creep process) is the main mechanism and occurs during the whole creep process. Dislocation creep process occurs at a relative higher stress and the temperature above $0.3 \sim 0.5 T_m$ (usually not exceeds $0.7 T_m$) compared with the diffusion creep deformation (Zhang & Zhou, 2009).

Besides, in terms of the creep deformation and damage mechanism, as it is concluded that the creep dislocation process and creep diffusion process take the domination at different stress range conditions. For instance, at high stress range, the dislocation creep controls the deformation mechanism; at low stress range, the diffusion creep controls the deformation mechanism, although the dislocation creep occurs throughout the whole creep deformation process (University of Cambridge, 2014). In general, according to the classical power law theory ($\dot{\varepsilon} \propto \sigma^n$), stress exponent $n \approx 1$ when the diffusion deformation is operating; stress exponent $3 < n < 8$ when the dislocation deformation is operating.
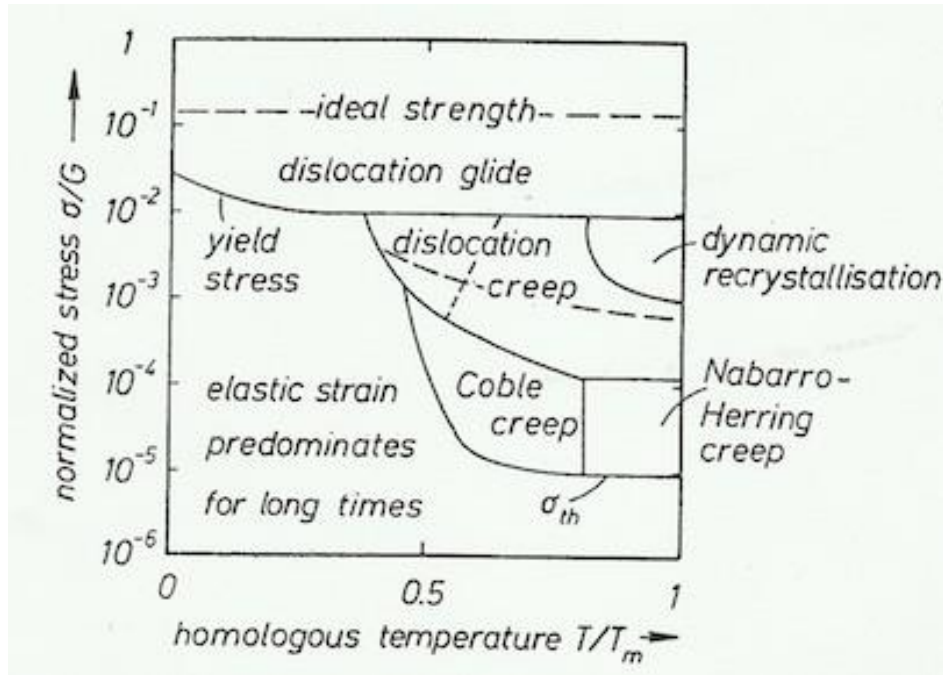
Figure 2. 4: Deformation mechanism Map (Riedel, 1987)

According to Riedel (1987), at high temperature condition, the creep diffusional deformation takes the domination at lower stress range, otherwise, the creep dislocation deformation takes over the domination to control the creep deformation mechanism at high stress range. The following Figure 2.4— deformation mechanism map represents the strain rate vs. temperature. From Figure 2.4, it can be seen that the different mechanisms dominate the creep deformation mechanism at different regions. For example, at a relative higher temperature and stress, the dislocation creep controls the creep damage mechanism.
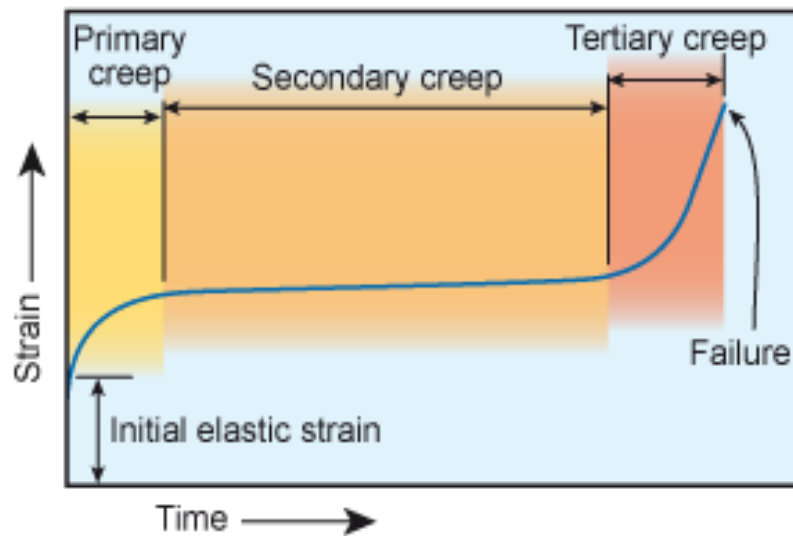
Figure 2. 5: Typical creep curve for steel (Mathers, 2014)

A standard creep curve which describes the process of creep deformation includes primary, secondary and tertiary creep stages together, as shown in Figure 2.5 (Mathers, 2014). An initial elastic strain is due to the application of the initial load. Firstly, the primary creep includes the strain hardening process which prevents the dislocation movements, and the relaxation process (redistribution of lattice defects). Secondly, the secondary creep includes the strain hardening process and softening process (recovery, recrystallization, strain softening and precipitates over-aging). The strain hardening effect and the softening effect are in equilibrium at secondary creep stage. Finally, tertiary creep is the damage process which includes the cavitation damage and the aging of the microstructural etc., based on the previous researchers, such as (Academic Resource Center; Gorash, 2008; Riedel, 1987).
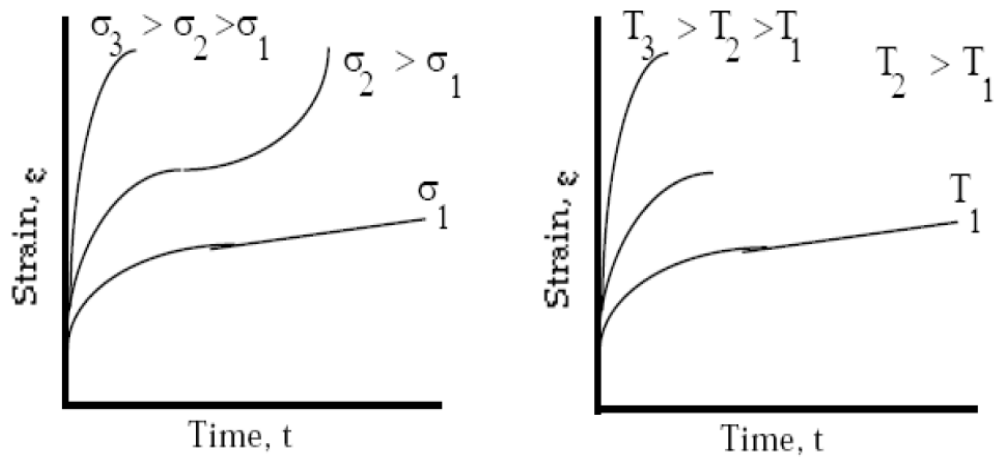
Figure 2. 6: Influence of stress and temperature on creep behaviour (Naumenko & Altenbach, 2007)

The shape of the creep curve is strongly depending on the stress and temperature, as shown in Figure 2.6 (Naumenko & Altenbach, 2007). In Figure 2.6, the left side figure shows the stress-dependent influence on the life span of materials; the right side figure shows the temperature-dependent influence on the life span of materials. When the temperature is a constant, the life span of materials decreases along with the increased stress, as shown in the left side in Figure 2.6. When the applied stress is a constant, the life span of materials decreases along with the increased temperature, as shown in the right side in Figure 2.6.
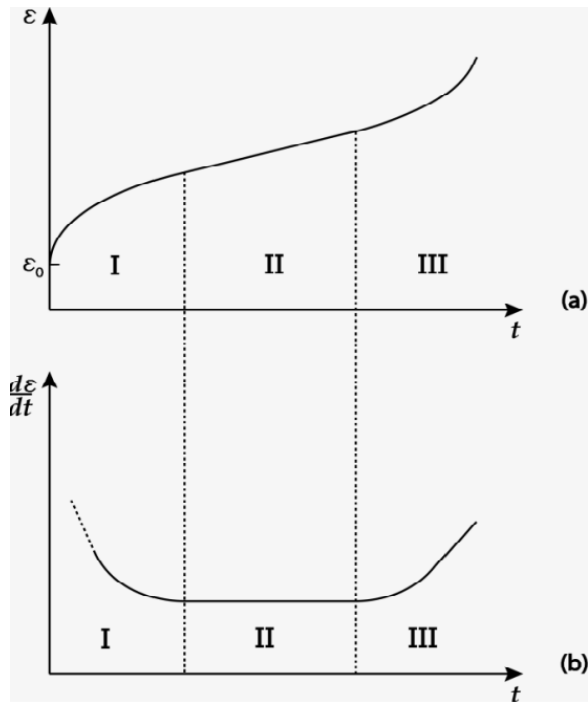
Figure 2. 7: Creep strain and creep strain rate under a constant loading test (Picard & Fafard, 2011)

The index used to describe the rate of creep deformation is called creep strain rate, as shown in Figure 2.7. It is the slope of the line in the standard creep curve (strain vs. time). The creep strain rate decreases in the primary creep stage until a critical value, stays stable in the secondary creep stage and increases in the tertiary creep stage eventually until the rupture of materials. The creep strain rate phenomenon has also been reported by many researchers, such as (Academic Resource Center; Naumenko, 2006; Naumenko & Altenbach, 2007; Riedel, 1987; Tu, 2005).

2.2 Creep fracture

2.2.1 Ductile fracture and brittle fracture

There are two typical types of fracture—ductile fracture and brittle fracture for most of the engineering materials. The difference between ductile fracture and brittle fracture is whether a large quantity of plastic deformation accompanied or not. The ductile fracture accumulates a large amount of plastic deformation. By contrast, the brittle fracture accumulates a small or no plastic deformation before the materials failure, based on the previous researcher (Bailey, 1997; Ballard, 1997; University of New South Wales Australia, 2014). In general, the different fracture modes can be identified by observing the surface of fracture materials, as it is shown in Figure 2.8 (ductile fracture—left, brittle fracture—right) (Charles Sturt University, 2015; University of New South Wales Australia, 2014).
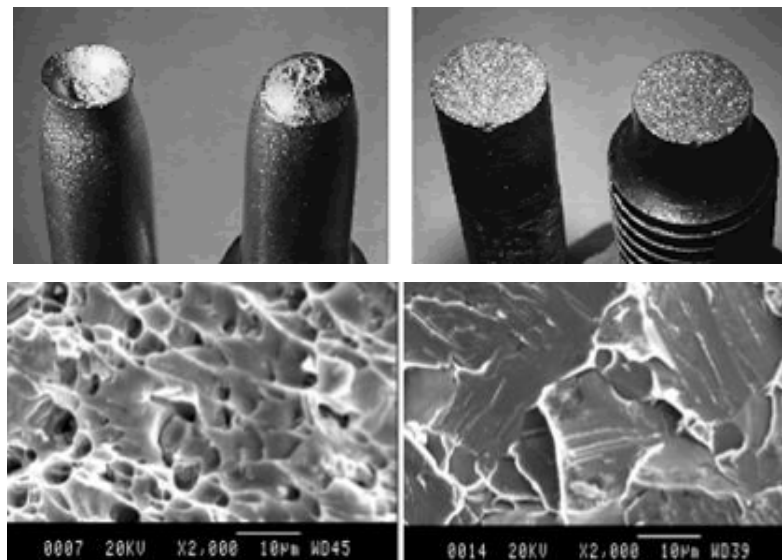
Figure 2. 8: Ductile fracture surface of metals (left) and brittle fracture surface of steels (right) (Charles Sturt University, 2015; University of New South Wales Australia, 2014)

In ductile fracture, the fracture surface of materials is a dimple-shaped surface at high magnification and a fibrous-shaped surface at low magnification. In brittle fracture, the fracture surface of materials is crystalline-shaped surface at high magnification and a radiating-shaped surface at low magnification. At the uniaxial creep tension condition, at high stress range, ductile fracture is usually observed; at lower stress range, brittle fracture is usually observed (Kachanov, 1986, p. 11).

2.2.2 Trans-granular creep fracture and inter-granular creep fracture

The initiation and propagation of cracks are the essential damage before a fracture. The cracks in ductile materials move slowly and will not extend unless increasing the applied stress. The cracks in brittle materials rapidly extend and spread before failure (Bailey, 1997). According to the path of crack propagation, there are two forms of fracture—trans-granular fracture when the cracks pass through the grains and inter-granular fracture when the cracks pass along the grain boundaries, respectively (Bailey, 1997).

According to Riedel (1987), trans-granular creep fracture and inter-granular creep fracture (grain boundary wedge cracks or grain boundary voids) are the two main creep fracture forms. Trans-granular creep fracture is anticipated at high stress range because of the reduction of dislocation network size. Inter-granular creep fracture results from cavities nucleation, growth and coalescence on grain boundary at high temperature.
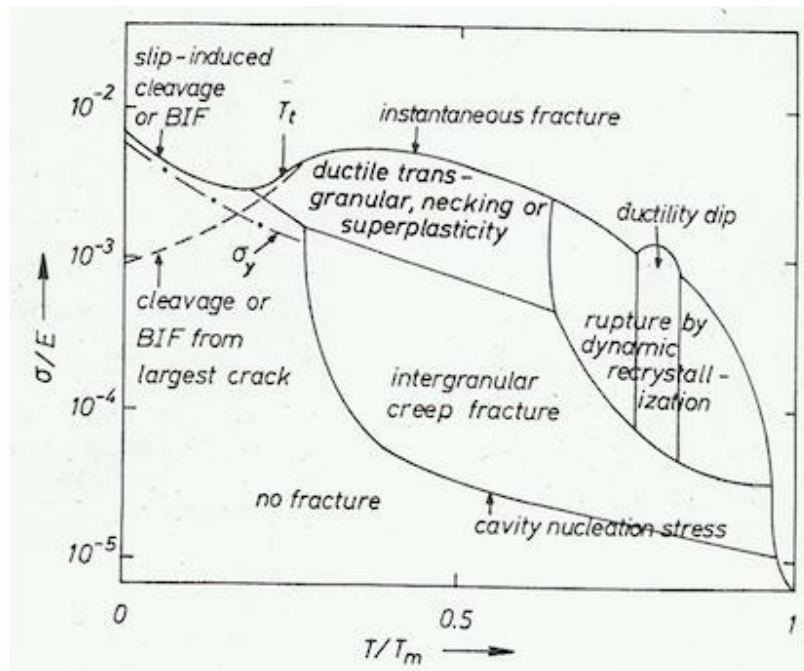
Figure 2. 9: Fracture mechanism map (Riedel, 1987)

In general, Figure 2.9 shows the fracture mechanism map of materials at different stresses and temperatures conditions (Riedel, 1987). For instance, at a certain temperature condition, Figure 2.9 shows that the ductile trans-granular creep fracture controls the fracture mechanism at the high stress range; the brittle inter-granular creep fracture controls the fracture mechanism at the lower stress range. Different types of creep fracture control the different fracture mechanisms of materials, supported by Kasyanov (1986).

2.3 High chromium steels P91

2.3.1 The development of high chromium alloy steel P91

The materials with high creep resistance and high strength properties are highly required since 20 years ago in power plant industries. Element chromium makes possibilities to develop materials which satisfy the requirements of industries.

Since 1990, due to the high resistance of corrosion, high creep strength and low oxidation speed of high chromium alloy steels (9-12%Cr), high chromium steels have been widely used in power plant industries as a component of steam boilers, pressure vessel, turbines, boiler drum, tubes, pipework etc., based on the literature review research from (Key to Metals AG, 2010, 2010 ; Saha, 2003).

In the 1950s in Germany, the material X20 (12%Cr-1%Mo-0.25%V) was primary produced and widely used in high temperature industries, like in power plant. However, X20 has been replaced by the high chromium alloy steel P91 (9%Cr-1%Mo-0.25%V) later on in 1980s in the US Oak Ridge National Laboratory; because of the limitations (the poor fabrication and welding properties) of material X20. Ideally, the material P91 compensates the limitations of X20, so the high chromium alloy steel P91 is popular for use in high temperature industries nowadays (Saha, 2003).

2.3.2 The properties of high chromium alloy steel P91

Grade 91 was developed in the 1970s by Oak Ridge National Laboratory (ORNL) in the USA as modified 9Cr-1Mo steel. It was used in many forms in ASTM/ASME specifications: seamless tube T91 (ASTM A213), seamless pipe P91 (ASTM A355), forged pipe FP91 (ASTM A369), forging F91 (ASTM A182) and casting C12A (ASTM A217) (Bendick et al., 2010). In order to fill the operating temperature gap between pearlite and austenitic steel, the martensitic heat resistant steel, like P91, are widely used between 550°C and 650°C.

Based on the previous research (Bendick et al., 2010; Eggeler et al., 1994; Johnzactruba & Lamar, 2011; Key to Metals AG, 2010 ; Materials & Welding, 2007), compared with its predecessor—T22 or P22, the high chromium alloy steel P91 has a higher creep resistance, higher creep rupture strength, higher thermal stability and higher oxidation resistance and a good fabrication properties. Some new elements (such as N, Nab, V) are added into the high chromium alloy steel P91 based on the previous 9Cr-1Mo steels. The element chromium improves the high temperature strength and increases the oxidation resistance and the corrosion resistance of materials. The element molybdenum increases the creep resistance ability.

The formation of P91 steel is by normalizing at 1050℃, air cooling down to 200℃, and then tempered by heating to 760℃. The chemical composition of P91 steel is listed in Table 2.1 (ThyssenKrupp, 2011).

By contrast, the chemical composition, heat treatment and mean creep rupture strength of the advanced high chromium steels P91, E911 and P92 are listed in Table 2.2, according to the European Creep Collaborative Committee (ECCC) in 1995 (Bendick et al., 2010).

Table 2. 1: Chemical composition (Heat analysis in %) (ThyssenKrupp, 2011)

Name	C	Si	Mn	P	S	Al
	0.08-0.12	0.20-0.50	0.30-0.60	≤0.020	≤0.010	≤0.040
	Cr	Mo	Ni	V	N	others
P91	8.0-9.50	0.85-1.05	≤0.40	0.18-0.25	0.03-0.07	Nb 0.06-0.10

Table 2.2: Chemical composition, heat treatment and mean creep rupture strength of advanced steels P91, P92 and E911 (Bendick et al., 2010)

Element	T/P91 (EN 1026-2)	E911 (ASME 213-335)	T/P92 (ASME 213-335)
C	0.08-0.112	0.09-0.13	0.07-0.13
Si	0.20-0.50	0.10-0.50	0.50max
Mn	0.30-0.60	0.30-0.60	0.30-0.60
P	0.020max	0.020max	0.020max
S	0.010max	0.010max	0.010max
Cr	8.00-9.50	8.50-10.50	8.50-9.50
Mo	0.85-1.05	0.9-1.10	0.30-0.60
Ni	0.40max	0.40max	0.40max
Al tot	0.04max	0.04max	0.04max
Cu	0.030max	/	/
Nb	0.06-0.10	0.06-0.10	0.04-0.09
Ti	/	/	/
V	0.18-0.25	0.18-0.25	0.15-0.25
N	0.03-0.07	0.04-0.09	0.03-0.07
W	/	0.09-1.10	1.5-2.0
B	/	0.0003-0.006	0.001-0.006
Normalising(600^0C)	1040-1090	1040min	1040min
Tempering(600^0C)	730-780	730min	730min
10^5h creep rupture strength at 600^0C	94MPa (ECCC 1995)	98MPa (ECCC 2005)	113MPa (ECCC 2005)

2.3.3 High chromium alloy steel P91 weldment properties

It is necessary to understand the creep deformation and creep damage mechanism to estimate the lifetime of high chromium alloy steel P91 weldment. Considering the weldment properties, some common issues occur in high chromium alloy steel P91 weldment, such as, type IV cracking/failure, reduced lifetime, reduced creep strength, changes in microstructure etc. This phenomenon was reported by (Tabuchi & Hongo, 2009).

In terms of the cavitation damage mechanism, Figure 2.10 illustrates the cavity growth mechanism. From part (a) in Figure 2.10, it can be seen that constrained cavity growth predominates at lower stress range; plasticity-controlled cavity growth will take the domination with stress increases, and lead to a high strain rate and short lifetime to rupture (Yao, Xuan, Wang, & Tu, 2007).
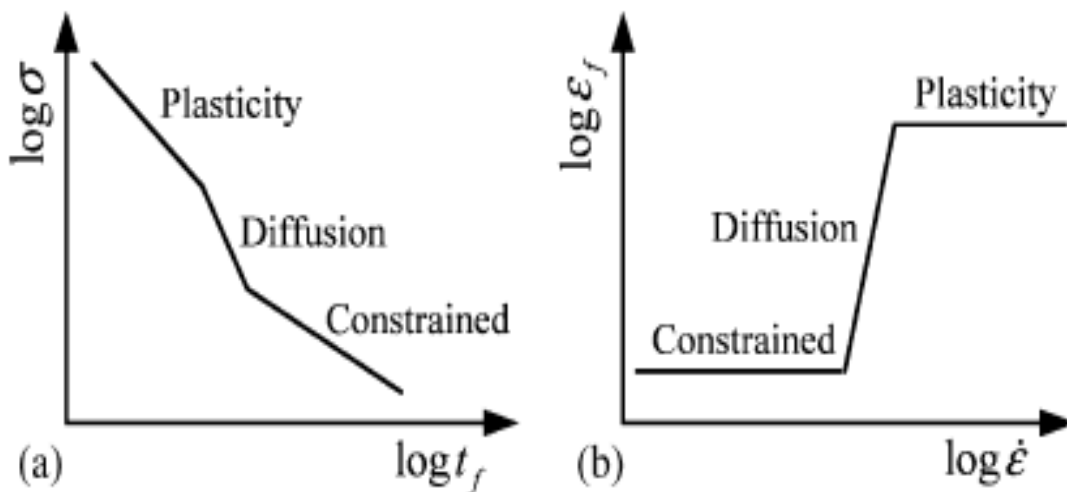
Figure 2. 10: The relationship between cavity growth mechanism and rupture time and rupture strain (Yao et al., 2007).

Many researchers investigated the creep damage behaviours of high chromium alloy steels weldment. The previous work reported that the weakest zone (lowest creep strength) in weldment materials is located within the weld metal zone, based on the previous researchers, such as (Bendick et al., 2010; Besson, Leclercq, Gaffard, & Gourgues-Lorenzon, 2009; Eggeler et al., 1994). Type IV failure could be affected by creep strain and the high multi-axial stress condition. The process of Type IV creep damage has been investigated by using a thick plate welded joint specimen by Li, Tabuchi and Hongo, (2009); Watanable and Tabuchi (2007). Their results reported that creep voids nucleation of high chromium alloy steel 91 starts at the early stage of creep rupture life (0.2 of life), increases with time till 0.7 of life, and then coalesces to form a macro crack after 0.8 of life. The current researcher argues that the cavity nucleation rate (voids density) has significant influence on the final fracture of materials.

2.4 Cavitation damage theory

Materials damage indicates the deterioration of materials' mechanical properties as a consequence of the development of cavities in microscopic, meso-scopic and macroscopic point of view. In microscopic point of view, the fracture of materials is the process of the micro-cavities or micro-cracks nucleation. In the macroscopic point of view, the fracture of materials is the extension of cracks which caused by cavities coalescence. Between these two points of view, i.e. in the meso-scopic viewpoint, the cavities nucleation, growth and coalescence leads to the initiation of a macroscopic crack (Murakami, 2012, p. 3).

Continuum damage mechanics, a branch of continuum mechanics, aims to describe the damage and fracture development in meso-scopic and macroscopic view. In the other words, the continuum damage mechanics is aiming to analyse the initiation of micro-cavities or micro-cracks to macro-cracks which finally leads to a fracture (Murakami, 2012, pp. 3-13). Continuum damage mechanics was originally introduced by Kachanov in 1958 for the case of creep damage (Kachanov, 1986). The assumption of continuum damage mechanics is the kinematics and the mechanical behaviours of materials are continuous. The damage variables are proposed to describe the homogeneous distribution of micro-defects, stress and strain rate. In the other words, according to Rice (1974), continuum damage mechanics is simulating the discrete material model as a continuum material model. Within the CDM framework, the damage variables were proposed to describe the damage process until macro-cracks of materials and to derive constitutive equations to solve the creep damage problems.

From the phenomenological view of the microstructure changes, an internal damage variable ω was introduced to describe the cavitated area fraction of grain boundary. The damage variable ω obeys the kinetic law and varies from the virgin material at 0 to the fractured material at 1 (Kachanov, 1986, p. 2; Riedel, 1987, p. 24). For the isotropic damage theory (cavities and cracks develop equally on all the directions), the damage variable ω is defined as (Kachanov, 1986, pp. 1-5)

$$\omega = \frac{A}{A_0}; 0 \leq \omega \leq 1 \qquad (2.1)$$

where A_0 is the initial undamaged area and A is the damaged area.

Conveniently, the expression 1- ω is denoted as Ψ

$$\Psi = 1 - \omega = \frac{A_0 - A}{A_0}; 0 \leq \Psi \leq 1 \qquad (2.2)$$

To coupling stress with damage, the actual stress (stress to the undamaged area section) σ_a in the uni-axial tension case is

$$\sigma_a = \frac{P}{A_0 - A} = \frac{P}{A_0(1-\omega)} = \frac{P}{A_0 \Psi} = \frac{\sigma}{\Psi} \qquad (2.3)$$

where σ is the nominal stress.

Later on, Rabotnov (1986) believed that the creep strain rate is not only stress-dependent, but also depending on the damage state. The creep strain rate should be (Naumenko & Altenbach, 2007)

$$\dot{\varepsilon} = \dot{\varepsilon}(\sigma, \omega) \qquad (2.4)$$

With the power law function of stress and the damage state, the constitutive equation may have the form as

$$\dot{\varepsilon} = A \frac{\sigma^n}{(1-\omega)^m} \qquad (2.5)$$

where m and n are constants (Naumenko & Altenbach, 2007).

Setting $m = n$, the equation 2.5 can be rewritten as

$$\dot{\varepsilon} = A\sigma_e{}^n \qquad (2.6)$$

where $\sigma_e = \frac{\sigma}{(1-\omega)}$, which is called effective stress (Naumenko & Altenbach, 2007).

According to TWI's report, the cavitation damage is the main reason which leads to a failure of materials eventually at creep damage situation (TWI, 2014). The cavities nucleate and grow during the creep deformation process before fracture. The cavities coalescence finally leads to the fracture of materials. Generally speaking, for metals or alloys, at high stress range, the dislocation creep deformation controls the deformation mechanism; at low stress range, the diffusion creep deformation controls the deformation mechanism (Riedel, 1987).

Depends on the TWI (2014) report, at low stress range, the cavities continuously nucleate around the large precipitates or particles on grain boundaries, and cavities grow constrained by a local creep strain, and eventually cavities coalescence to form a crack. At high stress range, the cavities nucleate both at grain boundary and within the grains; cavities grow by grain boundary sliding or plasticity growth, and the plastic process leads the final failure (TWI, 2014). A brief summary of cavity nucleation and cavity growth is listed as below (Kassner & Perez-Prado, 2004, p. Chapter 10; Riedel, 1987, pp. Chapter11, 12 & 16).

2.4.1 Cavity nucleation

A. Ways of creep cavity nucleation

In metals and alloys, the cavity nucleation theories are classified into three ways: grain-boundary sliding, vacancy condensation and dislocation pile-ups respectively. However, the cavity nucleates by which mechanism is not clear, expect the observation of cavity nucleation sites are around grain boundaries (Kassner & Hayes, 2003; Kassner & Perez-Prado, 2004, pp. 218-222). Figure

2.11 gives a clear description of each cavity nucleation mechanisms. The tensile stress is σ. The arrows in Figure 2.11 indicate the directions of tensile stress and the movement of cavities.
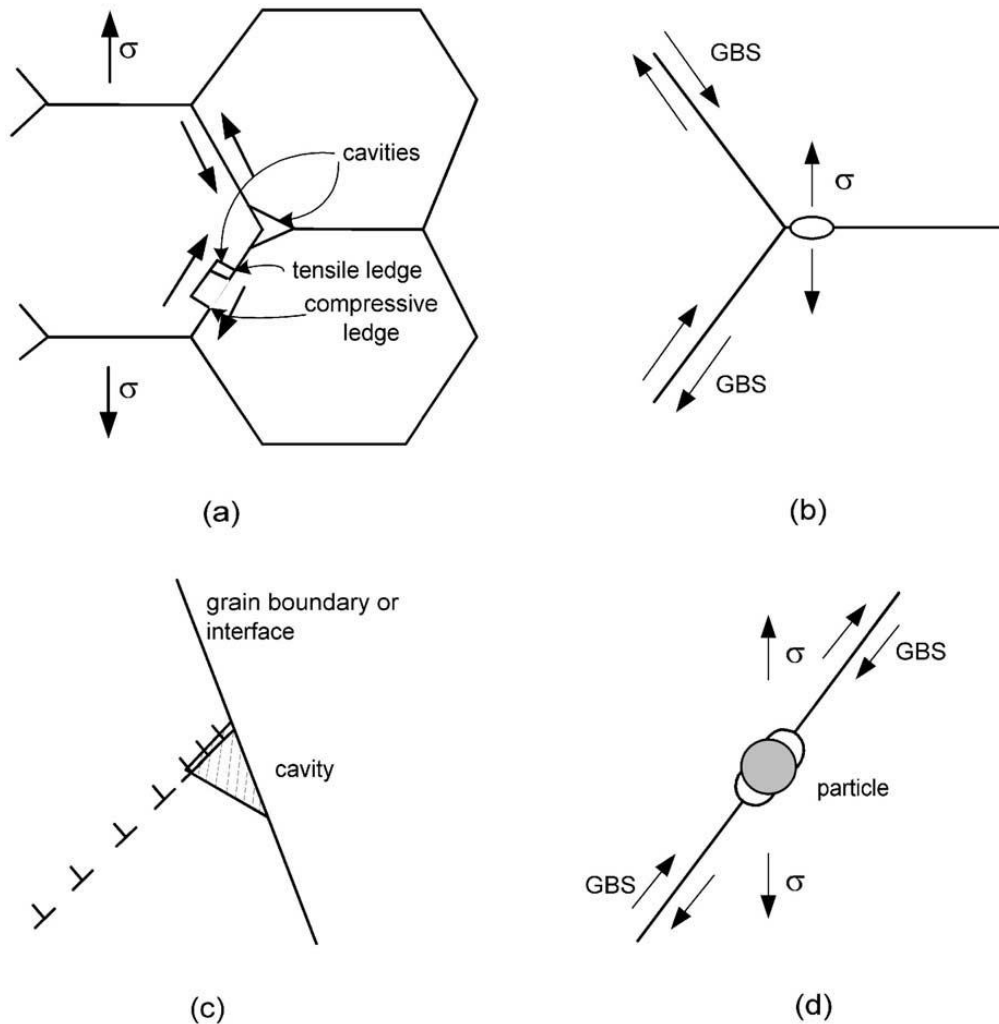
Figure 2. 11: a) grain boundary sliding, b) vacancy condensation; c) dislocation pile-ups; d) formation of a cavity from a particle-obstacle in conjunction with the mechanisms described in (a-c) (Kassner & Hayes, 2003)

In Figure 2.11 (a), grain-boundary sliding leads to a cavitation from ledges (triple points), the formation of voids is located at the head of a boundary or by the tensile grain-boundary ledges. However, the grain-boundary sliding either

accelerates cavities nucleation or cavity growth is vague (Kassner & Hayes, 2003).

In Figure 2.11 (b), vacancy condensation leads to a cavity nucleation, usually at high stress region, especially at the stress concentration area around grain boundary. Normally, the high stress (>10^4MPa) is required (Kassner & Hayes, 2003).

In Figure 2.11 (c), cavity nucleates at the head of dislocation pile-ups. The pile-ups against hard particles might accelerate the nucleation of cavities, but, the cavity might grow slowly than that at grain boundaries (Kassner & Hayes, 2003; Kassner & Perez-Prado, 2004, pp. 218-222).

In Figure 2.11 (d), cavity nucleates from a particle-obstacle in conjunction with the mechanisms of grain boundary sliding, vacancy condensation and dislocation pile-ups (Kassner & Hayes, 2003).

B. Constitutive equations for cavity nucleation

The cavity nucleation rate is classified as time-dependent and time-independent respectively (Kassner & Hayes, 2003; Kassner & Perez-Prado, 2004; Riedel, 1987, p. 232). The time-independent cavity nucleation rate is also well known as the strain rate-dependent cavity nucleation. The related equations are listed as below.

1) Time-dependent cavity nucleation rate $\dot{N}$

$$\dot{N} = A_2 t^\gamma \qquad (2.7)$$

Generally combine with the cavity growth rate $\dot{R}$

$$\dot{R} = A_1 R^{-\beta} t^{-\alpha}$$ (2. 8)

(Riedel, 1987, p. 226)

where A_1, A_2, α, β and γ may possible depend on stress and strain rate, but not on time nor on the cavity size (Riedel, 1987).

2) Time-independent cavity nucleation rate $\dot{N}$

$$\dot{N} = \alpha' \dot{\varepsilon}$$ (2. 9)

(Riedel, 1987, p. 63)

where N is the number of cavities, $\dot{N}$ is the cavity nucleation rate per unit grain boundary, α' is an empirical factor of proportionality (m^{-2}), $\dot{\varepsilon}$ is strain rate.

2.4.2 Ways of creep cavity growth

There are 6 ways of cavity growth reported by Kassner, Hayes and Perez-Prado (2003; Kassner & Perez-Prado, 2004). In summary, cavity growth are controlled by 1) grain boundary diffusion, 2) surface diffusion, 3) grain-boundary sliding, 4) constrained diffusion, 5) plasticity and 6) coupled diffusion and plastic (Kassner & Hayes, 2003; Kassner & Perez-Prado, 2004, pp. 91-96).

A. Cavity growth is controlled by grain boundary diffusion (unconstrained)

Cavity growth in size is controlled by grain boundary diffusion. This cavity growth theory was originally prosed by Hull and Rimmer in 1959 (Kassner & Hayes, 2003). Figure 2.12 illustrates the cavity growth mechanism. The rate of cavity growth is derived from

$$J_{gb} = -\frac{D_{gb}}{\Omega kT}\nabla f \qquad\qquad (2.\,10)$$

$$\nabla f \sim \frac{\Omega}{\lambda_s}\left(\sigma - \frac{2\gamma_m}{\alpha}\right) \qquad\qquad (2.\,11)$$

where J_{gb} is the flux, D_{gb} is diffusion coefficient at grain boundary, Ω is the atomic volume, $f = -\sigma_{loc}\Omega$, σ_{loc} is the local normal stress on the grain boundary, α is the cavity radius, σ is the remote or the applied stress to the grain boundary, λ_s is the cavity separation.

By substituting the sintering stress $\sigma_0 = \frac{2\gamma_m}{\alpha}$ into equations 2.10 and 2.11, the diffusive cavity growth rate $\frac{d_a}{d_t}$ is

$$\frac{d_a}{d_t} \cong \frac{D_{gb}\delta\left(\sigma - \frac{2\gamma_m}{a}\right)\Omega}{2kT\lambda_s a} \qquad\qquad (2.\,12)$$

where δ is the grain boundary width, γ_m is surface energy terms of metal, k is Boltzmann constant, T is temperature (Kassner & Hayes, 2003).

Later on, to improve the unconstrained cavity growth rate, the diffusion lengths, stress redistribution, cavity geometry and the "jacking" effect (atoms deposited on the grain boundary cause displacement of grains) have been considered to modify. The similar improved equation for unconstrained cavity growth rate of widely spaced voids is (Kassner & Hayes, 2003, p. 1729)

$$\frac{d_a}{d_t} \cong \frac{D_{gb}\delta(\sigma - \sigma_0)\Omega}{1.22kT\ln(\lambda_s/4.24a)\alpha^2} \qquad\qquad (2.\,13)$$

where $\alpha = \lambda_s/2$, $\sigma_0 = \frac{2\gamma_m}{\alpha}$.
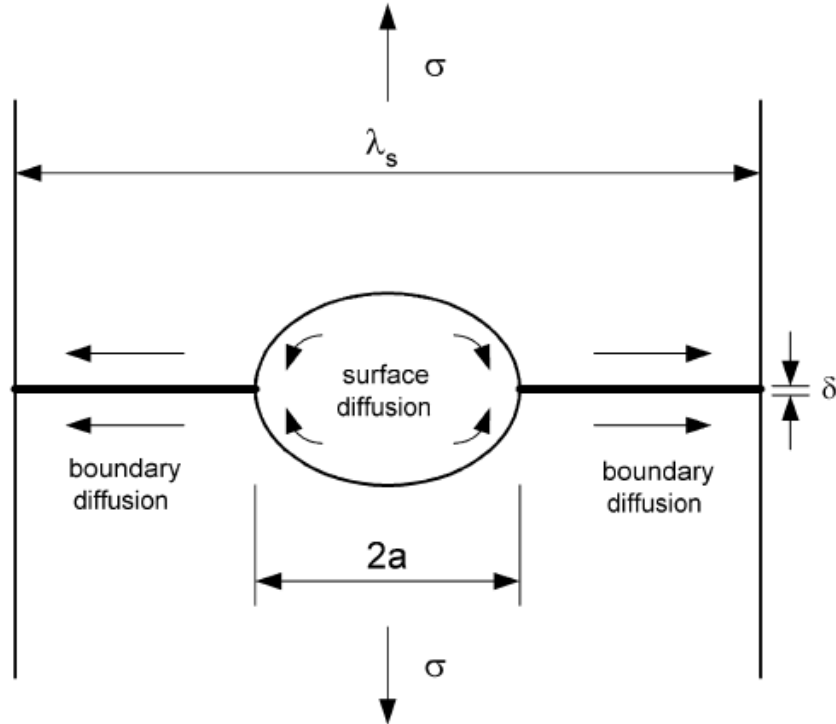
Figure 2. 12: Cavity growth from diffusion across the cavity surface and through the grain boundaries due to a stress gradient (Kassner & Hayes, 2003).

B. Cavity growth is controlled by surface diffusion

Later on, some other researchers argued that the surface diffusion might control the cavity growth rate at low stresses rather than the grain boundary diffusion (Kassner & Hayes, 2003), as it is shown in Figure 2.12. The cavity growth rate of surface diffusion is

$$\frac{da}{dt} \cong \frac{D_s \Omega \delta}{2kT(\gamma_m)^2} \sigma^3 \tag{2. 14}$$

The cavity growth rate is linear with a three-power law stress. However, at high stresses, the three-power relationship varies as $\sigma^{3/2}$. This cavity growth rate in

equation 2.14 is reasonable when the cavity continuous nucleation occurs with strain and the variation of nucleation rate is proper stress dependent.

In summary, whether cavity growth is controlled by grain boundary diffusion or surface diffusion, the relations between cavity growth rate and the applied stress is represented in equations 2.12—2.14. However, these equations are not satisfied with the Monkman-Grant phenomenology with the common five-power creep law. The Monkman-Grant relation suggests that the cavity growth rate should be proportional to the stress with the five-power creep law instead of three-power creep law (Kassner & Hayes, 2003).

C. Cavity growth is controlled by grain boundary sliding

Grain boundary sliding is one of the creep deformation mechanics. Grain boundary sliding is grain size dependent and usually occurs at high temperature (Wadsworth, Ruano, & Sherby, 1998). The shape of grain size usually changes in order to slide pass each other, as shown in Figure 2.13 (Chen, 1983a).

(a)   (b)
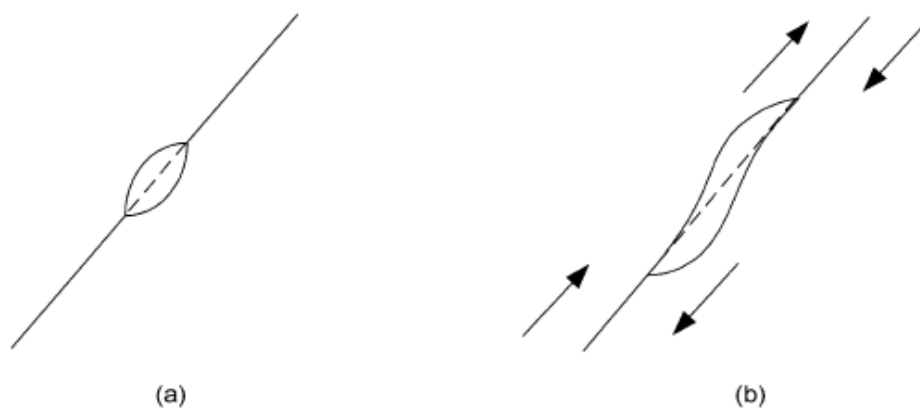
Figure 2. 13: grain boundary sliding in 304 stainless steel (Chen, 1983b)

The shape of a cavity is asymmetric between the two half surfaces at beginning. The grain boundary sliding might be observed at high strain rates and closely spaced cavities (Chen, 1983a). However, it is not clear if grain boundary sliding affects the cavity growth.

D. Cavity growth rate is controlled by constrained diffusion

Dyson in 1976 and 1979 originally proposed the constrained diffusive cavitation mechanism to balance the rate of the volume increased by the diffusive cavitation is compatible with the deformation rate of the surrounding materials (Kassner & Perez-Prado, 2004, p. 230; Riedel, 1987, p. 172). A back stress is exerted on the cavitated grain boundary to adjust that constrained diffusive cavitation (Riedel, 1987, p. 172). The constrained diffusional cavity growth equation is derived from:

The total growth rate of the whole facet by diffusive cavitation is

$$\dot{V}_f = \frac{2\pi^2 d^2 \Omega \delta D_b}{\lambda^2 kT q(\omega)} [\sigma_b - (1-\omega)\sigma_0] \tag{2. 15}$$

where ω is the cavitated area fraction of the boundary, $\omega = (\frac{2R}{\lambda})^2$, σ_0 is the sintering stress of an isolated cavity and is defined as $\sigma_0 = 2\gamma_s sin\Psi/R$, $q(\omega)$ is defined as $q(\omega) = -2\ln(\omega) - (3-\omega)(1-\omega)$, d is the grain size, Ω is atomic volume, λ is the cavity spacing, k is the Boltzmann constant ($k = 1.38 \times 10^{-23} J/K$), δD_b is diffusion constant for the grain boundary diffusion.

The volume growth rate of the facet by creep deformation of the matrix is

$$\dot{V}_f = \dot{\varepsilon}_e^\infty d^3 \left(1 + \frac{3}{n}\right)^{-\frac{1}{2}} (\sigma_I^\infty - \sigma_b)/\sigma_e^\infty \tag{2.16}$$

where σ_I is the initial stress, σ_b is the back stress, σ_e is the effective stress.

The equivalent strain rate is $\dot{\varepsilon}_e^\infty = B(\sigma_e^\infty)^n$ and the applied equivalent stress for axisymmetric loading is $\sigma_e^\infty = |\sigma_I^\infty - \sigma_T^\infty|$.

For compatibility, the volume growth rates by diffusive cavitation should equal to the volume growth rate by the creep deformation. Therefore, by solving the equations 2.15 and 2.16, the back stress is

$$\sigma_b = (1 - \omega)\sigma_0 + \frac{\sigma_I^\infty - (1-\omega)\sigma_0}{1 + 2\Omega\delta D_b q' \sigma_e^\infty / [kTq(\omega)d\lambda^2 \dot{\varepsilon}_e^\infty]} \tag{2.17}$$

The abbreviation $q' = \pi^2(1 + \frac{3}{n})^{1/2}$.

For an axisymmetric, equilibrium cavity, the linear cavity growth rate is

$$\dot{R} = \frac{2\Omega\delta D_b[\sigma_b - \sigma_0(1-\omega)]}{kTh(\psi)q(\omega)R^2} \tag{2.18}$$

By substituting equation 2.17 into equation 2.18, the constrained cavity growth rate is

$$\dot{R} = \frac{\sigma_I^\infty - (1-\omega)\sigma_0}{h(\psi)R^2 \left[\frac{q(\omega)kT}{2\Omega\delta D_b} + \frac{q'\sigma_e^\infty}{\dot{\varepsilon}_e^\infty d\lambda^2}\right]} \tag{2.19}$$

When the creep strain rate is very small, σ_b approximates to the sintering stress σ_0, with $q' = 12.5$ and $h(\psi) = 0.61$. The constrained cavity growth rate becomes

$$\dot{R} = 0.13\dot{\varepsilon}_e^\infty d\left(\frac{\lambda}{R}\right)^2 \frac{\sigma_I^\infty - (1-\omega)\sigma_0}{\sigma_e^\infty} \qquad (2.\,20)$$

To determine whether the cavity growth is constrained or not, the given strain rate should be less than the equivalent creep strain rate. The equivalent creep strain rate is

$$\dot{\varepsilon}_e^\infty = \frac{2q'\Omega\delta D_b\sigma_e^\infty}{q(\omega)kT\lambda^2 d} \qquad (2.\,21)$$

$$\dot{\varepsilon}_e^\infty = B(\sigma_e^\infty)^n \qquad (2.\,22)$$

where n is the steady-state stress exponent, d is the grain size, σ_e^∞ and $\dot{\varepsilon}_e^\infty$ are the steady-state stress and strain rate respectively. The steady-state strain rate is

$$\dot{\varepsilon}_{ss} = A_0 \exp\left[-\frac{Q_c}{kT}\right]\left(\frac{\sigma_{ss}}{E}\right)^n \qquad (2.\,23)$$

If the strain rate (applied stress) is smaller than this critical value of strain rate (back stress), the cavity growth is constrained; reversely, the cavity growth is unconstrained (Riedel, 1987, p. 175).

When cavity growth is constrained, time to calescence was used to identify the failure of materials. The time to coalescence is derived from

The cavitated area fraction $\overline{\omega}$ is obtained by integrating the areas πR^2, occupied by the individual cavities multiplied by their density, NdR

$$\overline{\omega} = \int \pi R^2\, N(R,t)\, dR = I(\alpha,\beta,\gamma)A_2A_1^{2/(\beta+1)}t^{\alpha+\gamma+(1-\alpha)(\beta+3)/(\beta+1)} \quad (2.\,24)$$

The dimensionless factor $I(\alpha,\beta,\gamma)$ is defined as integral

$$I = \pi(1+\beta)^{(\beta+3)/(\beta+1)}\int_0^U x^{\beta+2}[1-(1-\alpha)x^{\beta+1}]^{(\alpha+\gamma)/(1-\alpha)}dx \qquad (2.\,25)$$

with $U = \infty$ if $\alpha > 1$ and $U = ((1 - \alpha)^{-1/(\beta+1)}$ if $\alpha < 1$. Material constants $A_1, A_2, \alpha, \beta, \gamma$ are might stress and strain rate dependent, but in-dependent on the time and cavity size.

When the continuous cavity nucleation is time-independent ($\gamma = 0, \alpha = 1, \beta = 2$), cavity growth is constrained, the time to cavity coalescence on isolated grain boundary facets is

$$t_c = \left[\frac{3\pi\left(1+\frac{3}{n}\right)}{J^*}\right]^{\frac{1}{3}} * \left(\frac{\sigma_e^\infty}{\sigma_I^\infty} * \frac{h(\varphi)}{\dot{\varepsilon}_e d}\right)^{\frac{2}{3}} * \frac{\omega_f}{2\Gamma(\frac{2}{3})} \qquad (2.26)$$

If the cavity nucleation is creep strain-controlled, i.e. $\dot{N} = \alpha' \dot{\varepsilon}$. The time to coalescence is

$$\dot{\varepsilon} t_c = \frac{(5\pi)^{1/3} * (0.61)^{\frac{2}{3}} * \omega}{(\alpha')^{1/3} * (d)^{\frac{2}{3}} * 2.708} = 0.6652 * (\alpha' * d^2)^{-\frac{1}{3}} * \omega \qquad (2.27)$$

with constants $n = 4.5, \frac{\sigma_e^\infty}{\sigma_I^\infty} = 1, h(\varphi) = 0.61, \Gamma\left(\frac{2}{3}\right) = 1.354$ (Riedel, 1987).

The constrained diffusional cavity growth with continuous cavity nucleation was represented by Riedel (1987) in his book chapters 11, 12, 16 and 17. He pointed out that the time to coalescence is no big difference whether the cavity is continuous or instantaneous with the constrained cavity growth mechanism, if the cavitated area at failure $\omega_f = \frac{\pi}{4}$ (Riedel, 1987). The lifetime of materials predicted by constrained cavity growth mechanism is questionable. The predicted constrained cavity growth rate is much smaller than cavity nucleation rate.

E. Cavity growth is controlled by plasticity

The cavity growth rate is

$$\frac{dr}{dt} = r\dot{\varepsilon} - \frac{\gamma}{2G}$$

(2. 28)

This plasticity model is not well understood so far. This model only suits for the high strain rate conditions at creep deformation which is consistent with the plasticity growth of materials (Kassner & Hayes, 2003).

F. Cavity growth rate is controlled by coupled diffusional and plasticity

The coupling between diffusional and plastic growth theory was suggested by many researchers (Kassner & Hayes, 2003). The illustration of coupled cavity growth is shown in Figure 2.14. The coupling is shown in Figure 2.15. In Figures 2.14 and 2.15, λ is cavity spacing, Λ is diffusion length, a is cavity radius.
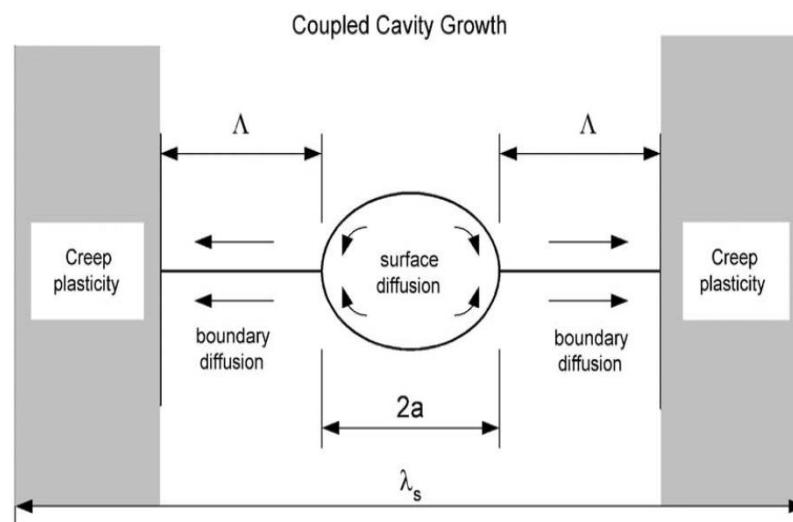
Figure 2. 14: The model for coupled diffusive cavity growth with creep plasticity. The diffusion length is suggested to be reduced by plasticity ahead of the cavity (Kassner & Hayes, 2003)
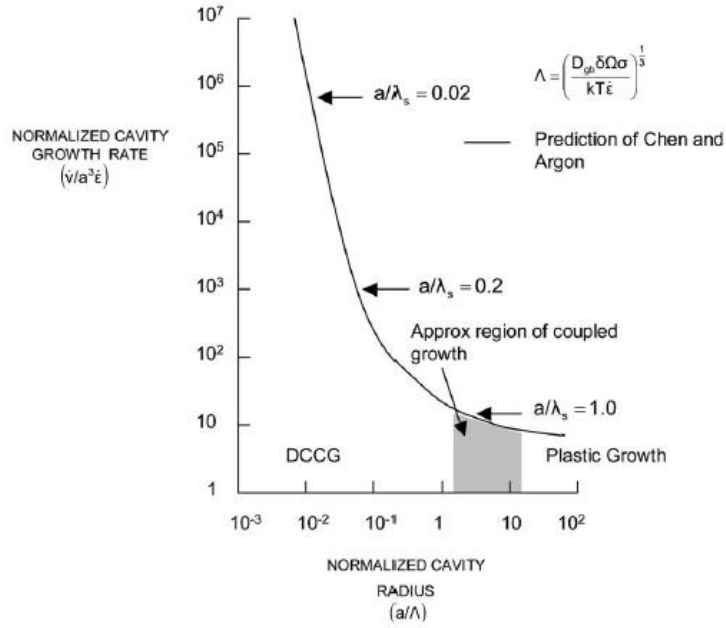
Figure 2. 15: Prediction of growth rate for different ratios of cavity spacing λ and diffusion zone sizes Λ (Kassner & Hayes, 2003)

When $\Lambda << a \ and \ \lambda_s$, the growth by diffusion is not applicable anymore at low temperature situation. At high temperature situation, when the creep strain rate is very small, $\Lambda \cong \frac{\lambda_s}{2}$, the normalized cavity radius α/Λ is relatively small, the diffusional-controlled cavity growth takes the domination. As Figure 2.15 shows, if the ratio of α/Λ in the middle value, the coupled diffusional and plastic growth were considered. The diffusion length Λ is

$$\Lambda = (\frac{D_{gb}\Omega\delta\sigma}{kT\dot{\varepsilon}})^{1/3} \tag{2. 29}$$

The coupling between diffusional and plastic growth is

$$\frac{dV}{dt} = \dot{\varepsilon}2\pi\Lambda^3/[\ln\left(\frac{a+\Lambda}{a}\right) + \left(\frac{a}{a+\Lambda}\right)^2 * \left(1 - \frac{1}{4}\left(\frac{a}{a+\Lambda}\right)^2\right) - \frac{3}{4}] \tag{2. 30}$$

67

For pure metals, the influence of plasticity is important only for $\frac{\sigma}{G} > 10^{-3}$ at high stress range when the temperature $T > 0.5T_m$. Riedel (1987) suggested using the diffusive growth mechanism for the whole creep test.

2.4.3 Dyson's cavitation damage theory

In Dyson's (1988, 2000) articles, the cavitation damage theory is classified into three types. The first type of cavitation damage theory is called thermally induced damage. Thermally induced damage includes the influence of coarsening and solute depletion. The second type of cavitation damage theory is called environmentally induced damage. Environmentally induced damage includes the influence of corrosion and oxidation. The third type of cavitation damage theory is called strain-induced damage. Strain-induced damage includes the influence of grain boundary cavitation, dynamic sub-grain coarsening and mobile dislocation multiplication.

The strain-induced cavitation damage theory is also classified into two types of cavity damage mechanisms. The first type of cavity damage mechanism is named constrained cavity nucleation controlled cavity damage mechanism. The constrained cavity nucleation controlled creep damage mechanism assumes that the cavity continuously nucleates throughout the creep deformation and damage process. The second type of cavity damage mechanism is named constrained cavity growth controlled creep damage mechanism. The constrained cavity growth controlled cavity damage mechanism assumes that an amount of cavities

are nucleated at the beginning and then certain number of cavities grows until fracture.

The creep damage variables D_N and D_G are proposed to describe the cavity nucleation damage mechanism and cavity growth damage mechanism respectively. The related equations of damage parameter, damage rate and strain rate at different cavitation damage mechanisms are listed as below (Dyson, 1988, 2000).

1) Cavitation damage is controlled by constrained cavity nucleation

The dimensionless damage parameter D_N indicates the area fraction of grain boundary facets cavitated. When cavity evolution is growth controlled, the rate of cavity nucleation is $\dot{D}_N = 0$. When cavities continuously nucleates, the evolution of D_N is

$$\dot{D}_N = \frac{K_N}{\varepsilon_{fu}}\dot{\varepsilon} \qquad (2.\ 31)$$

where K_N has an upper limit of $\approx \frac{1}{3}$ when all transverse boundaries are cavitated, ε_{fu} is the uniaxial strain at fracture.

The effect of continuous cavitation nucleation damage is to reduce the load-bearing area by $(1 - D_N)$. Therefore, the stress in the equation of creep strain rate becomes $\frac{\sigma}{(1-D_N)}$. The creep strain rate at any instant is

$$\dot{\varepsilon} = \dot{\varepsilon}_0 \mathrm{sinh}(\frac{\sigma}{\sigma_0(1-D_N)}) \qquad (2.\ 32)$$

where $\dot{\varepsilon}_0$ is a temperature creep parameter at the arbitrary normalizing stress σ_0 (Dyson, 1988, 2000).

2) Cavitation damage is controlled by constrained cavity growth

The dimensionless damage parameter D_G indicates the volume fraction of grain boundary facets cavitated. When cavity evolution is growth controlled, the rate of cavity nucleation is

$$\dot{D}_G = \frac{d}{2lD_G}\dot{\varepsilon} \qquad (2.\ 33)$$

where l is the inter-cavity spacing, d is the grain size (Dyson, 1988, 2000).

According to Dyson (1988, 2000), the effect of cavitation growth damage is same as the cavitation continuous nucleation damage to reduce the load-bearing area by $(1 - D_G)$. The stress in the equation of creep strain rate becomes $\frac{\sigma}{(1-D_G)}$. The creep strain rate at any instant is

$$\dot{\varepsilon} = \dot{\varepsilon}_0 \sinh(\frac{\sigma}{\sigma_0(1-D_G)}) \qquad (2.\ 34)$$

where $\dot{\varepsilon}_0$ is a temperature creep parameter at the arbitrary normalizing stress σ_0 (Dyson, 1988, 2000).

2.5 Classical creep constitutive equations models within continuum damage mechanics

From literature review research, creep damage constitutive equations are proposed to depict the behaviours of materials during a creep damage (deformation and rupture) process within the framework of continuum damage mechanics. Constitutive equations are required to reflect the time-dependent creep deformation process, such as hardening/recovery effect and damage process. However, from simple phenomenological to complex constitutive, the majority of the creep constitutive equations models are used to present the creep strain and creep rupture ductility behaviours of materials (Holdsworth & Merckling, 2003).

Generally speaking, there are two relationships which are used to predict the rupture lifetime of materials. They are Monkman-Grant relationship $(\dot{\varepsilon}_{min} t_r = k)$ and Larson-Miller parameter/relation $LM = T(log t_r + C_{LM})$. Monkman-Grant is more popular than the latter equation. Monkman-grant relationship describes the relation between minimum creep strain rate $\dot{\varepsilon}_{min}$ and failure time t_r of materials with a material constant k. The minimum creep strain rate is inversely proportional to the rupture time of materials in Monkman-Grant relationship. In Monkman-Grant relationship, it also clarifies minimum creep strain rate controlled-creep deformation and damage process of materials (Dunand, Han, & Jansen, 1999; Sundararajan, 1989).

Larson-Miller parameter/relation is used to extrapolation experimental data on creep and rupture life of engineering materials. Larson-Miller relation is stress

independent. Larson-Miller relation relates the differences in rupture time to differences in temperatures at a certain stress, i.e. Larson-Miller parameter describes the equivalence time at a temperature at the thermally activated creep stress rupture process. T is the temperature in degrees Rankine (°F + 460); t_r is the rupture time in hours; C_{LM} is the material constants factor $C_{LM} \cong 20$ for low alloy steels or C-Mn materials; $C_{LM} = 30$ for the high alloy steels 9%Cr (TWI, 2015). However, LM parameter is used for short-term tests, and not applicable for the primary and secondary creep stages.

Within the CDM theory, the creep damage mechanism is divided into three categories which were proposed by Dyson (1988, 2000). These three creep damage categories are 1) loss of external section—the stress increases progressively due to the deceasing of the cross seaction area; 2) microstructral degradation; and 3) loss of internal section—this is well known as the cavitation damage which leads to the inter-granular fractures along the grain boundary. The detailed creep damage categories and mechanims are listed in Table 2.3 (Dyson, 1988). The definition of symbols in Table 2.3 are listed in Table 2.4.

In addition, the development of creep strain-controlled creep deformation constitutive equaions are listed in Table 2.5 (Holdsworth et al., 2008; Holdsworth & Merckling, 2003). The definition of the symbols in Table 2.5 is given in Table 2.6. As Table 2.5 shows, the relation between creep strain rate and stress was identified as power law originally. Until Dyson's model, the power law relation has been replaced by the hyperbolic law in order to compensate the inconvience of using power law. Besides, except the classical power law and hyperbolic law,

there are also theta and omega relations. The theta projection concept was used to extrapolate short term data to long term data. The theta projection only works under constant stress and temperature conditions. The theta projection also requires at least 17 material paramters to predict the material behaviours. The omega relations are suggested for the thermally induced damage conditions (Dyson, 2000).

Table 2. 3: Creep damage categories and mechanisms (Dyson, 1988, 2000)

Creep damage category	Mechanism	Damage parameter ω	Damage evolution rate $\dot{\omega}$	Strain rate $\dot{\varepsilon}$	$C_m = \dot{\varepsilon}_i t_f$	ε_f	$\lambda = \frac{\varepsilon_f}{C_m}$
					$\omega_f = 1$		
Loss of external section	Uniform straining under constant load	$1 - \dfrac{A}{A_i}$	$\dot{\varepsilon}_i[\dfrac{1}{1-\omega}]^{n-1}$	$\varepsilon_i[\dfrac{1}{1-\omega}]^n$	$\dfrac{1}{n}$	$\propto$	$\propto$
	Periodic failure of corrosion-product	$\dfrac{2X}{R}$	$\varepsilon_i[\dfrac{1}{1-\omega}]^n$	$\varepsilon_i[\dfrac{1}{1-\omega}]^n$	Not applicable to large ω		
Microstructural degradation	Thermal coarsening of particles	$1 - \dfrac{S_i}{S}$	$(1-\omega)^4\dfrac{K'}{3}$	$\dot{\varepsilon}_{ip}[1 + K^n\omega]^n$	$\propto$	$\propto$	$\propto$
	Instability of the dislocation substructure	$1 - \dfrac{\rho_i}{\rho}$	$C\dot{\varepsilon}_i$	$\dot{\varepsilon}_i[1-\omega]^{-1}$	$\dfrac{1}{C}$	$\propto$	$\propto$
Loss of internal section	Environmentally-induced damage	$\dfrac{2X}{R}$	$\dfrac{2K}{R^2\omega}$	$\dot{\varepsilon}_i[\dfrac{1}{1-f_\omega}]^n$	Not applicable to large ω		
	Cavity growth by grain boundary diffusion	$(\dfrac{r}{l})^2$	$\dot{\varepsilon}_{ig}\dfrac{d}{2l\omega^{1/2}}\dfrac{ln1/\omega_i}{ln1/\omega}$	$\dot{\varepsilon}_{ig}\dfrac{ln1/\omega_i}{ln1/\omega}$	$-\dfrac{4}{3}\dfrac{1}{d}$	$-\dfrac{8}{3}\dfrac{1}{d}$	-2
	Cavity nucleation with creep-constrained growth	F	$\dot{\varepsilon}_{in}[\dfrac{1}{1-k\omega}]^m$	$\dot{\varepsilon}_i[\dfrac{1}{1-k\omega}]^n$	$\dfrac{\dot{\varepsilon}_i[1-(1-k)]}{(n+1)\dot{\omega}_i}$	$\dfrac{k\dot{\varepsilon}_i}{\dot{\omega}_{in}}$	-2

Table 2. 4: Definitions of symbols in Table 2.3 (Dyson, 1988, 2000)

D: Dame parameter, subscripts indicate specific mechanism
ρ: dislocation density, subscript i denotes initial value
P: particle spacing, i denotes initial value
K_p: Rate constant for particle coarsening
$\bar{C}_t$: Mean concentration of W/Mo in matrix at time t
C_0: Concentration of W/Mo in matrix at $t = 0$
K_s: Rate constant for precipitated particles
X: Thickness of oxidising/corroding phase
K_c: Rate constant for surface corrosion product
ε^*: Strain required to fracture corrosion product
K_{ox}: Rate constant for internal oxidation
N: Number density of cavitated grain boundary facets
R: Radius of test piece or component
r_{sg}: Subgrain radius; subscript i denotes initial value
K_N: Cavitation constant ≤1/3
$\varepsilon_{f,u}$: Uni-axial strain at fracture
l: Intercavity spacing
r: Cavity radius
T: Temperature
σ: Uni-axial stress

Table 2. 5: Creep strain equations (Holdsworth & Merckling, 2003)

Norton	$\dot{\varepsilon}_{f,min}=a_1 * \exp\left(\frac{Q}{RT}\right) * \sigma^n$
Modified Norton	$\dot{\varepsilon}_{f,min}=b_1 * \exp\left(\frac{Q_B}{RT}\right) * \sigma^n + c_1 * \exp\left(\frac{Q_C}{RT}\right) * \sigma^n$
Norton-Bailey	$\varepsilon_f = d_1 \sigma^n t^p$
Bartsch	$\dot{\varepsilon}_f = e_1 * \exp\left(\frac{Q_1}{RT}\right)\sigma * \exp(b_1\sigma)t^p + e_2 * \exp\left(\frac{Q_2}{RT}\right)\sigma * \exp(b_2\sigma)t$
Garofalo	$\varepsilon_f = \varepsilon_1[1 - \exp(-b_1 t)] + \dot{\varepsilon}_{f,min}t$
Modified Garofalo	$\varepsilon_f = \varepsilon_n\left[1 - \exp\left(-g_1(\frac{t}{t_{12}})^u\right)\right] + \dot{\varepsilon}_{f,min}t + c_{23}(\frac{t}{t_{23}})^f]$
BJF	$\varepsilon_f = n_1[1 - exp(-\underline{t})]^\beta + n_2\underline{t}$, where, $\underline{t}=(\sigma/A_1)^{n} * \exp(-\frac{Q}{RT})$
Theta	$\varepsilon_f = \theta_1[1 - \exp(-\theta_2 t)] + \theta_3[1 - \exp(\theta_4 t) - 1]$, where, $\log(\theta_t)=a_i + b_i T + c_i\sigma + d_i\sigma T$
Modified Theta	$\varepsilon_f = \theta_1[1 - \exp(-\theta_2 t)] + \theta_m t + \theta_3[1 - \exp(\theta_4 t) - 1]$, where, $\theta_m = A\sigma^n\exp(-\frac{Q}{RT})$
Rabotnov-Kachanov	$\dot{\varepsilon}=\frac{h_1\sigma^n}{(1-\omega)}$ $\dot{\omega}=\frac{k_1\sigma^v}{(1-\omega)^\zeta}$
Dyson & McClean	$\dot{\varepsilon}_f = \dot{\varepsilon}_o'*(1+D_d)\exp\left(\frac{Q}{RT}\right)\sinh(\frac{\sigma(1-H)}{\sigma_0(1-D_p)(1-\omega)})$
IMechE	$R_{u/t/T}=(a_1 + \frac{b_1}{\varepsilon} - c_1\varepsilon^2)R_{\varepsilon/t/T} + d_1 + \frac{e_1}{\varepsilon} + \frac{f_1}{\varepsilon^2} - g_1\varepsilon^2)$
Bolton	$\varepsilon_f(\sigma)= \varepsilon(R_{u/t/T}/R_{\varepsilon/t/T}\text{-}1)/(R_{u/t/T}/\sigma\text{ -}1)$
Omega	$\dot{\varepsilon}_f = \dot{\varepsilon}_{f,min}/(1\text{-}\dot{\varepsilon}_{f,min}\Omega t)$

Table 2. 6: Definitions of the symbols in Table 2.5 (Holdsworth & Merckling, 2003)

n: stress exponent

p: time exponent
Q: Activation energy for creep
R: Universal gas constant
R$_{u/t/T}$, R$_{u/t/T}$: Creep strength and rupture strength for a given time and temperature
T: time
t_u, $t_{u,max}$: observed time to rupture, maximum observed time to rupture
ω,$\dot{\omega}$: damage, rate of damage accumulation
ε, $\dot{\varepsilon}$, $\dot{\varepsilon}_{f,min}$: creep strain, creep strain rate, minimum creep strain rate
θ_1, θ_2, θ_3, θ_4: constants in Theta equation
θ_m: additional constant in modified Theta equation σ, σ_0: stress, initial stress

2.6 The development of KRH constitutive equations

2.6.1 Kachanov-Rabotnov theory

Kachanov proposed a new damage variable to describe the internal damage process of materials in 1958 (Kachanov, 1986; Murakami, 2012, pp. 218-233). Later on, Kachanov's constitutive equation was modified by Rabotnov in 1969 for the uni-axial tension case study. In Kachanov-Rabotnov theory, the uni-axial form of single state variable of the creep constitutive equations with the damage evolution equation are given as (Murakami, 2012, p. 218)

$$
\begin{cases}
\dot{\varepsilon}^c = B\dfrac{\sigma^n}{(1-D)^q} \\
\dot{D} = A\dfrac{\sigma^m}{(1-D)^p}
\end{cases}
\tag{2.35}
$$

where m, n, p, q, A and B are material constants. D, σ and $(\dot{\ })$ are the damage variables, stress and the differentiation with respect to the time t respectively. The relation between creep strain rate and the applied stress is power law.

In terms of multi-axial stress state, the uni-axial form of single variable creep constitutive equations can be extended to (Murakami, 2012)

$$
\begin{cases}
\dot{\varepsilon}_{ij}^c = \dfrac{3}{2}B\dfrac{\sigma_{EQ}^n}{(1-D)^q}\dfrac{\sigma_{ij}^D}{\sigma_{EQ}} \\
\dot{D} = A\dfrac{\chi^m}{(1-D)^p} \\
\chi(ij) = \alpha\sigma_1 + \beta\sigma_{EQ} + 3(1-\alpha-\beta)\sigma_H
\end{cases}
\tag{2.36}
$$

where $\chi(ij)$ denotes the damage stress criterion for creep rupture, α and β are material constants. σ_1 and σ_{EQ} are the maximum stress and equivalent stress respectively. The hydrostatic stress is $\sigma_H = (\frac{1}{3})\sigma_{kk}$. The deviatoric stress tensor is

$\sigma_{ij}^D = \sigma_{ij} - (\frac{1}{3})\sigma_{kk}\delta_{ij}$.

The multi-axial stress state form of Kachanov-Rabotnov single variable creep constitutive equations are also rewritten by Hyde, Becker, Sun and Williams (2006a)

$$
\begin{bmatrix}
\dot{\varepsilon}_{ij}^c = \frac{3}{2}\frac{S_{ij}}{\sigma_{eq}}A'(\frac{\sigma_{eq}}{1-\omega})^n t^m \\
\dot{\omega} = B'\frac{\sigma_r^x}{(1-\omega)^\emptyset}t^m \\
\sigma_r = \alpha\sigma_1 + (1-\alpha)\sigma_{eq}
\end{bmatrix}
\tag{2.37}
$$

where A', B', n, m, x, $\emptyset$ and α are material constants. The constant α is related to the multi-axial stress state behaviour of materials. σ_1, σ_{eq} and σ_r are the maximum principal stress, equivalent stress and rupture stress respectively. ω is the damage variable, which varies from 0 to 1 (0< ω<1). The hydrostatic stress is related to the volume change of materials. The hydrostatic stress does not cause the plastic deformation. The hydrostatic stress is ignored to the fracture of materials at the creep condition.

2.6.2 Kachanov-Rabotnov-Hayhurst theory

Afterwards, the Kachanov-Rabotnov constitutive equations were modified again by Leckie and Hayhurst in 1974 and 1977, especially used for the multi-axial stress state condition within the continuum damage mechanism (Liu & Murakami, 1998). The hyperbolic law replaces the power law relation between the creep strain rate and the applied stress. The modified constitutive equations are recorded here as Kachanov-Rabotnov-Hayhurst theory for multi-axial stress state condition. In this project, the Kachanov-Rabotnov-Hayhurst theory is simplified as KRH constitutive equations. The uni-axial form of three variables KRH constitutive equations are (Evans & Wilshire, 1993; Hyde et al., 2006a)

$$\left[\begin{array}{l} \dot{\varepsilon} = A \sinh(\dfrac{B\sigma(1-H)}{(1-\varphi)(1-\omega)}) \\[2mm] \dot{H} = \dfrac{h}{\sigma}\left(1 - \dfrac{H}{H^*}\right)\dot{\varepsilon}_c \\[2mm] \dot{\varphi} = \dfrac{K_C}{3}(1-\varphi)^4 \\[2mm] \dot{\omega} = D\dot{\varepsilon}_c \end{array}\right. \qquad (2.38)$$

The multi-axial form of three variables KRH constitutive equations are (Evans & Wilshire, 1993; Hyde et al., 2006a)

$$\left[\begin{array}{l} \dot{\varepsilon}_{ij} = \dfrac{3}{2}\dfrac{S_{ij}}{\sigma_{eq}} A \sinh(\dfrac{B\sigma(1-H)}{(1-\omega_2)(1-\varphi)}) \\[2mm] \dot{H} = \dfrac{h}{\sigma_{eq}}\left(1 - \dfrac{H}{H^*}\right)\dot{\varepsilon}_c \\[2mm] \dot{\varphi} = \dfrac{K_C}{3}(1-\varphi)^4 \\[2mm] \dot{\omega}_2 = DN\dot{\varepsilon}_c\left(\dfrac{\sigma_1}{\sigma_{eq}}\right)^\nu \end{array}\right. \qquad (2.39)$$

where $N = 1, \sigma_1 > 0\ (tensile); N = 0, \sigma_1 < 0\ (compressive)$. $A, B, h,\ H^*,\ K_c$ and D and ν are material constants, where ν is the index of multi-axial stress state of materials. The damage variable $H\ (0 < H < H^*)$ indicates the strain hardening effect during primary creep stage. The value of H increases from 0 until the maximum value H^* from primary creep stage to secondary creep stage. The damage variable φ indicates the evolution of the spacing of the carbide precipitates. The damage variable φ varies from 0 to 1 $(0 < \varphi < 1)$. The damage variable ω_2 represents the inter-granular cavitation damage. The value of the damage variable ω_2 indicates the cavitated area fraction of cavitation damage at failure, which in uni-axial case $\omega_2 \cong \frac{1}{3}$; in multi-axial stress state case, $\omega_2 \cong 1$ (Hyde et al., 2006a).

The stress ranges depends on the different materials, different temperatures. In the original Kachanov-Rabotnov model, the relationship between creep strain

rate and stress was identified as power law with a stress exponent n (Kachanov, 1986). At different stress levels, the tress exponent n is varies from high stress range to low stress range. In terms of the definition of stress range, the previous research work has only classified into high stress range and lower stress range.

In the current research project, the districts of stress ranges are high, transition and low stress range respectively for high chromium alloy steel P91 under 600^0C. For instance, the stress district is divided into three regions—low stress range, transition stress range and high stress range respectively. The stress exponent $n = 1$ at low stress range; $n = 4\ or\ 5$ at the transition stress range and $n > 10$ at high stress range respectively for high chromium alloy steel P91 under 600^0C (Chen et al., 2011).

The accuracy of applying the KRH constitutive equations at lower stress range is doubtable by the extrapolation method from high stress range to lower stress range. The inconvenient of Kachanov-Rabotnov constitutive equations is the changing of stress exponent n at different stress ranges. In order to avoid this, the relationship between creep strain rate and stress was modified by hyperbolic law. In Kachanov-Rabotnov-Hayhurst model, the hyperbolic law has been widely accepted to compensate the disadvantages of power law function. At high stress range, the KRH constitutive equations could accurately predict the life span of materials. However, at lower stress range, the life span of materials has been over-estimated by the extrapolation method from high stress range to lower stress range. Many researchers have also supported this point of view, such as (Xu, 2000, 2001; Xu & Barrans, 2003; Xu, Wright, & Xu, 2011). Simply, the

hyperbolic law was blindly adopted because of the differences of creep deformation and cavitation damage mechanisms at different stress ranges. Thus, the predicting result of materials' life span is questionable.

2.7 Experimental data classification and analysis for high chromium alloy steel P91 and weldment

Temperature and stress are two main factors to affect the creep deformation and damage mechanism (Perrin & Hayhurst, 1996b; Zhang & Zhou, 2009). In this section, the current project tries classify the experimental data at different stress ranges and different temperatures. According to the classification of the experimental data, the current project tries to analyse the influence of stress and temperature on the fracture of parent materials and weldment.

The special existing uni-axial creep testing data of high chromium alloy steel P91 and its weldment will be represented in the following sections, based on the previous research and NRIM creep dataset No.43 (Besson et al., 2009; Eggeler et al., 1994; Hyde et al., 2006b; National research institute for metals, 1996; Ogata, Sakai, & Yaguchi, 2010b, 2010c; Sawada et al., 2011; Shu, Zhao, Xue, Zhang, & Zhang, 2010; Ule & Nagode, 2007; Vivier et al., 2010)

2.7.1 Creep curves under constant load and constant stress
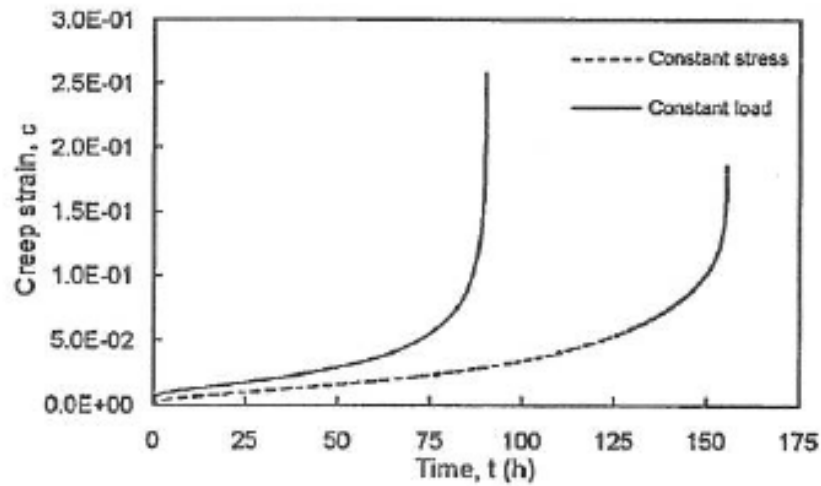
Figure 2. 16: Creep strain and rupture time in the constant-load and constant stress creep tests at 180MPa and under 625°C (Nagode, Ule, Jenko, & Kosec, 2007)
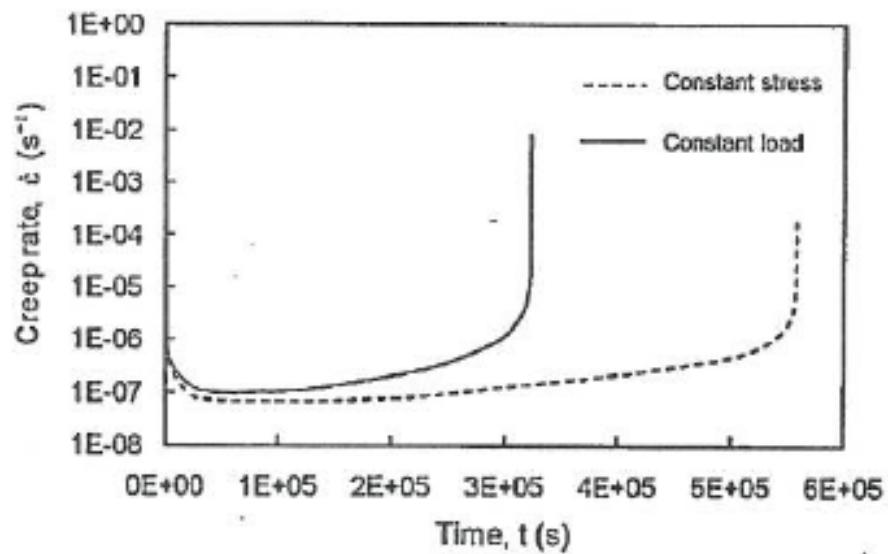
Figure 2. 17: Creep strain rate in the constant-load and constant stress creep tests at 180MPa and under 625°C (Nagode et al., 2007)

Figure 2.16 and Figure 2.17 show the creep strain rate and the minimum strain rate for high chromium alloy steel P91 at 180MPa under 625°C. As it can be seen that the minimum creep strain rate is smaller, the life span of materials is

longer at the constant stress condition. The creep strain rate at constant stress is about 2 times smaller than the creep strain rate at the constant load. The life span of materials at constant load is two times shorter than the life span at constant stress. The influence of the stress (constant load condition) on failure of materials is higher than the influence of the load (constant stress condition).

2.7.2 Creep curves under different stress levels and different temperatures
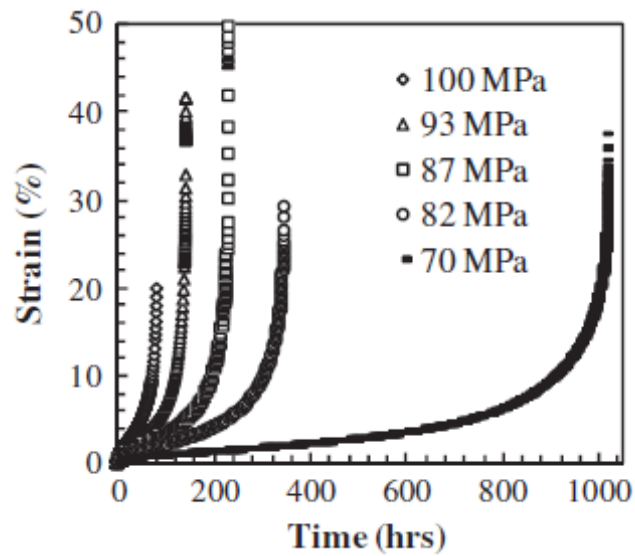
Figure 2. 18: Uni-axil creep data for high chromium alloy steel P91 PM under 650°C (Hyde et al., 2006a)
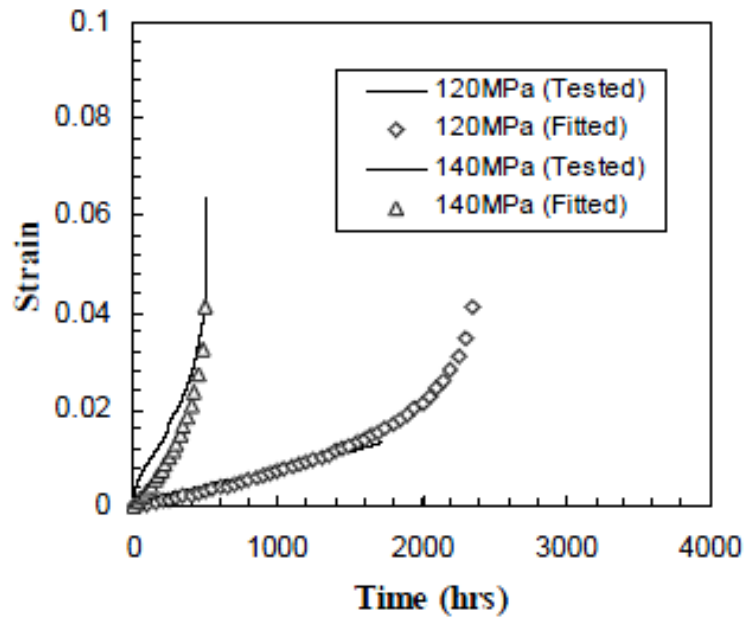
Figure 2. 19: Uni-axial creep data for P91 WM under 625°C (Hyde, Saber, & Sun, 2010b)
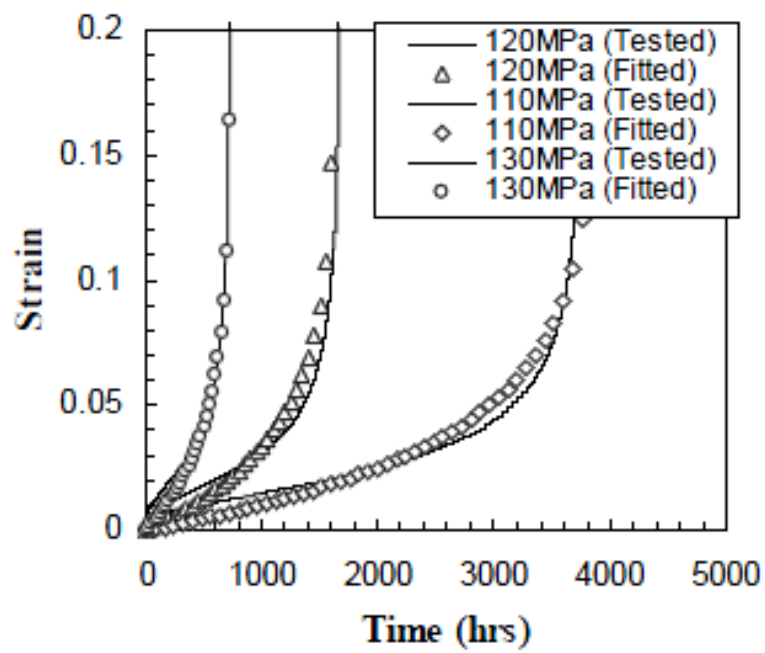
Figure 2. 20: Uni-axial creep data for P91 WM under 625°C (Hyde et al., 2010b)
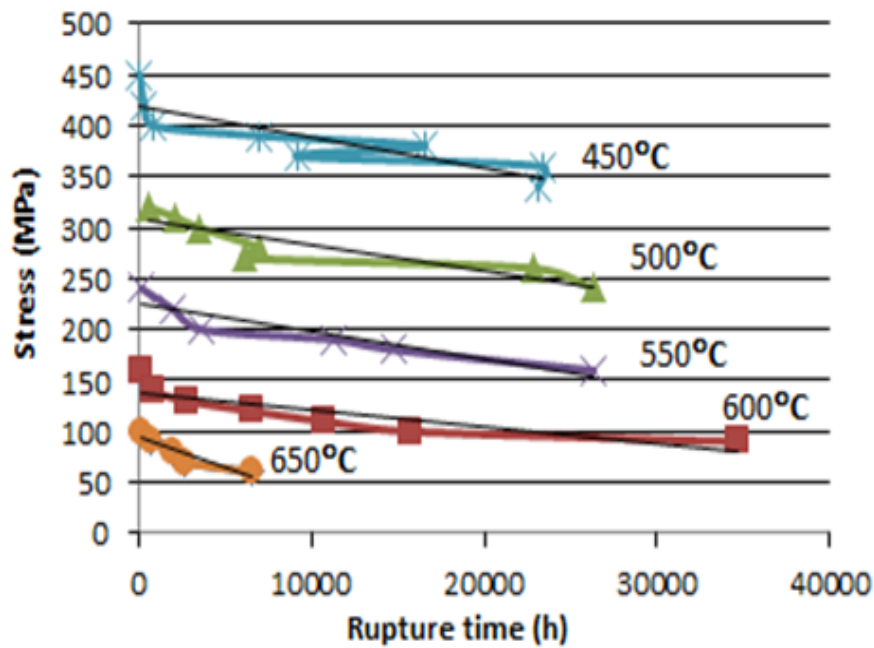
Figure 2. 21: Rupture time at different stress levels and different temperature, data from (National research institute for metals)

For high chromium alloy steel P91 parent materials, Figure 2.18 shows the creep strain curves at different stress levels 70—100MPa under 650^0C. In Figure 2.18, the creep strain at failure varies from 20% to 50%. It seems that there is no trend of the creep strain at failure at different stress levels. However, the current researcher argues that the stress 87MPa might be a boundary stress between high stress range and transition stress range for high chromium alloy steel P91 under 650^0C. For instance, if stress 87MPa is the critical value between high stress range and transition stress range, there is a decreasing trend with stress increases at the high stress range (left side) and a decreasing trend with stress decreases at the transition stress range (right side). However, according to Dyson's cavitation damage theory ($\omega = \frac{1}{3}$ at uni-axial stress), the current researcher argues that creep strain at failure could be simplified as a constant

within the same stress range. However, from high stress range to lower stress range, the creep strain at failure increases. For instance, for high chromium alloy steel P91 weldment under 625^0C, Figure 2.19 and Figure 2.20 show the creep strain curves at the high stress range. The values of creep strain at failure in both figures could be assumed as a constant.

NRIM creep data sheet reported the experimental data of 9Cr-IMo-V-Nb steel tubes (T91) and steel plates and pressure vessels (P91) (National research institute for metals). There were three NRIM reference codes---MgA, MgB and MgC had been used to record the creep data at different temperatures 450°C, 500°C, 550°C, 600°C and 650°C (National research institute for metals). Take the reference code MgB into account in the current research, the influence of stress and temperature is shown in Figure 2.21, experimental data obtained from NRIM data sheet No.43 (National research institute for metals).

In Figure 2.21, the rupture time decreases against with stress increases. In the other words, under a constant temperature, the higher the stress is, the shorter the life span will be. In addition, assumes if the rupture time is a constant, at higher temperature, the applied stress is smaller than the stress applied into a lower temperature. The temperature also has influence on the failure of materials. If stress is constant, the higher temperature is, the shorter life span will be.

2.7.3 Creep curves in base metal (BM), inter-critical heat-affect-zone (IC-HAZ) and weld metal (WM)
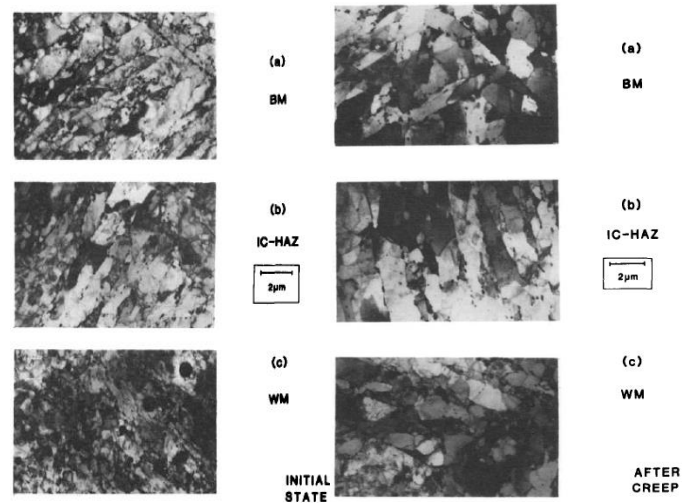
Figure 2. 22: Transmission electron micrographs for BM, IC-HAZ and WM, before creep (left); after creep (right) (Eggeler et al., 1994)
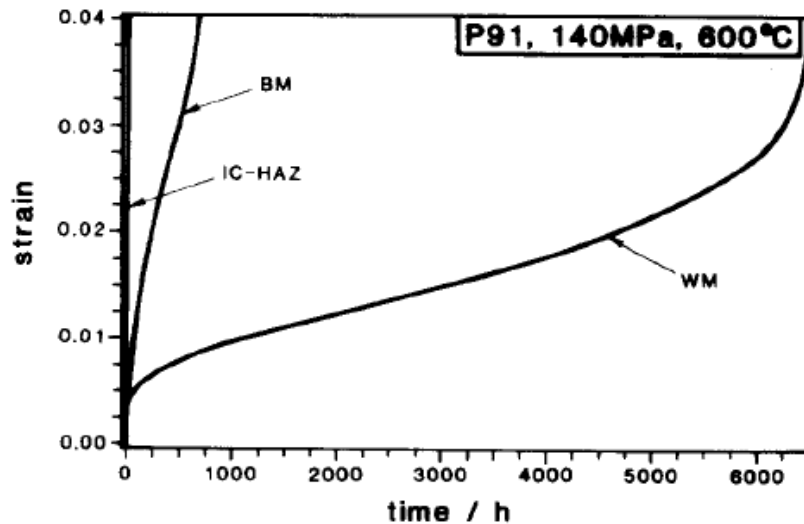
Figure 2. 23: A standard creep curve for the three material states at 140MPa under 600°C (Eggeler et al., 1994)
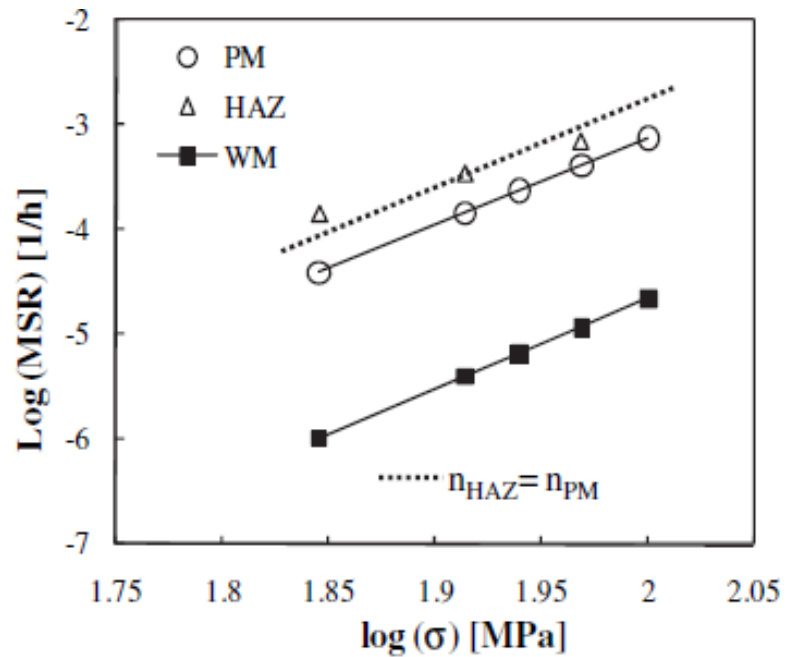
Figure 2. 24: Minimum strain rate vs stress for P91 weldment tested under 650°C (Hyde, Saber, & Sun, 2010a)

For high chromium alloy steel P91, at the stress of 140MPa under 600⁰C, Figure 2.22 shows the sub-grain size before and after creep in BM, IC-HAZ and WM respectively (Eggeler et al., 1994). The previous research reported that the largest sub-grain size locates at the IC-HAZ before creep and after creep. The smallest sub-grain size locates at the WM area before and after creep (Eggeler et al., 1994). The growth of sub-grain is strongly depending on the creep damage. Some of the sub-grain grows during the thermal aging period, but much more sub-grain grows after creep (Panait et al., 2010a; Panait et al., 2010b).

The creep strain curves in BM, IC-HAZ and WM for high chromium alloy steel P91, at 140MPa under 600⁰C, are shown in Figure 2.23. The life span in weld metal is more than 6 times longer than the life span in base metal. The life span

of IC-HAZ is shortest. The fracture of weldment is observed at IC-HAZ. The coarsening effect of sub-grain during creep might lead to the fracture.

Figure 2.24 shows the logarithm function between minimum strain rate and stress in BM, HAZ and WM for high chromium alloy steel P91 under 650^0C, stress varies from 70—100Mpa. It can be seen that the Log (Minimum strain rate) is proportional to the Log (stress) in different materials zones. The power law function with different stress exponent in WM ($n = 7.65$) and HAZ (HAZ=PM=8.462) was applied into different areas (Hyde et al., 2010a). The minimum creep strain rate in HAZ is highest.

2.8 Constitutive equations which are used for high chromium alloy steel P91

2.8.1 Classical constitutive equations of creep strain analysis method

Constitutive equations were used for high chromium alloy steel P91 and its weldment could be summarized as: Norton's Law, Robinson Model, Liu and Murakami, Hill's anisotropic potential function, Kachanov-Rabotnov and Xu's formulation, based on reviewing of the previous work. The classical constitutive equations representations of primary, secondary and tertiary creep are listed in Table 2.7 (Holdsworth et al., 2008). However, creep strain characteristics may not be acceptably modelled by certain creep constitutive equations for overall creep stages (primary, secondary and tertiary stages) of materials (Holdsworth & Merckling, 2003).

Table 2. 7: Classical representations of primary, secondary and tertiary creep (Holdsworth et al., 2008)

Model equation	Forms
Primary creep	
Power law	$\varepsilon_f = At^p \rightarrow \varepsilon_f = A\sigma^n t^p$
Logarithmic	$\varepsilon_f = B\log(1+bt)$
Exponential	$\varepsilon_f = C(1-\exp(-ct))$
Sinh law	$\varepsilon_f = D^* \sinh(ct^{1/3})$
Secondary creep	
Power law	$\dot{\varepsilon}_{f,min} = A'\sigma^n$
Sinh law	$\dot{\varepsilon}_{f,min} = \dot{\varepsilon}_0 \sinh(\sigma/\sigma_0)$
Tertiary creep	
Exponential	$\varepsilon_f = M(\exp(-mt)-1)$, $\dot{\varepsilon}_f = \dfrac{a\,\sigma^n}{(1-\omega)^q}$ where, $\dot{\omega} = \dfrac{c\,\sigma^k}{(1-\omega)^r}$
Omega	$\dot{\varepsilon}_f = \dot{\varepsilon}_0 \exp(\Omega\varepsilon)$

2.8.2 Typical constitutive equations of rupture ductility method

At high stress range, rupture ductility method is widely used for high chromium steels. The rupture mechanisms associated with the identified ductility regimes can differ for different alloy systems, as shown in Figure 2.25. Regime-I is the ductile rupture which causes by the formation of voids. Regime-II is a transition region. In regime-II, the ductility decreases because of the grain boundary cavitation effects. Regime-III is the ductile rupture which causes by the cavities nucleation and diffusive growth at grain boundary. Regime-IV is a recovery of ductility region because the influence of microstructural over-aging reduces the rate of cavity nucleation and/or growth (Holdsworth & Merckling, 2003).

The assessment of creep-ductility is complicated, but it can represent rupture characteristics in up to four different mechanism regimes at high temperature. However, the analytical representation of rupture ductility data has not previously received significant attention (Holdsworth & Merckling, 2003). Only few rupture ductility equations are listed in Table 2.8.
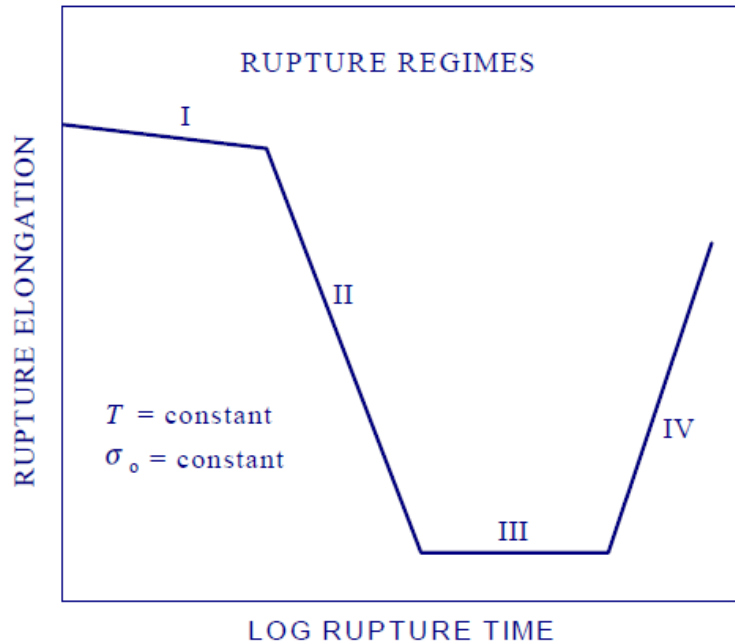
Figure 2. 25 Schematic representation of regimes of rupture ductility (Holdsworth & Merckling, 2003)

Table 2. 8 Rupture ductility equations (Holdsworth & Merckling, 2003)

Spindler	$\ln(A_u)$=MIN$\left\lfloor[\ln(A_1) + \frac{\Delta Q}{RT} + n_1\ln(\dot{\varepsilon}_{av}) + m_1\ln(\dot{\sigma})], \ln(A(t))\right\rfloor$
Evans & Wilshire	$\ln(A_u)$=MIN$[[a_1 + b_1\sigma + c_1 T + d_1\sigma T], \ln(A(t))]$
Anon	$\ln(A_u)$=MIN$[[a_1 + b_1\ln(\sigma) + c_1/T + d_1\ln(\sigma)/T], \ln(A(t))]$
Soviet Model	$\ln(A_u)$=MIN$\left\lfloor[a_1 + b_1\log(T) + c_1\log(\sigma) + \frac{d_1}{T} + e_1\sigma/T], \ln(A(t))\right\rfloor$

where A, A_u are tensile elongation and elongation at rupture. T is temperature. t is time. R is universal gas constant.

2.8.3 Constitutive equations were used for high chromium alloy steel P91

A. Norton's law

$$\dot{\varepsilon}=k\,\sigma_{eff}^{n} \tag{2.40}$$

<div align="right">(Eggeler et al., 1994)</div>

B. Robinson model

$$
\begin{cases}
\dot{\sigma} = D\left(\dot{\varepsilon} - \dot{\varepsilon}_p\right) & (1) \\[2mm]
\dot{\varepsilon}_p = A\left(\dfrac{\Sigma:\Sigma}{2K} - 1\right) n\,\dfrac{\Sigma}{\sqrt{\Sigma:\Sigma/2}} = \begin{cases}1 & if\ (\Sigma:\Sigma) > 2K\ and\ (s:\Sigma) > 0 \\ 0 & else\end{cases} & (2) \\[4mm]
\dot{a} = -R\left(\dfrac{a:a}{2K_0^2}\right)^{m-\beta}\dfrac{a}{\sqrt{a:\dfrac{a}{2}}} + H\dot{\varepsilon}_p = \begin{cases}\left(\dfrac{a:a}{2K_0^2}\right)^{-\beta} & if\ \left(a:\dfrac{a}{2}\right) > \dfrac{\alpha_0^2}{3}\ and\ (s:a) > 0 \\ \left(\dfrac{\alpha_0^2}{3K_0^2}\right)^{-\beta} & else\end{cases} & (3) \\[4mm]
\dot{K} = S\,\dot{W}_p\,e^{-\frac{W_p}{W_0}} & (4) \\[2mm]
\dot{W}_p = s:\dot{\varepsilon}_p & (5)
\end{cases}
$$

<div align="right">(2.41)</div>
<div align="right">(Eggeler et al., 1994)</div>

These variables in the Robinson model are

State variables

Total strain	ϵ
Plastic strain	ϵ_p
Stress	σ
Deviatoric stress	$s = \sigma - T_r(\sigma)/3$
Effective stress	$\Sigma = s - a$
Kinematic hardening	a
Isotropic hardening	K
Plastic strain work	W_p

Material constants

Elastic stiffness matrix	D

Special model	A, n, R, H, m
Parameters	$\beta, k_0, a_0, S, W_0, K_0$
Initial conditions	Except from the isotropic hardening ($K(0) = K_0$, all the other state varaibles are set to 0 from the unload material

In Robinson's model, there are two assumptions. The first assumption is at a steady temperature and stress, the creep damage is proportional to the fraction of the rupture lifetime. The second assumption is the damage results from each loading period is independent (Dyson, 2000). In the Robinson model, these variables not only just describe the creep damage behaviours, but also the fatigue damage. The Robinson model cannot simply used in the uni-axial creep data analysis (Eggeler et al., 1994). The Robinson's model and the Omega parameters are more likely applicable at temperature condition rather than stress, i.e. these models are applicable at thermal induced creep damage theory (Dyson, 2000).

C. Kachanov- Rabotnov-Hayhurst formulation

Single-state variable uni-axial equations

$$
\begin{cases}
\dot{\varepsilon} = A'(\frac{\sigma}{1-\omega})^n \, t^m \\
\dot{\omega} = B' \frac{\sigma^x}{(1-\omega)^\varphi} t^m
\end{cases}
\tag{2.42}
$$

Single-state variable multi-axial equations

$$
\begin{cases}
\dot{\varepsilon}_{ij}^c = \frac{3S_{ij}}{2\sigma_{eq}} t^m A' \left(\frac{\sigma_{eq}}{1-\omega}\right) \\
\dot{\omega} = B' \frac{\sigma_r^x}{(1-\omega)^\varphi} t^m \\
\sigma_r = \alpha\sigma_1 + (1-\alpha)\sigma_{eq}
\end{cases}
\tag{2.43}
$$

Three-state uni-axial variable equations

$$
\begin{cases}
\dot{\varepsilon} = A \sinh\left(\frac{B\sigma(1-H)}{(1-\varphi)(1-\omega_2)}\right) \\
\dot{H} = \frac{h}{\sigma}\frac{d\varepsilon^c}{dt}\left(1 - \frac{H}{H^*}\right) \\
\dot{\varphi} = \frac{K_c}{3}(1-\varphi)^4 \\
\dot{\omega}_2 = D\frac{d\varepsilon^c}{dt}
\end{cases}
\qquad (2.\,44)
$$

Three-state variable multi-axial equations

$$
\begin{cases}
\dot{\varepsilon}_{ij}^c = \frac{3S_{ij}}{2\sigma_{eq}} A \sinh\left(\frac{B\sigma_{eq}(1-H)}{(1-\varphi)(1-\omega_2)}\right) \\
\dot{H} = \frac{h\dot{\varepsilon}_e^c}{\sigma_{eq}}\left(1 - \frac{H}{H^*}\right) \\
\dot{\varphi} = \frac{K_c}{3}(1-\varphi)^4 \\
\dot{\omega}_2 = DN\dot{\varepsilon}_e^c\left(\frac{\sigma_1}{\sigma_{eq}}\right)^v
\end{cases}
\qquad (2.\,45)
$$

(Evans & Wilshire, 1993; Hyde & Sun, 2006)

Single state variables

$A', m, n, B', \chi, \varphi, a$	Material constants in single state equations, a is related to the multi-axial stress state behavior of the materials
σ_{eq}	Equivalent stress
σ_1	Maximum principal stress
σ_r	Rupture stress

Three state variables

A, B, h, H^*, K_c, D, v	Material constants in the three-state equations, v is related to the tri-axial stress state sensitivity of the materials
$H\ (0 < H < H^*)$	Strain hardening at primary creep
$\varphi\ (0 < \varphi < 1)$	Evolution of the spacing of carbides precipitates

ω_2 (0< ω_2 < 1/3)   Inter-granular cavitation damage

D. Activation energy method

Generally speaking, steady state behaviours of materials are described by using power law theory. The stress exponent n and activation energy Q_c are two variables according to different temperatures and stresses. The activation energy Q_c was introduced because of the vacancy movements are controlled by the diffusion mechanism in most metals and alloys at lower stress range (Evans & Wilshire, 1993). Activation energy is by plotting the natural logarithm of creep strain rate against the reciprocal of temperature.

In most pure metals, the vacancy movements are also called self-diffusion process. The energy of vacancy movements is called self-diffusion activation energy— Q_{SD}. However, during the temperature around 0.4—0.6T$_m$, activation energy for creep Q_c is significant less than Q_{SD}, even those activation energy can be considered equally in high temperatures (Evans & Wilshire, 1993).

Ule and Nagode (2007) proposed an improved stress dependent energy barrier to describe the minimum creep strain rate for high chromium alloy steel P91. The threshold stress concept and stress dependent activation energy concept were used in their project. The threshold stress varies with temperatures and applied stresses. Therefore, the threshold stress concept cannot well describe the behaviours of materials and predict the creep strain rate when the experimental data is not available.

Compared with the threshold stress concept, stress dependent activation energy is proposed on two assumptions. The first assumption is the applied stress will have an effect on the energy barrier to overcome transition from an initial to final state within a local region. The second assumption is using power law stress function instead of hyperbolic function. However, the multiple creep mechanisms are still not developed yet (Ule & Nagode, 2007).

E. Spindler model

Spindler model is the initial model to assess the mean rupture ductility based on grain boundary cavity nucleation and growth mechanism. This Spindler model was developed to determine creep damage at tertiary creep stage by considering the fracture elongation with the strain rate in high stress range (Holdsworth & Merckling, 2003).

F. Xu's formulations

$$
\begin{cases}
\dot{\varepsilon}_{iJ} = \dfrac{3S_{ij}}{2\sigma_e} \operatorname{Asinh}\left(\dfrac{B\sigma_e(1-H)}{(1-\varphi)(1-\omega_d)}\right) \\[2ex]
\dot{H} = \dfrac{h}{\sigma_e}\left(1 - \dfrac{H}{H^*}\right)\dot{\varepsilon}_e \\[2ex]
\dot{\varphi} = \dfrac{K_C}{3}(1-\varphi)^4 \\[2ex]
\dot{\omega} = CN\dot{\varepsilon}_e f_2 \\[1ex]
\dot{\omega}_d = \dot{\omega} f_1
\end{cases}
$$

$$
\begin{cases}
f_1 = \left[\dfrac{2\sigma_e}{3S_1}\right]^a \exp\left\{b\left[\dfrac{3\sigma_m}{S_s} - 1\right]\right\} \\[2ex]
f_2 = \left(\exp\left\{p\left[1 - \dfrac{\sigma_1}{\sigma_e}\right] + q\left[\dfrac{1}{2} - \dfrac{3\sigma_m}{2\sigma_e}\right]\right\}\right)^{-1}
\end{cases}
\tag{2.46}
$$

(Xu, 2007)

The influence of the stress state was considered in Xu's formulation based on the KRH constitutive equations. But, depending on the different materials at various conditions, the fundamental creep deformation mechanism, and microstructural degradation influence were not considered in his formulation.

2.9 Deficiencies of KRH constitutive equations and considerations of improving constitutive equations

2.9.1 Deficiencies of KRH constitutive equations

To develop or improve the current widely used constitutive equations (KRH) is essential. Xu (2000, 2001, 2004) has reported that the deficiencies of KRH constitutive equations. However, Xu's new formulation of constitutive equations is also needed to be improved in rupture criterion, influence of stress level, and thorough validation under non-proportional multi-axial loading condition. Hyde and Sun (2006) tried to depicte the life span of high chromium alloy steel P91 pipe weldment by applying the KRH constitutive equations together with another set of constitutive equations models. However, which type of constitutive equations could accurate estimate the life span of materials is not identified. In addition, Hosseini, Holdsworth and Mazza (2012) have compared five different types of current constitutive equations models in order to analyze the effectiveness of finite-element analysis method. In some extent, their research has releaved that the confusion and uncertain of each constitutive equations model. Besides, these evidence also prove that the demand of a new set of consitutitve equations to accurately predict the creep behaviours and life span of materials at lower stress range. European Creep Collaborative Committee (ECCC) has also reported that

98

the requirement of improving the constuitutive equations on both strain rate analysis method and ductility analysis method (Holdsworth & Merckling, 2003).

2.9.2 Considerations of improving constitutive equations model

Xu and Barrans (2000, 2001, 2004; Xu & Barrans, 2003) attempted to improve the methodology for developing and validating the creep constitutive equations. Their critical review has revealed that the deficiencies in the KRH constitutive equations creep constitutive equations model. As discussed above, the KRH constitutive equations are the most widely used for the creep damage problems under a multi-axial stress state condition within the continuum damage mechanics. However, the KRH constitutive equations approach was blindly adopted and even with some compromise in the determination of the stress sensitively index (Xu, 2000). The primary deficiency is unable to depict the creep deformation accurately by KRH constitutive equations. The second deficiency is unbale to depict the multi-axial stress state effect on the creep deformation, damage and rupture by the multi-axial stress state index v (Xu, 2000, 2001, 2004; Xu & Barrans, 2003).

There are two fundamental requirements for developing constitutive equations. These requirements are consistency of creep strain rate and consistency of creep damage evolution during the whole creep deformation and damage process. Xu (2000, 2001) has improved the KRH constitutive equations for multi-axial stress state condition for 0.5Cr-0.5Mo-0.25V ferritic steel under 590°C. However, xu's formulation was just able to satisfy the creep strain rate consistence requirement. Xu's formulation is limited into a high stress range at multi-axial stress state. The influence of the stress state has been improved in xu's formulation. Besides, Xu

(2001) reported that the new creep constitutive equations should consider a wider range of stress range, a better coupling of the states of stress on damage, and rupture criterion.

In the current project, the framework of improving a constitutive equations is based on the KRH constitutive equations. There are several aspects to improve the KRH constitutive equations for high chromium alloy steel P91. Firstly, at the certain temperature 600^0C, identify the different stress ranges, especially at the transition stress range. Secondary, identify the creep deformation and damage mechanism at the transition stress range. Thirdly, determine the power law function or hyperbolic function to describe the relation between creep strain rate and stress. Fourthly, define the dimensionless damage variables in each constitutive equation according to the microstructural degradation evolution process (strain hardening, particle coarsening and cavitation damage). Afterwards, investigate the cavitation damage on cavity size, cavity density to determine whether cavitation damage mechanism is cavity nucleation-controlled or cavity growth-controlled. Finally, identify the failure criterion for high chromium alloy steel P91 at the transition stress range.

Chapter 3

Methodology

3.1 Introduction

The experimental data in the current research project is selected from the previous researches. The selection required experimental data aims for high chromium alloy steel P91 at the transition stress range under 600℃. However, it is difficult to collect creep experimental data for high chromium alloy steel P91 at the transition stress range. In realistic, a creep test may take years until the fracture of materials. For example, the lifetime of materials is about 13 years until fracture at a transition stress of 80MPa under 600℃ for high chromium alloy steel P91.

In practical, the common used temperatures for high chromium alloy steels vary from 550℃ to 650℃. In order to investigate the influence of stress on creep damage evolution, the experiments usually conduct at a higher stress with a lower temperature or at a lower stress with a higher temperature to reduce the testing time. It is impossible in the current research to obtain the primary experimental data within the PhD research period time.

From literature review in the current research, the temperature under 600℃ is chosen because there is more required experimental data under 600℃ than the other temperatures and the applied stresses are lower in the transition stress range. When the temperature is certain, however, the existing experimental data

for high chromium alloy steel P91 at the transition stress range under 600℃ is limited based on the literature review research.

In summary, the majority of previous researches investigated the creep behaviours and estimated the lifetime of high chromium alloy steel P91 at the high stress range under different temperatures. The majority of previous researchers reported that the over-estimated lifetime of high chromium alloy steel P91 by the extrapolation method from high stress range to lower stress range. The accurate prediction of lifetime of high chromium alloy steel P91 at the lower stress range is essential. Some of the previous researches investigated the microstructural degradation evolution of high chromium alloy steel P91 at the transition stress range, such as the French group Panait et al. (2010a; 2010b) investigated the microstructural degradation evolution of high chromium alloy steel P91at the stress of 80MPa under 600℃. However, their research work did not combine the microstructural degradation damage with the creep constitutive equations models. Only few of previous researchers tried to modify the creep constitutive equations models combined with the microstructural degradation damage, such as in 2006, Yin's research (2006) of high chromium alloy steel P92 under 600℃ at the stress range 132MPa-180MPa; in 2010, Chen's research (2011) of high chromium alloy steel P91 under 600℃ at the stress range 130MPa-200MPa. However, the stresses used in their projects are still higher than the transition stress range for high chromium alloy steel P91 under 600℃.

3.2 Quantitative and qualitative research methods

Quantitative research method provides a measure of what people think from a statistical and numerical point of view. Quantitative research method collects numerical data or information that can be easily converted into numbers for analysis. Qualitative research method investigates why and how of the decision making, not what, where, when or who. Case study is one of the popular methods of qualitative research approach. Smaller but focused samples are more often used than large samples in qualitative research method (The British Library Board). Qualitative research method quantitative research method emphasis different aspects, as listed in Table 3.1

Table 3. 1 Differences between qualitative and quantitative research methods

Qualitative	Quantitative
Emphasis on understandings	Emphasis on testing and verification
Focus on understanding from respondent's/informants's point of view	Focus on facts and/or reasons for social events
Interpretation and rational approach	Logical and critical approach
Observations and measurements in natural settings	Controlled measurement
Subjective 'inside view 'and closeness to data	Objective 'outside view' distant from data
Explorative orientation	Hypothetical-deductive; focus on hypothesis testing
Process oriented	Result oriented
Holistic perspective	Particularistic and analytical
Generalization by comparison of properties and contexts of individual organism	Generalization by population membership

(Ghauri & Gronhaug, 2010, p. 105)

In summary, qualitative research method is adopted in the current research. The small but focused samples are selected because of the limitation of the experimental data. Case study is selected to validate the creep constitutive

equations in the current research. The process of research method is illustrated in Figure 3.1.
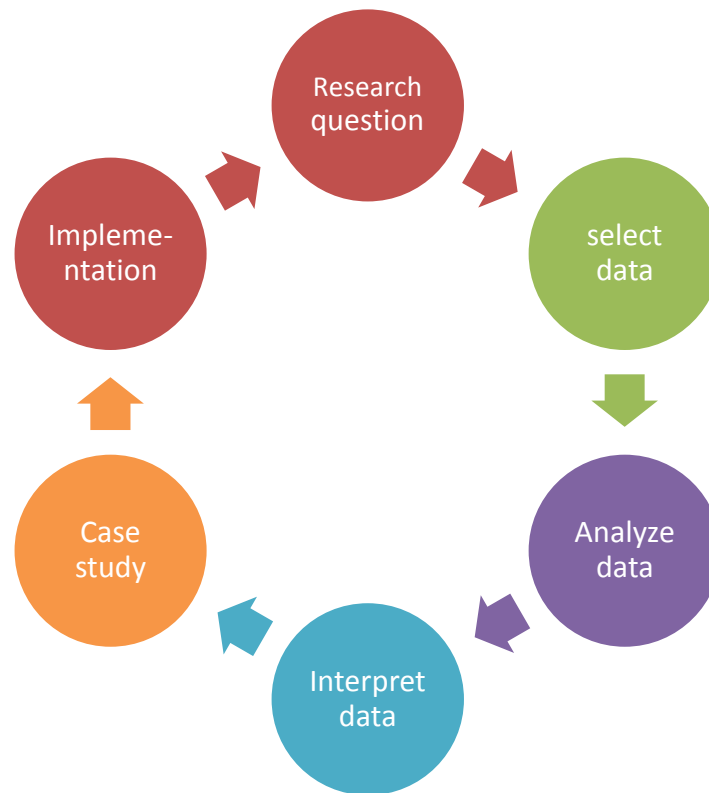
Figure 3. 1 The current research method flowchart based on (Ghauri & Grønhaug, 2005, p. 33; Sheridan, 2010)

3.3 Process of the current research project

The process of the current research project includes 5 steps. Each step is illustrated as below.

1) Determine the creep deformation and damage mechanism for high chromium alloy steel P91 at the transition stress range

Based on the classification of the stress ranges at a certain temperature for high chromium alloy steel P91, the first step is to determine the creep deformation

mechanism at different stress ranges, especially at the transition stress range. By analysing the relation between creep strain rate and stress to decide whether power law or hyperbolic law could be applied. Microstructural degradation evolution damage mechanism includes the changings of Lave phase, Z-phase, M23C6, MX precipitates and cavitation damage.

2) Determine the damage variables which are used to describe the creep damage process of high chromium alloy steel P91 at the transition stress range

In the current research, the second step is to develop the dimensionless damage variables for each damage mechanism in the constitutive equations. Based on the KRH constitutive equations, the damage variable H was proposed to describe the strain hardening effect at primary creep stage. The damage variable φ was proposed to describe the particle coarsening effect at secondary creep stage. The damage variable ω was proposed to describe the cavitation damage at tertiary creep stage.

3) Determine the failure criteria for uni-axial and multi-axial stress states conditions of high chromium alloy steel P91 at the transition stress range

In the current research, the third step is determining the failure criteria according to the cavitation damage mechanism. In KRH constitutive equations, cavity continuous nucleation is regarded as the cavitation damage mechanism during creep. At multi-axial stress state, the failure criterion was identified by the ratio of maximum principal stress and equivalent stress for high chromium alloy steels. At

uni-axial condition, the maximum principal stress equals to the equivalent stress. The cavitated area at fracture was identified as $\omega_f = 1/3$ at uni-axial stress; $\omega_f = 1$ at multi-axial stress state (Dyson, 2000)

4) Determine the material parameters and formation of the proposed creep constitutive equations of high chromium alloy steel P91 at the transition stress range

The next step is to determine the material parameters in the proposed creep constitutive equations model. In KRH constitutive equations, the material parameters are determined by fitting a number of uni-axial strain-time curves obtained from creep tests at a given temperature. At multi-axial stress state, the stress state index is determined from FE modelling of the notched bar creep rupture tests.

5) Validation of the proposed creep constitutive equations

The final step is to validate the feasibility of the proposed creep constitutive equations. Case study research method is adopted in the validation section. Case study 1 is to validate the feasibility of the proposed creep constitutive equations at the stress of 80MPa for high chromium alloy steel P91 under 600℃ by comparing the predicted lifetime and creep behaviours with the experimental data. Case study 2 is to validate the feasibility of the proposed creep constitutive equations at the critical stress of 70MPa for high chromium alloy steel P91 under 600 ℃ by comparing the predicted lifetime and creep behaviours with the experimental data.

Chapter 4

Characteristics of experimental data and evaluation for high chromium alloy steel P91

4.1 Introduction

Chapter 1 is an introduction of the current research project. Chapter 1 introduces a general background of creep damage and the importance of investigating of creep damage in high temperature industries. Chapter 1 also illustrates the gap between the previous research and the current project.

Chapter 2 summaries a fundamental knowledge of creep damage, properties of high chromium alloy steel P91, cavitation damage mechanism and the creep constitutive equations within continuous damage mechanics. Chapter 2 discovers the essential of developing or improving constitutive equations for high chromium alloy steels at the lower stress range, especially for high chromium alloy steel P91 at the transition stress range.

Chapter 3 is the methodology of the current research project. Methodology includes an introduction of how to choose the research methods for the current project and a comparison between quantitative and qualitative research methods. In addition, chapter 3 illustrates the process of how to conduct the current research project.

In summary, the previous chapters provide a basic knowledge and direction for chapter 4. Chapter 4 summarizes the characteristics of experimental data and evaluation of selected experimental data. The primary step in chapter 4 is selection of the existing experimental data for high chromium alloy steel P91 under 600℃. The required experimental data in the current research includes 7 aspects. They are

1) Experimental data selection of stress regions

At a given temperature 600℃ for high chromium alloy steel P91, the stress regions of high, transition and low stress should be identified before selecting the other experimental data. In the current research, creep damage within the transition stress range is the main objective to investigate.

2) Experimental data selection of creep deformation and rupture mechanism

Creep deformation and rupture mechanism at different stress ranges provide a fundamental theory for selecting creep constitutive equations.

3) Experimental data selection of creep strain rate and stress

The aim of selecting the experimental data of creep strain and stress is to analyse the relation between creep strain rate and stress within the transition stress range for high chromium alloy steel P91. The relation between creep strain rate and stress will decide whether use power law function or hyperbolic law function in the proposed creep constitutive equations model.

4) Experimental data selection of strain hardening effect

These experimental data aims to investigate the influence of strain hardening on the failure of materials for high chromium alloy steel P91 at the transition stress range under 600℃. The dimensionless damage variable of strain hardening will be selected to describe the strain hardening effect in the proposed creep constitutive equations model.

5) Experimental data selection of particle coarsening effect

Same as the last step, these experimental data aims to investigate the influence of particle coarsening on the failure of materials for high chromium alloy steel P91 at the transition stress range under 600℃. The dimensionless damage variable of particle coarsening will be selected to describe the particle coarsening effect in the proposed creep constitutive equations model.

6) Experimental data selection of cavitation damage effect

The aim of investigating the influence of cavitation damage on failure of materials is to decide whether cavity continuous nucleation in density mechanism or cavity growth in size mechanism takes the domination for high chromium alloy steel P91 at the transition stress range under 600 ℃. The selection of creep constitutive equations depends on which cavitation damage mechanism is controlled. Ideally, in the current research, the experimental data of cavity size, cavity density, cavitated area and volume fraction at fracture surface are aimed to select.

7) Experimental data selection of failure criteria

These experimental data are mainly investigating the failure criteria for multi-axial stress state situation. In KRH constitutive equations, the failure criterion is identified as the ratio of maximum stress and principal stress at multi-axial stress state. The uni-axial situation is the special case when the maximum stress equals the principal stress. In the current research, the aim of these experimental data is to investigate the influence of hydrostatic stress on the failure of materials.

In conclusion, the required experimental data in the current research for high chromium alloy steel P91 at the transition stress range under 600 °C can be summarised in Table 4.1.

Table 4. 1: Required experimental data selection in the current research

Required experimental data	Aims of these required experimental data
Stress regions	Classifying the low, transition and high stress range at a given temperature 600℃.
Creep deformation and rupture mechanism	Determining the creep deformation and rupture mechanism in order to select creep constitutive equations.
Creep strain rate and stress	Determining whether power law or hyperbolic law function to describe the relation between creep strain rate and stress.
Strain hardening	Determining the dimensionless damage variable according to strain hardening effect.
Particle coarsening	Determining the dimensionless damage variable according to particle coarsening effect.
Cavitation damage	Determining whether cavity continuous nucleation or cavity growth-controlled cavitation damage mechanism.
Failure criteria	Determining whether hydrostatic stress has influence on failure of materials or not

4.2 Experimental data selection and evaluation of stress regions

4.2.1 Definition of stress exponent

Generally, the stress exponent n is generally identified as

$$n = \frac{\Delta(\ln(\dot{\varepsilon}_s))}{\Delta(\ln(\sigma))}$$
(4. 1)

The stress exponent n can be obtained by plotting the creep strain rate as a function of stress, as shown in Figure 4.1 (University of Cambridge). The gradient

is the value of the stress exponent. According to the classical power law theory ($\dot{\varepsilon} \propto B\sigma^n$), the stress ranges could be classified combine with the values of stress exponent. In general, at low stress, the exponent is $n \approx 1$. At high stress, the exponent is $3 < n < 8$. The stress exponent n is strongly temperature dependent. The higher temperature is, the lower stress exponent n will be (Chen et al., 2012; Ule & Nagode, 2007).
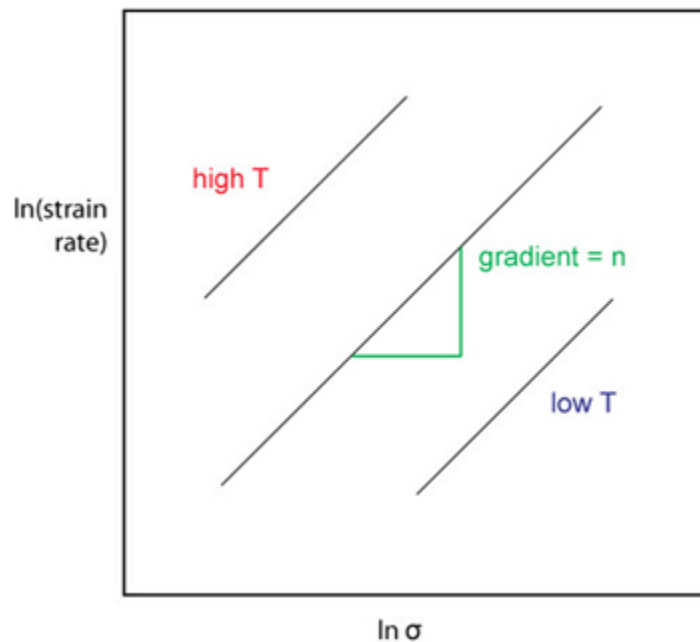
Figure 4. 1: Creep strain rate as a function of stress (University of Cambridge)

4.2.2 Stress regions for high chromium alloy steel P91 under 600℃

Many researchers have redefined the value of stress exponent n for low stress range for 9-12%Cr alloy steels, such as (Besson et al., 2009; Chen et al., 2011; Czyrska-Filemonowicz, ZieliÅ„ska-Lipiec, & Ennis, 2006; Kloc & Sklenička, 2004). The investigation of stress exponent n for high chromium alloy steel P91 has been summarised by a chronological order. In 2004, for high chromium alloy steel P91 under 600℃, Kloc & Sklenička (2004) has found that the stress

exponent n for stress changes is approximate 4.5, which is much higher than the stress exponent $n \approx 1$ for low stress range and much lower than the stress exponent $n \approx 12$ for high stress range. An illustration of the stress exponent for stress changes is plotted in Figure 4.2.
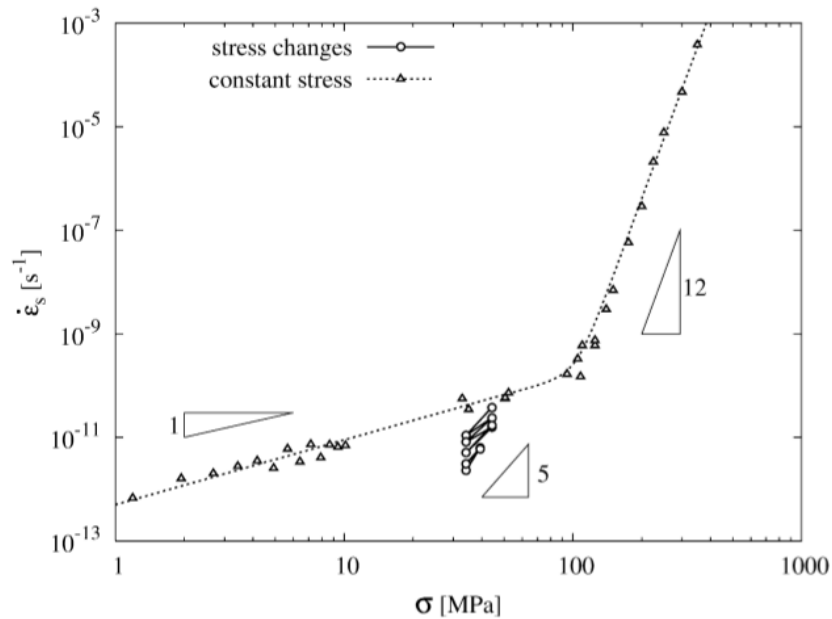
Figure 4. 2: Stress exponents with stress changes for high chromium alloy steel P91 under 600℃

In 2006, for high chromium alloy steels (P91, E911 and P92) under the temperature 600℃—650℃, Czyrska-Filemonowicz et al. (2006) reported that the stress exponent n varies from 6 to16 from lower stress to high stress range at different temperatures. In 2009, for high chromium alloy steel P91 weldment under 625℃, Besson et al. (2009) pointed out that the stress exponent n =5.4 at the stress changes. The stress of 70MPa is identified as stress changes between low stress and high stress. In 2009, for high chromium alloy steel T91 under 600℃ ($t_f = 94,000h$), Haney et al. (2009) also reported the different stress

exponents at different temperatures, as shown in Table 4.2. Haney et al. (2009) pointed out that there is a changing of creep damage mechanism according to the stress levels. It is essential to accurately model the relation between power law creep and viscous creep independently or find out dependency of power law creep and viscous creep.

Table 4. 2: Stress exponents with stress changes at different temperatures for high chromium alloy steel T91 (Haney et al., 2009)

Temperature	High stress exponent n	Low stress exponent n	Transition stress
500℃	18.566	3.024	170-210MPa
600℃	11.929	0.781	70-100MPa
625℃	10.700	1.729	50-90MPa

In 2011, for high chromium alloy steel P91 under 600℃, Chen et al. (2011) has reported different values of stress exponent n for low, transition and high stress ranges. The stress exponent n for stress changes is approximate 4. In summary, Table 4.3 summarises the creep deformation mechanisms, stress exponent and stress values for low, transition and high stress ranges. Orowan stress is required to force a dislocation pass an obstacle. Orowan stress is inversely proportional to the particle separation. The high stress range is when the applied stress higher than Orowan stress. The transition stress range is when the applied stress lower than Orowan stress. The low stress is when the applied stress is very small.

Table 4. 3: Stress ranges for high chromium alloy steel P91 under 600℃, data from (Chen et al., 2011)

P91 600℃	High stress range	Transition stress range	Low stress range
Creep deformation	Dislocation (Orowan stress)	Dislocation (Climbing)	Diffusion
Stress exponent n	>10	≈4	=1
Stress σ (MPa)	>130	70<σ<110	<50

In conclusion, the stress exponent for stress changings for high chromium alloy steels under different temperatures is on-going. In the current research, the stress exponent n for high chromium alloy steel P91 under 600℃ is classified in Table 4.4. The transition stress range is complicated and deserving a further research on the creep deformation mechanism, reduction of area at fracture and creep strain rate etc. (Haney et al., 2009).

Table 4. 4: Stress exponent and stress changings for high chromium alloy steel P91 under 600℃

Temperature	High stress exponent n	Low stress exponent n	Transition stress exponent n
600℃	>10	≈4	≈1
Stress (MPa)	>130	70<σ<110	<50

4.3 Experimental data selection and evaluation of creep deformation and rupture mechanism

4.3.1 Dislocation-assisted ductile rupture mechanism at the high stress range

For most of the materials, the dislocation creep deformation occurs through the whole creep damage process. But, the dislocation creep deformation mechanism takes the domination at the high stress range and a low temperature condition. The diffusion creep deformation takes the domination at a relative lower stress and a high temperature condition. For majority of metals, the cavitation damage is the main reason which leads to a final fracture. According to Dyson's (2000) theory, the cavitation damage mechanism is divided into cavity nucleation-controlled and cavity growth-controlled mechanisms. If unconstrained cavity nucleation controls the cavitation damage mechanism, a low density of cavities is observed at the high stress range under a low temperature condition.

At the high stress range, for high chromium alloy steel P91, the ductile fracture (trans-granular) assisted by the dislocation creep deformation is identified as the creep deformation and rupture mechanism. This point of view was supported by many researchers, such as (Bendick et al., 2010; Gaffard et al., 2004; Gaffard et al., 2005; Massé & Lejeail, 2013; Panait et al., 2010a; Vivier et al., 2010). Moreover, the previous researcher Lim et al. (2011) reported that a low density of cavities and a low volume fraction of cavities (≈10%) were observed for high chromium alloy steel P91 at the high stress range. The failure criterion is based on the reduction in cross-section at fracture (Lim et al., 2011). Masse et al. (2012

also investigated the creep deformation and rupture mechanism for high chormium alloy steel P91 at the stress range under 600℃. Masse et al. (2012) argued that the time to rupture at a 10% strain as a failure criterion. In addition, Masse et al. (2012) argued that the viscoplasticity-assisted ductile rupture mechanism is idetified at the high stress range. The cavity nucelation preferentially begins along the grain boundary, mainly in the stress concentration area. The cavity growth is assisted by grain deformation and cavity coalescence of small inter-granular cavities. The ductile fracture is because of the necking phenomenon which is caused by the microstructural recovery (Lim et al., 2011; Massé & Lejeail, 2012).

4.3.2 Diffusion-assisted brittle rupture mechanism at the transition stress range

Figure 4.3 shows the diffusion angles of grain boundaries by Electron Back Scattered Diffraction (EBSD) after creep for high chromium alloy steel at the transition stress of 80MPa under 600℃. The majority of grain boundaries' rotation angle is $\theta > 15°$. Some of grain boundaries' rotation angle is $5° < \theta < 15°$ after creep process. The Nabarro-Herring (N-H) creep deformation was argued as the creep mechanism at the lower stress range (Massé & Lejeail, 2012, 2013). This point of view is also supported by Gaffard et al. (2005).
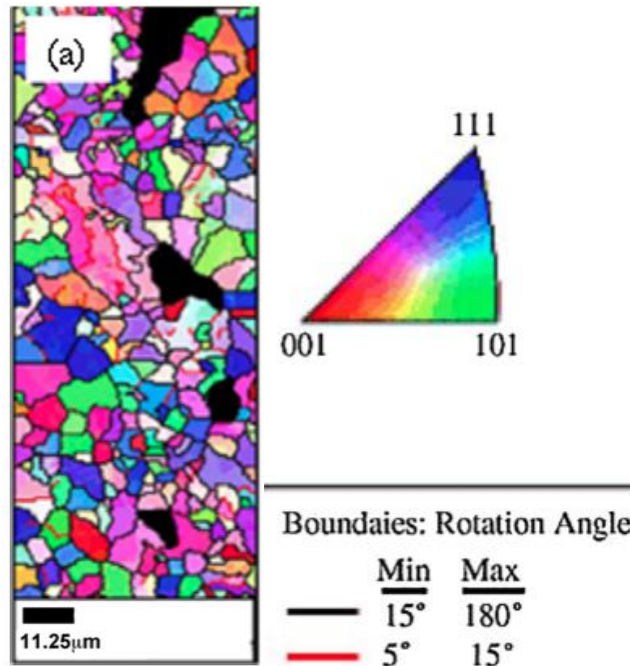
Figure 4. 3: EBSD map near rupture area, creep teat at 90MPa ($t_f = 7000h$), illustrates diffusion-assisted cavitation damage. Black lines indicate high angle boundaries ($> 15°$), grey and red lines indicate low angle boundaries ($5° < \theta < 15°$) (Massé & Lejeail, 2012, 2013).

According to TWI' report (2014), for most of metals, the cavitation damage mechanism at the lower stress range is identified as that cavities continuously nucleate around large participates or particles on the grain boundary. Cavities growth by diffusion (constrained by local creep strain) and coalescence of cavities or large precipitates lead to a micro- or macro-crack eventually.

For high chromium alloy steel P91 at the transition stress range under 600℃, the rupture mechanism is argued as N-H diffusion-assisted brittle rupture mechanism. The brittle rupture is caused by the cavitation damage during creep. This cavitation damage starts with cavity nucleation at grain boundary at the beginning, then cavity growth assisted by diffusion along the grain boundaries,

cavity coalescence leads to a final micro or macro-cracks eventually (Massé & Lejeail, 2012, 2013).

4.4 Experimental data selection and evaluation of creep strain rate and stress

4.4.1 Relations between creep strain rate, strain at failure and stress

The relation between creep strain rate and stress is determining whether power law function or hyperbolic law function used in constitutive equations model. For high chromium alloy steel P91 under 600℃, the current researcher finds out that the required experimental data to describe the relation between creep strain rate and stress is inadequate, especially at the transition stress range. Therefore, the current researcher expands the specific material to 9-12%Cr alloy steels and temperature 600℃ to temperature range 550℃-650℃.

The overall experimental data of creep strain rate, strain at failure and stress are collected from 9 relative published papers. The experimental data of creep strain rate, strain at failure and stress are roughly read from these published papers. These required experimental data are summarised in Table 4.5. However, for high chromium alloy steel P92 under 600℃, the applied stress 132MPa and 110MPa are still slightly higher than the transition stresses.

Table 4. 5: Experimental data selection of creep strain rate, strain at failure and stress

Temperature	Reference	Material	Creep strain rate	Strain at failure	Stress
600℃	(Yin & Faulkner, 2006)	P92	$8.33 \times 10^{-8} h^{-1}$	0.0475	132Mpa
600℃	(Pétry & Lindet, 2009)	P92	$5.00 \times 10^{-8} h^{-1}$	0.02	110MPa
600℃	(Panait et al., 2010a)	P91	$1.80 \times 10^{-7} h^{-1}$	0.0475	80MPa
600℃	(Sawada et al., 2011)	P91	$1.13 \times 10^{-8} h^{-1}$	0.035	70MPa
600℃	(Abe, 2012)	P91	$4.50 \times 10^{-7} h^{-1}$	0.0998	100MPa
625℃	(Massé & Lejeail, 2013)	T91	$5.25 \times 10^{-7} h^{-1}$ $6.25 \times 10^{-7} h^{-1}$	0.005 0.0122	60MPa 80MPa
650℃	(Yin & Faulkner, 2006)	P92	$6.25 \times 10^{-8} h^{-1}$	0.051	81MPa
650℃	(Hyde et al., 2006a)	P91	$5.00 \times 10^{-8} h^{-1}$	0.142	70MPa
650℃	(Abd El-Azim et al., 2013)	P91 weld	$4.00 \times 10^{-8} h^{-1}$	0.05	55MPa
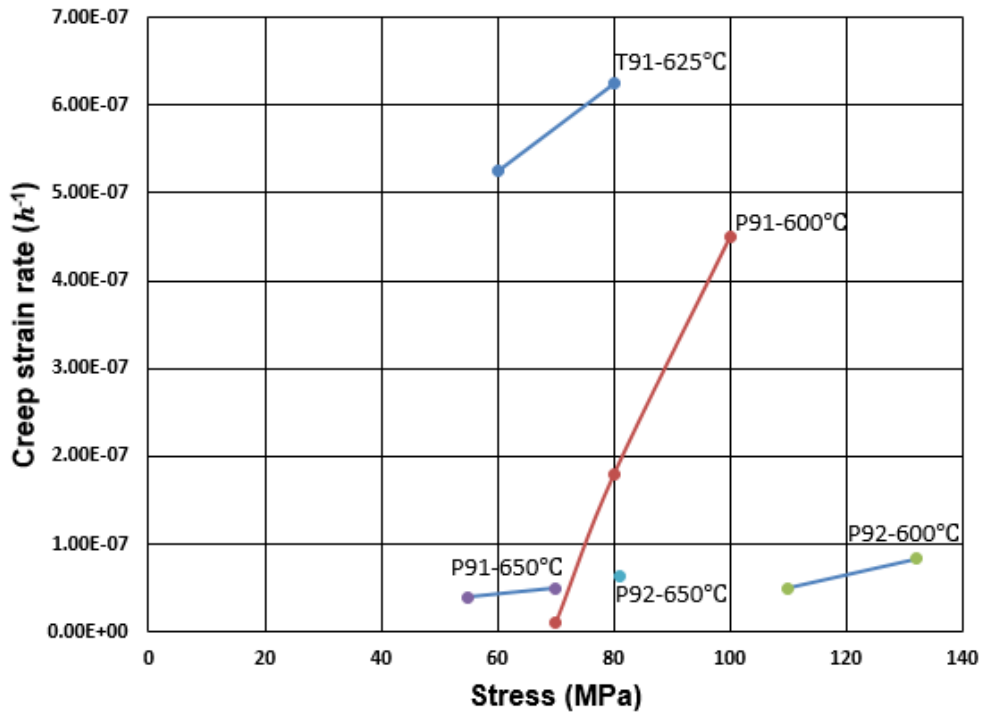
Figure 4. 4: Relation between creep strain rate and stress for high chromium alloy steels
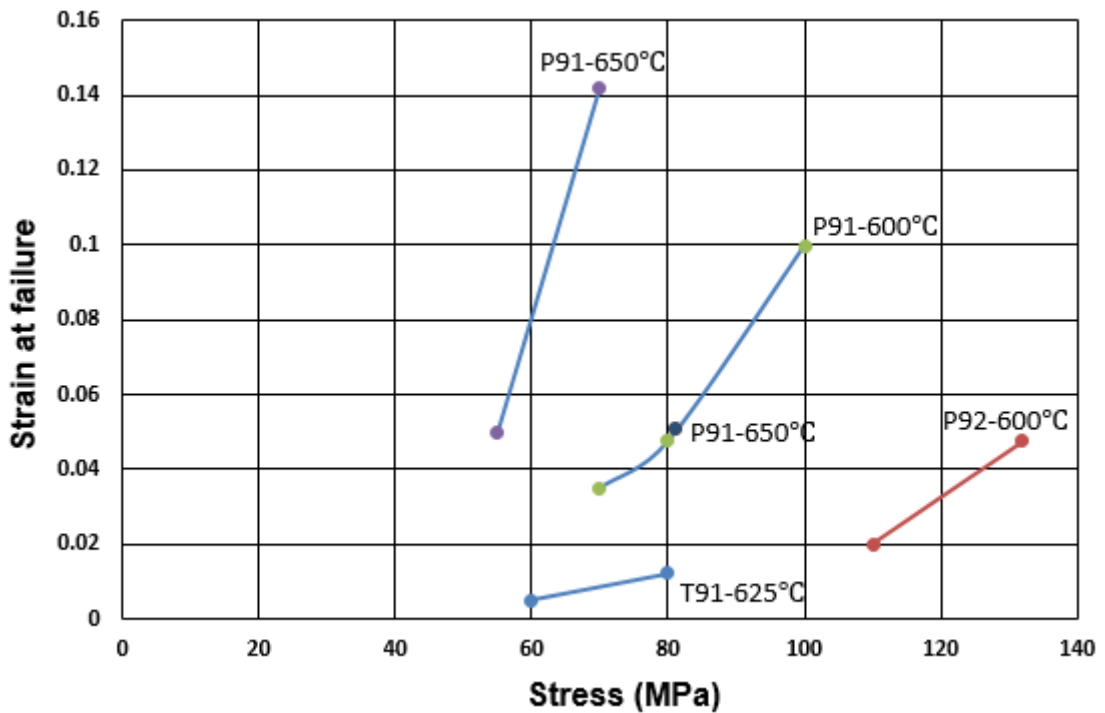
Figure 4. 5: Relation between strain at failure and stress for high chromium alloy steels

According to Table 4.5, for 9%-12%Cr steels, the relation between creep strain rate and stress is plotted in Figure 4.4. The relation between strain at failure and stress is plotted in Figure 4.5. Firstly, the creep strain rate is assumed approximately proportional to the stress in Figure 4.4. Within the transition stress range, the creep strain rate is stress-controlled. The creep strain rate increases with the stress is increasing. However, the experimental data listed in Figure 4.4 are less substantial to support these points of view because of the inadequate data. For example, the linear relation between creep strain rate and stress is not accurate according to the inadequate selected data. Even though, there are 3 selected data for high chromium alloy steel P91 under 600℃, however, the stress at 132MPa for high chromium alloy steel P91 under 600 ℃ is slight higher than the transition stress.

Secondly, the strain at failure is assumed as stress-controlled at a given temperature. The strain at failure at a higher stress level is higher than the strain at failure at a lower stress level if the temperature is certain. However, the current researcher assumes that the strain at failure is approximately to a certain value within the same stress range. The average value of strain at failure could be regarded as the strain at failure for high chromium alloy steel T91 at the stresses of 60MPa and 80MPa under 625℃.

4.4.2 Constitutive equations for N-H diffusion creep at the transition stress range

In general, the value of stress exponent n depends on creep deformation mechanism. If diffusion creep mechanism takes the domination at the low stress range, the stress exponent $n \approx 1$. If dislocation creep mechanism takes the domination at the high stress range, the stress exponent $3 < n < 8$ according to the classical power law theory. When the N-H creep deformation takes the domination, the minimum creep strain rate is

$$\dot{\varepsilon} = \frac{\alpha_v \sigma^n \Omega D_v}{kTd^2} = A\sigma^n \tag{4.2}$$

where stress exponent $n \approx 1$ at the low stress range, Ω is atomic volume, k is the Boltzmann constant($k = 1.38 * 10^{23} \frac{J}{K}$), T is the absolute temperature in Kelvin, d is grain size, α_v is a dimensionless numerical factor whose magnitude depends on the shape of the grains, $\alpha_v = 24$ (for equi-axed, hexagonal grains). D_v is the diffusion coefficient in the grains. The diffusion coefficient D_v is (Riedel, 1987)

$$D_v = D_{v0} \exp\left(-\frac{Q_v}{RT}\right) \tag{4.3}$$

The power law function between creep strain rate and stress could provide a flexibility of stress exponent n at different stress ranges for high chromium alloy steel P91 under $600\,°C$. Based on the selected experimental data of creep deformation mechanism for high chromium alloy steel P91 at the transition stress range under a given temperature, the N-H creep deformation is argued as the creep deformation mechanism, see in section 4.3. At a given temperature $600°C$,

the stress exponent n varies from the low stress range to high stress range for high chromium alloy steel P91. Therefore, the minimum creep strain rate is

$$\dot{\varepsilon} \propto A\sigma^n \qquad (4.4)$$

where $n \approx 1$ at the low stress range, $n \approx 4$ at the transition stress range, $n > 10$ at the high stress range for high chromium alloy steel P91 under 600℃.

The determination of material proportional parameter A could be obtained from

$$A = \frac{\alpha_v \Omega D_v}{kTd^2} \qquad (4.5)$$

where the material proportional parameter A is related to the activation energy, grain size, temperature, atomic volume etc. The material proportional parameter A for high chromium alloy steel P91 under 600^0C approximately equals 2.5×10^{-16}. The material parameters are listed in Table 4.6 for high chromium alloy steel P91 under 600℃. These material parameters $(\alpha_v, \Omega, D_{v0}, Q_v, d)$ are selected from the previous researches (Abd El-Azim et al., 2013; Riedel, 1987; Shrestha et al., 2013). Material parameters k, R, T are constant.

Table 4. 6: Material parameters for high chromium alloy steel P91 under 600℃

Constants	α_v	Ω	D_{v0}	Q_v
Values	24	$1.21 \times 10^{-29} m^3$	$1.8 \times 10^{-5} m^3/s$	$270\ KJ/mol$
Constants	d	T	k	R
Values	$0.35 \times 10^{-6} m$	600℃(873K)	$1.38 \times 10^{-23} J/K$	$8.315 J/molK$

4.5 Experimental data selection of strain hardening effect

Strain hardening process is making a metal harder and stronger by preventing the dislocation movements and the relaxation process. The strain hardening of material is inevitable at the primary creep stage whether at the high stress range or the transition stress range. The strain hardening effect is considered as one of the damage variable in the creep constitutive equations model. Based on the KRH constitutive equations, the current expressions of strain hardening effect on high chromium steels at the transition stress range are adopted.

Within the CDM theory, the isotropic hardening method is widely used under a creep damage condition. In Dyson's paper (2000) cited in (Ion, Barbosa, Ashby, Dyson, & McLean, 1986), he reported that the dimensionless variable H is used to describe the isotropic strain hardening. This classical expression of isotropic strain hardening effect H is frequently used by many researchers for high chromium steels at different stress ranges. This is supported by many researchers, such as (Dyson, 1988, 2000; Hayhurst, Mustata, & Hayhurst, 2005; Hayhurst, Vakili-Tahami, & Hayhurst, 2009; Hyde et al., 2006a; Hyde, Sun, Becker, & Williams, 2004; Yin & Faulkner, 2006) and so forth.

The strain hardening effect has been illustrated by a dimensionless variable *H*. The expression of the strain hardening is

$$H = \frac{\sigma_i}{\sigma} \qquad\qquad (4.6)$$

where σ_i is the an internal back stress generated during stress redistribution within hard regions of microstructure (particles, sub-grain and others), σ is the uniaxial applied stress

The evolution rate of strain hardening *H* is

$$\dot{H} = \frac{h'}{\sigma} * \left(1 - \frac{H}{H^*}\right) * \dot{\varepsilon} \tag{4. 7}$$

where $0 < H < H^* < 1$, constant $h' = E * \phi$ (E is Young's Modulus, $\phi \geq \phi_p$ is the volume fraction of all phase lead to the stress redistribution) (Dyson, 2000)

4.6 Experimental data selection and evaluation of particle coarsening effect

4.6.1 Introduction

The microstructure degradation process significantly affects the strength and the failure of materials at creep. In order to investigate the microstructural degradation process for high chromium alloy steel P91 at the transition stress range, the experimental data of MX precipitates, M23C6 carbides, Laves phases and Z-phase are selected and analysed in the current research.

The previous researchers state that the microstructural degradation is the most likely reason to cause the premature failure at the lower stress range. This point of view was supported by several researchers, such as (Armaki, Chen, Maruyama, & Igarashi, 2010; Kalck et al., 2010; Kimura et al., 2002; Magnusson & Sandström, 2007; Naumenko & Kostenko, 2009; Panait et al., 2010a; Panait et al., 2010b; Sawada, Bauer, Kauffmann, Mayr, & Klenk, 2010; Sawada et al., 2011; Sklenička; Spigarelli, 2013; Vivier et al., 2008).

The premature failure is the process of large precipitates appear, cavities rapidly coalesce at the tertiary creep stage at the long-term creep test. This process is also re-defined as the inhomogeneous recovery at the lower stress range by Kimura (2002). The different preferential recovery mechanisms of martensite at the prior austenite grain boundary (PAGB) are homogeneous and inhomogeneous recovery at the high stress range and lower stress range respectively (Kimura et al., 2002). The inhomogeneous recovery of tempered martensite lath structures in 9-12%Cr materials might be the reason for the premature failure. The inhomogeneous recovery is because of the loss of the MX and M23C6 precipitates (Armaki et al., 2010).

4.6.2 Changings of MX precipitates, M23C6 carbides, Lave phases and sub-grain

Firstly, the MX type of precipitates and M23C6 carbides nucleate and grow at tempering condition. The MX precipitates and M23C6 carbides are only coarsening at creep damage (Magnusson & Sandström, 2007). The previous researchers reported that there is no changes of MX precipitates in size, shape and spatial distribution during the creep process for high chromium alloy steel P91 at the transition stress of 80MPa under $600°C$. The average size of MX precipitates is about $20 - 40nm$ before creep. By contrast, the average size of M23C6 carbides is about $70nm - 100nm$ before creep. M23C6 carbides is coalescence up to $300nm$ during creep process with a number of M23C6 carbides decreasing (Panait et al., 2010a; Panait et al., 2010b; Spigarelli, 2013).

Secondly, for high chromium alloy steel P91 at the transition stress of 80MPa under 600℃, Lave phases nucleate and grow significantly during the creep process. The mean radius of Lave phases reaches up to $500nm$ after 50,000 hours under 600℃. The equivalent diameter of Lave phases is about $400nm$ before coarsening. The mean diameter of Lave phases is plotted in Figure 4.6 (Panait et al., 2010a). In a contrary manner, for high chromium alloy steel P91 at the transition stress of 80MPa under 600℃, the Z-phase has only a small influence or no influence on the failure of material at the long-term creep test. There were only 41 Z-phase precipitates out of 640 identified precipitates which had been observed after creep (Panait et al., 2010a). The formation of Z-phase does not affect significantly of a long-term creep properties for high chromium alloy P91 steel (Parker, 2013). In addition, the changings of precipitates for Mod.9Cr-1Mo steel under 600℃ and 650℃ are shown in Figure 4.7. The Z-phase is more likely observed at a high temperature situation, however, the Lave phases were observed preferentially at a relative lower temperature (Kimura et al., 2002; Kimura, Toda, Kushima, & Sawada, 2010).

Thirdly, the sub-grain growth occurred during thermal exposure, but the sub-grain growth is strongly enhanced by creep. The sub-grain size increased up to 70, 000 hours during creep. After that, the coarsening of sub-grain rapid occurred (Panait et al., 2010a; Panait et al., 2010b; Sawada et al., 2011).
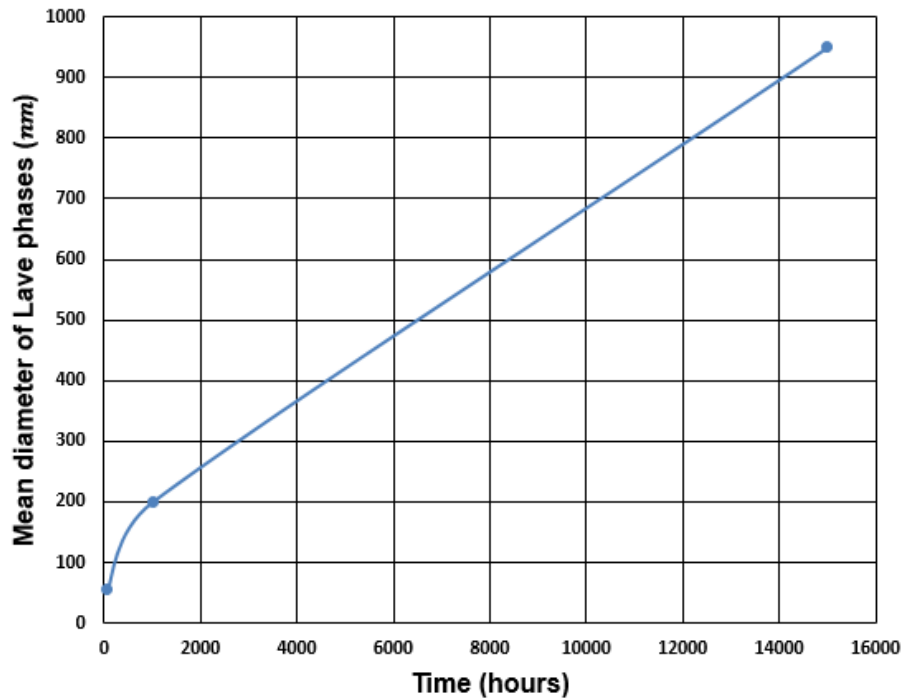
Figure 4. 6: Mean diameter of Laves phase for Mod.9Cr-1Mo at 80Mpa under 600°C, data from (Panait et al., 2010a; Panait et al., 2010b)
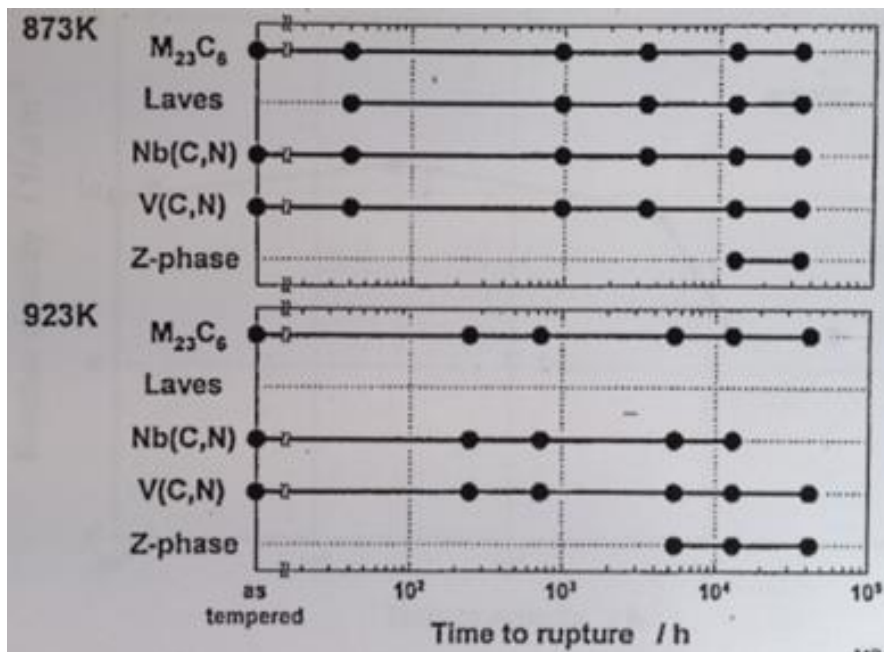
Figure 4. 7: Microstructural changings of Mod.9Cr-1Mo steel (Kimura et al., 2002)

4.6.3 Constitutive equations for particle coarsening effect

The coarsening of large precipitates is one of the reasons to cause the material softening at creep damage. As discussed above, for high chromium alloy steel P91 at the transition stress range under $600\,^{\circ}\text{C}$, the coarsening of large precipitates and sub-grains have significant influence on the failure of materials. The particle coarsening concept was proposed by Dyson in 1988 (1988). This particle coarsening effect has been widely used for high and low chromium alloy steels (Hyde & Sun, 2006; Yin & Faulkner, 2006).

The coarsening process of large precipitates obeys the Lishitz-Wagner form

$$d^3 = d_0{}^3 + Kt \tag{4.8}$$

where d is the particle size at arbitrary time and d_0 is the initial particle size.

The dimensionless damage variable of particle coarsening D_p is

$$D_p = 1 - \frac{P_i}{P_t} \tag{4.9}$$

where P_i is the initial spacing and P_t is the arbitrary time of particle spacing.

The evolution rate of particle coarsening $\dot{D}_p$ is determined from the particle coarsening equation at a constant volume fraction. The evolution rate of particle coarsening is

$$\dot{D}_p = \frac{K_p}{3}\left(1 - D_p\right)^4 \tag{4.10}$$

where K_p is a parameter which is inversely proportional to the cube of the initial particle radius ($\frac{1}{r^2}$) and proportional to the form of $\exp(-\frac{Q_c}{RT})$, which is

$$K_p \propto D * \exp\left(-\frac{Q_c}{RT}\right) \qquad (4.\,11)$$

where D is the diffusivity constant, Q_c is the sum of activation energy for diffusion creep deformation and the enthalpy of solution of the rate controlling element, R, T are universal gas constant ($8.351\ J/mol$) and temperature respectively (Dyson, 2000). The activation energy is obtained from by plotting the natural log of creep strain rate against the reciprocal of temperature, as shown in Figure 4.8.
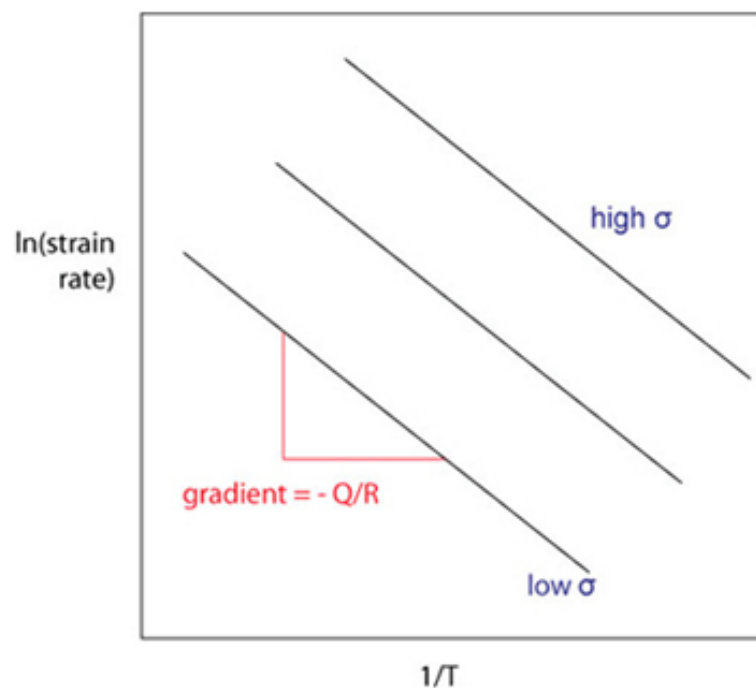
Figure 4. 8: The logarithm of creep strain rate against the reciprocal of temperature

4.7 Experimental data selection and evaluation of cavitation damage effect

4.7.1 Introduction

Cavitation damage is the most important reason which leads to the failure of materials according to the report by TWI (2014). The current research aims to investigate the changings of numbers and size of cavities to determine the cavitation damage mechanism for high chromium alloy steel P91 at the transition stress range under 600℃. However, the current researcher points out that the experimental data of numbers of cavities and size of cavities for high chromium alloy steel P91 under 600℃ are inadequate. Within the transition stress range, the current researcher has selected as much as possible experimental data of cavitation damage for high chromium alloy steels under different temperatures, uniaxial and multi-axial stress states conditions.

In this section, it includes the experimental data selection and evaluation of continuous cavity nucleation and constrained diffusional cavity growth mechanism for high chromium alloy steels under different temperatures, uniaxial and multi-axial stress states conditions.

4.7.2 Experimental data selection and evaluation of continuous cavities nucleation for 9-12%Cr alloy steels

In Dyson's theory (2000), the cavitation damage mechanism includes cavity nucleation-controlled damage mechanism and cavity growth-controlled damage mechanism. When the cavitation damage is cavity nucleation controlled, a large density of cavities is normally observed at a lower stress and high temperature

condition. The continuous cavity nucleation mechanism assumes that the cavity nucleates at the beginning, grows in numbers continuously during creep, and coalesces before the fracture of materials.

For high chromium alloy steel P91 at the transition stress of 80MPa under 600℃, the previous researcher observed that cavity nucleation started less than 50 hours around the large precipitates at grain boundary. The minimum equivalent diameter of cavities is about $0.7um$ at the magnification of x400. At the fracture surface, the average numbers of cavities are about 31—33 on areas of $342\mu m \times 214\mu m$ along the creep specimen axis, and the average equivalent cavity diameter is about $5.5\mu m$. The brittle fracture of high chromium alloy steel P91 is argued due to the high density of cavities nucleation, rapid growth and then coalescence of cavities and large precipitates (Dyson, 2000; Panait et al., 2010a; Panait et al., 2010b). The high density of cavities at fracture surface has also been reported by many other researchers, such as (Gupta et al., 2013; Massé & Lejeail, 2012, 2013; Parker, 2013; Rauch, Maile, & Ringel, 2004).

A. Uni-axial data collection and evaluation for 9-12%Cr alloy steels under 600℃ and 650℃

Firstly, for 9-12% chromium alloy steels under 600℃, the selected experimental data of cavitation damage process at different stress ranges are shown in Table 4.7, 4.8 and 4.9. According to the stress classification for high chromium alloy steel P91 under 600℃, the low stress range is when the applied stress $\sigma < 50$Mpa, and the transition stress range is when the applied stress $70 < \sigma < 110$Mpa. Table 4.7 and Table 4.8 summarize the experimental data of cavitation

damage for high chromium alloy steel P91 under 600℃ at the low stress range

and the transition stress range, respectively.

Table 4. 7: Experimental data of cavitation damage for high chromium alloy steel

P91 under 600℃ at the low stress range

Low stress range	σ <50 MPa
Cavity nucleation	There is no observation on cavitation damage for high chromium alloy steel P91 at the low stress range.
Cavity growth	

Table 4. 8: Experimental data of cavitation damage for high chromium alloy steel

P91 under 600℃ at the transition stress range, data from (Panait et al., 2010a)

Transition stress range	$\sigma = 80MPa$
Cavity nucleation	The number of cavities at fractured surface: 31—33 on areas of $342\mu m \times 214\mu m$
Cavity growth	Cavity size at as received: 0.7 μm, at fractured: 5.5 μm
Minimum strain rate	$1.8 \times 10^{-7} \ h^{-1}$
Reduction of area	37%

Table 4.7 summarises the cavitation damage experimental data for high

chromium alloy steel P91 under 600℃ at the low stress range. However, the

current researcher argues that it is difficult to conclude that the influence of

cavitation damage at the low stress range. Table 4.8 summarises the cavitation

damage for high chromium alloy steel P91 under 600℃ at a transition stress of

80MPa. The numbers of cavities at the fracture surface (31—33 on areas of

$342\mu m \times 214\mu m$), the cavity size at beginning ($0.7\mu m$) and fracture ($5.5\mu m$)

could not identify the influence of continuous cavity nucleation and cavity growth on the fracture of materials after a long-term creep test.

Table 4. 9: Experimental data of cavitation damage for 9%Cr steel (CB8 steel) under 600℃ at the transition stress range, data from (Gupta et al., 2013)

Transition stress range	$120 < \sigma < 150$MPa		
Stress (MPa)	120	135	150
Cavity number density ($10^{-5}\mu m^{-3}$)	1.07	0.62	0.5
Size (μm)	298	300	800
Volume fraction (ppm) / (10^{-4}%)	106 /1.06	143/1.43	1310/13.1
Growth and coalescence fraction (%)	68	41	30

Table 4.9 summarizes the experimental data of cavitation damage for 9%Cr steel (CB8 steel) under 600℃ at different stresses. In Gupta et al. (2013) research, the applied stresses are classified into high stress range ($165 < \sigma < 180$MPa) and low stress range ($120 < \sigma < 150$ MPa). The aim of their research was to determine the natural of the spatial distribution and 3D cavitation characteristics of the creep voids with increasing creep exposure time by analysing the density of cavities, size of cavities, and volume fraction of cavities at different stresses (Gupta et al., 2013). The current researcher argues that the applied stress $120 < \sigma < 150$MPa should be considered as the transition stress range for CB8 steel under 600℃.
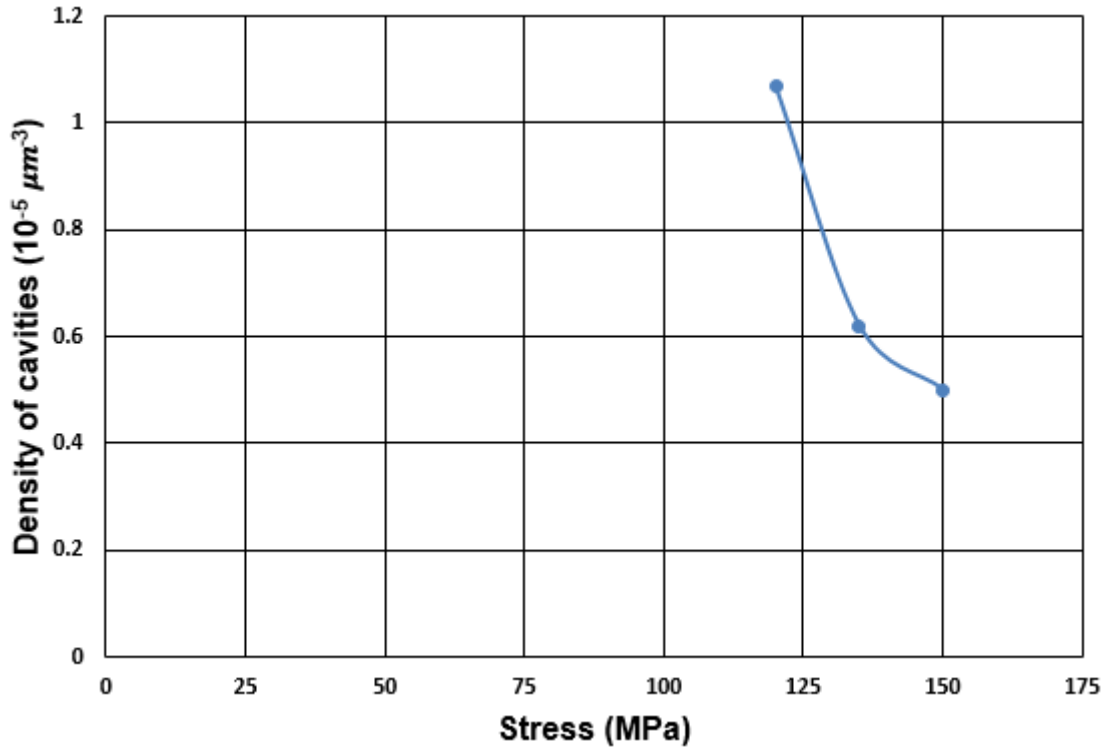
Figure 4. 9: Density of cavities and stress for 9%Cr steel (CB8 steel) under 600℃
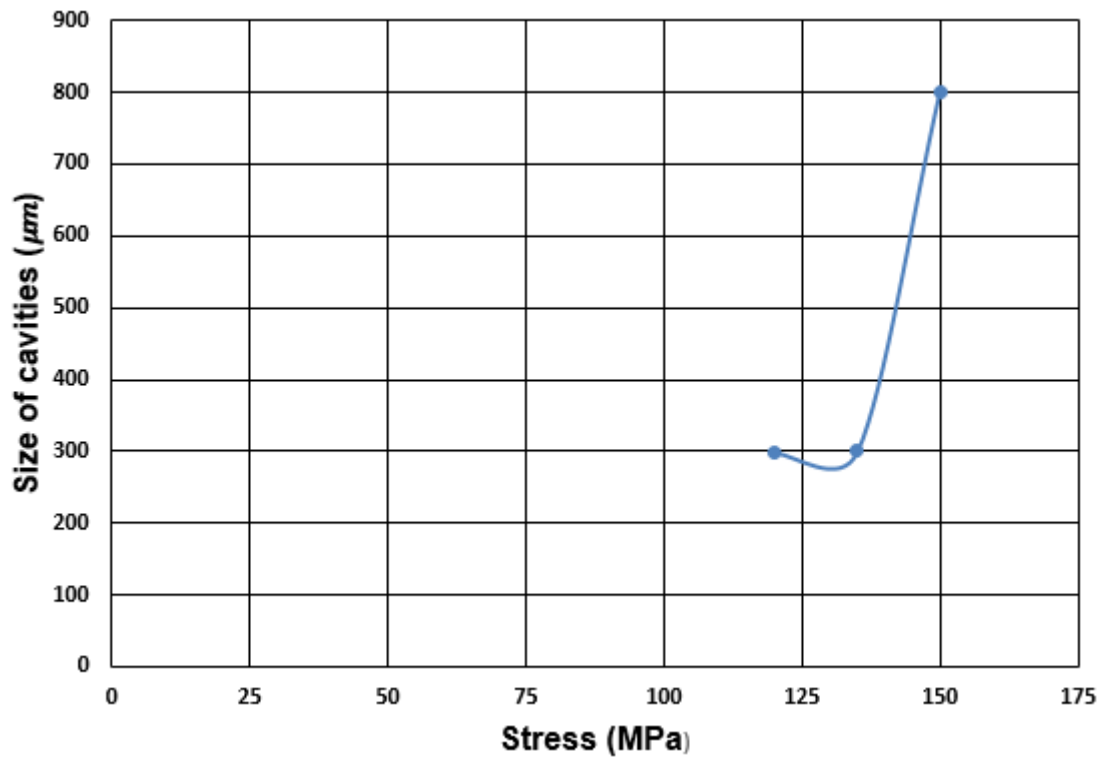
Figure 4. 10: Size of cavities and stress for 9%Cr steel (CB8 steel) under 600℃

Figure 4.9 illustrates the relation between density of cavities and stress for 9%Cr steel (CB8 steel) under 600℃. The density of cavities increases when the applied stress is decreasing. Figure 4.10 illustrates the relation between size of cavities and stress for 9%Cr steel (CB8 steel) under 600℃. The size of cavities decreases when the applied stress is decreasing. In the other words, a higher density but smaller size of cavities will be observed at a lower stress level. The volume fraction at the stress of 120MPa is much smaller than the volume fraction at the stress of 150MPa. However, the cavity growth and coalescence fraction at the stress of 120MPa is higher than the cavity growth and coalescence fraction at the stress of 150MPa. Therefore, the current researcher argues that the continuous cavity nucleation mechanism has more significant influence on the fracture of materials than the cavity growth (in size) mechanism.

Secondly, for 12% chromium alloy steels under 650℃, the selected experimental data of cavitation damage process at the stress of 80MPa are shown in Table 4.10. The relation between number density of cavities and strain is plotted in Figure 4.11. Figure 4.11 illustrates that the cavity nucleation is strain-dependent for 12%Cr-Mo-V steel under 650℃. The relation between number density of cavities and time is plotted in Figure 4.12. The cavity nucleation increases at an exponential rate. In Eggeler et al. (1989) research, he pointed out that the cavities nucleation were observed as early as 1% of strain. The constrained cavity growth method was applied into their research. However, the time to coalescence method as a rupture criterion overestimates the rupture life of materials.

Table 4. 10: Experimental data of cavitation damage for 12%Cr-Mo-V steel under 650℃, data from (Eggeler et al., 1989)

Transition stress range	$\sigma = 80MPa$		
Strain (%)	1	5	12
Time (hours)	23	200	250
Number density of cavities per evaluated cross-section area $(10^{-10}\mu m^{-2})$	0.25	0.62	1.355
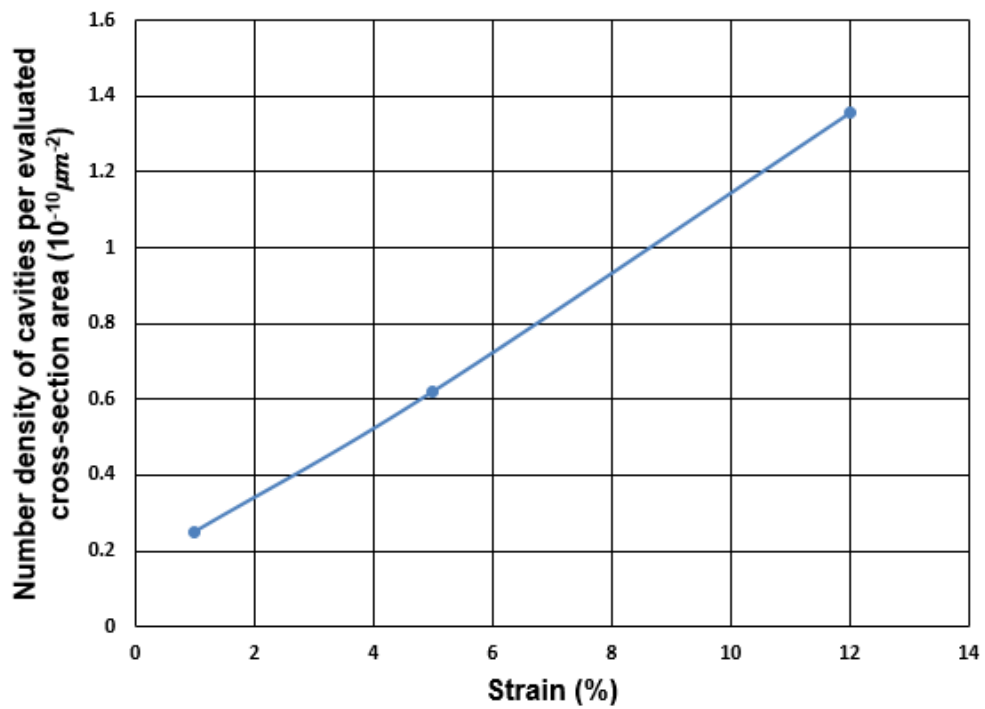
Figure 4. 11: Number density of cavities and strain for 12%Cr-Mo-V steel under 650℃
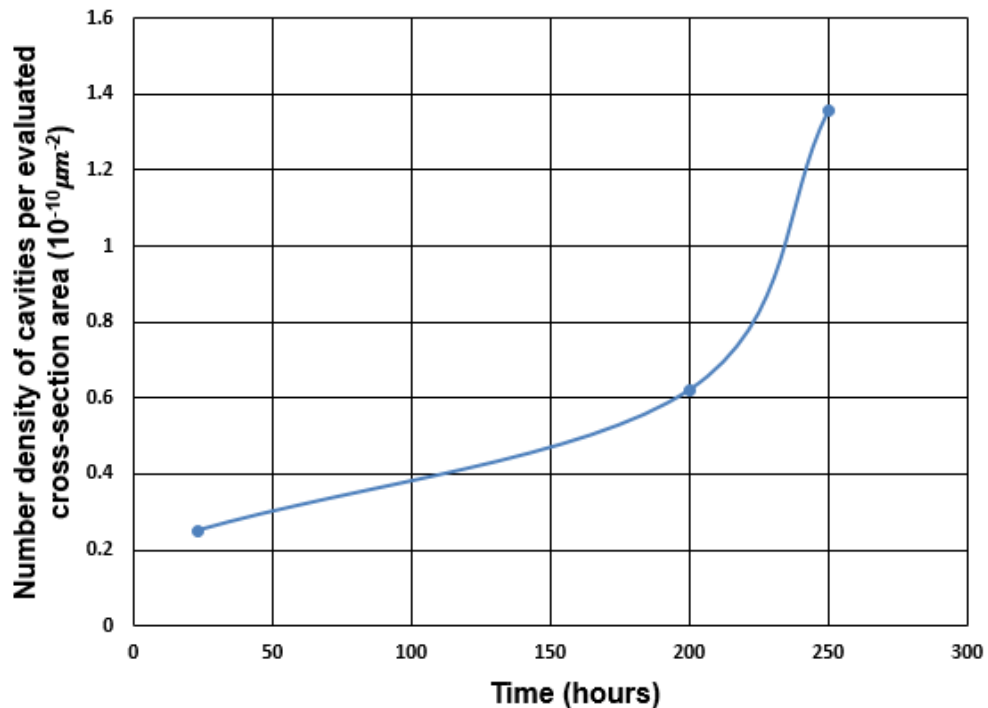
Figure 4. 12: Number density of cavities and time for 12%Cr-Mo-V steel under 650℃

B. Multi-axial stress state data collection and evaluation for 9-12%Cr weldment components under 600℃ and 740℃

Type-IV cracking is caused by cavities nucleation in the heat-affected zone (HAZ) of the welded components during a long-term creep exposure. It has been reported that the 9-12%Cr weldment in such high temperature power plants undergoes the Type-IV cracking (Ogata, Sakai, & Yaguchi, 2009a; Sawada et al., 2011; Tabuchi & Hongo, 2009).

The tri-axial stress state will accelerate the creep damage evaluation in the heat-affect-zone for 9%Cr weldment components. Ogata, Sakai, & Yaguchi (2009a; Ogata, Sakai, & Yaguchi, 2009b) has reported that the life span of HAZ material is approximately 1/5 shorter than the life span of parent material for high

chromium alloy steel P91. Cavities nucleate through the creep damage process. The highest number density of cavities was observed at the center of the fine-grained heat-affected zone. This observation has been supported by researchers, such as (Gaffard et al., 2004; Ogata et al., 2009a, 2010b; Sawada et al., 2010; Watanabe, Tabuchi, Yamazaki, Hongo, & Tanabe, 2006).

Table 4.11 summarizes the experimental data of cavitation damage for high chromium alloy steel P91 weldment component at the stress of 90MPa under 600℃ (Tabuchi & Hongo, 2009). The number density of cavities and the area fraction of cavities are plotted in Figures 4.13 and 4.14, respectively. The previous researcher reported that the creep cavities were initiated at an early stage of lifetime (Tabuchi & Hongo, 2009).

Table 4. 11: Experimental data of cavitation damage for high chromium alloy steel P91 weldment component under 600℃, data from (Tabuchi & Hongo, 2009)

Transition stress range	$\sigma = 90\text{MPa}$				
Time ($tr = 8853h$)	$0.2tr$ $= 2000$	$0.5\ tr$ $= 4425$	$0.7\ tr$ $= 6000$	$0.8\ tr$ $= 7040$	$0.9\ tr$ $= 7970$
Cavity nucleation (number/mm^2)	300	530	750	900	850
Area fraction of cavities	0.00067	0.0028	0.00528	0.0067	0.0082
Cavity growth	No data				
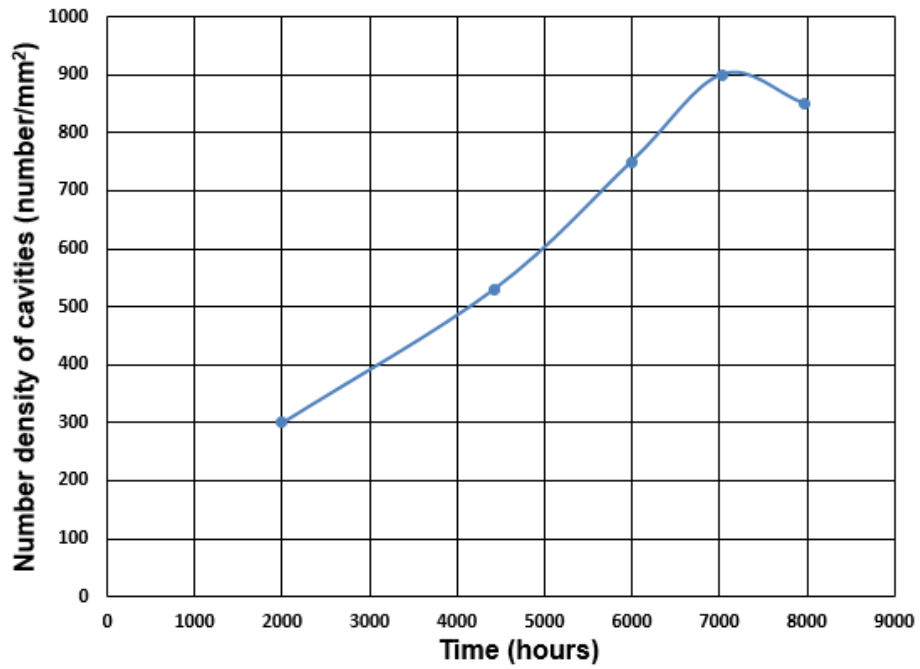
Figure 4. 13: Number density of cavities for high chromium alloy steel P91

weldment component under 600℃
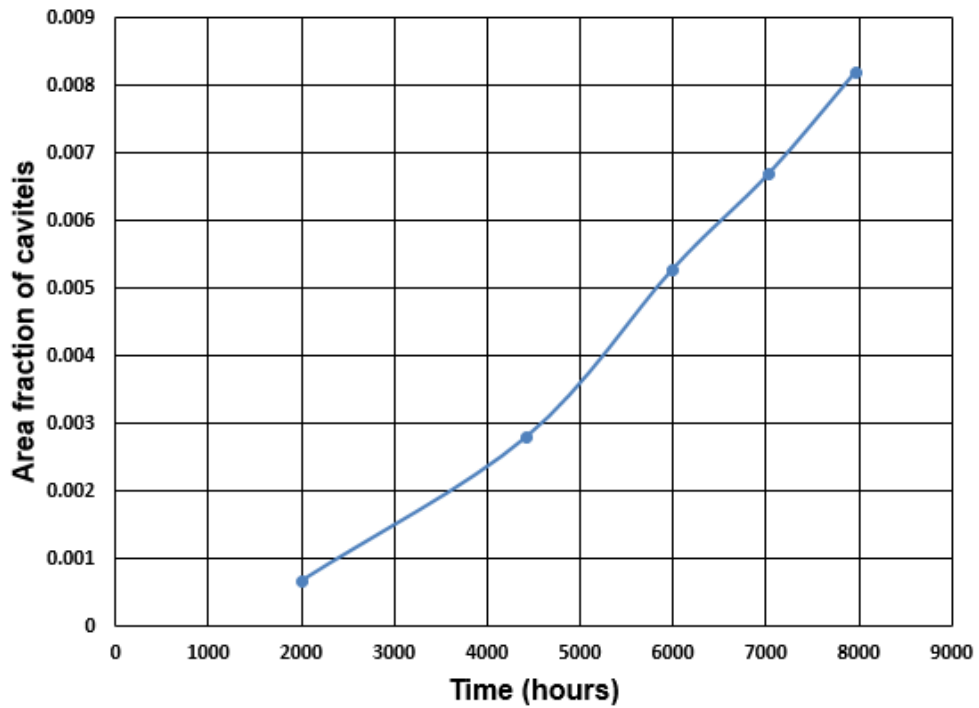
Figure 4. 14: Area fraction of cavities for high chromium alloy steel P91 weldment

component under 600℃

Figure 4.13 illustrates that the number density of cavities increases up to 80% of rupture life, and then the number density of cavities decreases rapidly until fracture for high chromium alloy steel P91 weldment component under 600℃. The drop of number density of cavities might be caused by the coalescence of cavities. Figure 4.14 illustrates that the area fraction of cavities increases until the fracture of material.

Ogata, Sakai and Yaguchi (2011) also reported that the cavity growth in numbers is controlled by diffusional creep deformation for 9%Cr weldment component at an internal pressure 21.7Mpa under 650℃. It has been reported that the cavities nucleate at less than 25% of creep damage and a small amount of cavities was observed at 32% of creep damage until 56% of creep damage. The cavities growth in size is just slightly increased during the creep damage process (Gaffard, Besson, & Gourgues-Lorenzon, 2008).

Table 4.12 summarizes the experimental data of cavitation damage for high chromium alloy steel P91 weldment component under 740℃, data from Ogata, T. Sakai, T. & Yaguchi, M. (2010a). The applied stresses in their research are $40 < \sigma < 70$ MPa. The cavities nucleation process is plotted in Figure 4.15. The number of cavities increases slowly up to 56% of creep damage. However, the number of cavities dramatically increases after 56% creep damage until fraction.

Table 4. 12: Experimental data of cavitation damage for high chromium alloy steel P91 weldment component under 740℃, data from (Ogata et al., 2010a)

Percentage of creep damage (%)	32%	56%	100%
Number of cavities per area ($1/mm^2$)	52	60	710
Time (hours)	2144	3752	6700
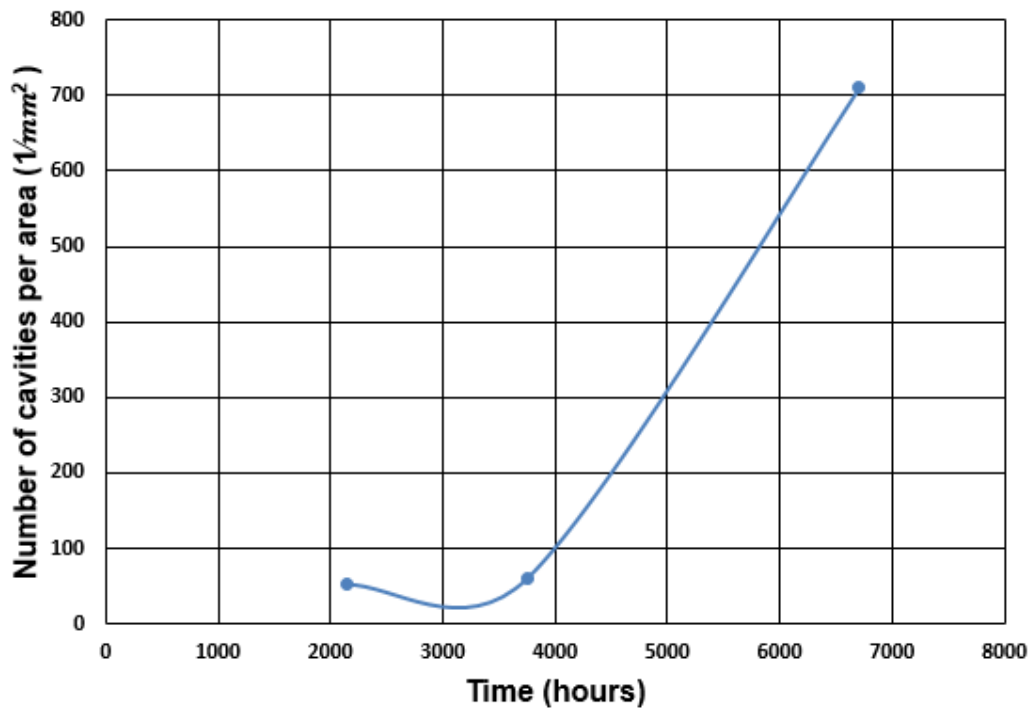
Figure 4. 15: Number of cavities per area in HAZ for high chromium alloy steel P91 weldment component under 740℃

In summary, the brittle fracture of materials is argued by the continuous cavity nucleation, growth and coalescence mechanism for 9-12%Cr weldment components. The cavity growth in size has less influence on the fracture of

materials for 9-12%Cr weldment components. The continuous cavity nucleation is strain-controlled, but, the stress might have influence on the formation of cavities at the beginning of creep for 9-12%Cr alloy steels (Rauch et al., 2004).

The constitutive equation of strain-controlled continuous cavity nucleation rate is

$$\dot{N} = \alpha' \dot{\varepsilon} \qquad (4.\ 12)$$

where $\dot{N}$ is the cavity nucleation rate, α' is material constant (Riedel, 1987).

4.7.3 Experimental data selection and evaluation of constrained diffusional cavity growth for 9-12%Cr alloy steels

A. Experimental data selection and evaluation of cavity growth for 9%Cr steel under 600℃

Recently, some researchers dispute that the continuous cavities nucleation combined with a diffusive growth of cavities and coalescence of large precipitates and cavities might finally lead to a micro or macro crack after a long-term creep test (Abe, 2012; Eggeler et al., 1994; Haney et al., 2009; Massé & Lejeail, 2012, 2013; Panait et al., 2010a; Panait et al., 2010b; Shrestha et al., 2013; Shrestha et al., 2012). Vöse, Otto, Frdelich & Eggeler (2014) also argued that the development of grain boundary cavitation damage at the low stress range is due to the continuous nucleation and diffusive growth of cavities for high chromium alloy steels. However, the cavity growth (in size) mechanism is less understood then the cavity nucleation mechanism (Sklenicka, 2003).

Based on the experimental data selection for 9%Cr alloy steel (CB8 steel) under 600℃ in Table 4.13, the volume fraction of cavities and stress is plotted in Figure 4.16. The growth and coalescence fraction and stress is plotted in Figure 4.17.

Table 4. 13: Experimental data of cavitation damage for 9%Cr steel (CB8 steel) under 600℃ at the transition stress range, data from (Gupta et al., 2013)

Transition stress range	$120 < \sigma < 150$MPa		
Stress (MPa)	120	135	150
Volume fraction (ppm)/(10^{-4}%)	106/1.06	143/1.43	1310/13.1
Growth and coalescence fraction (%)	68	41	30
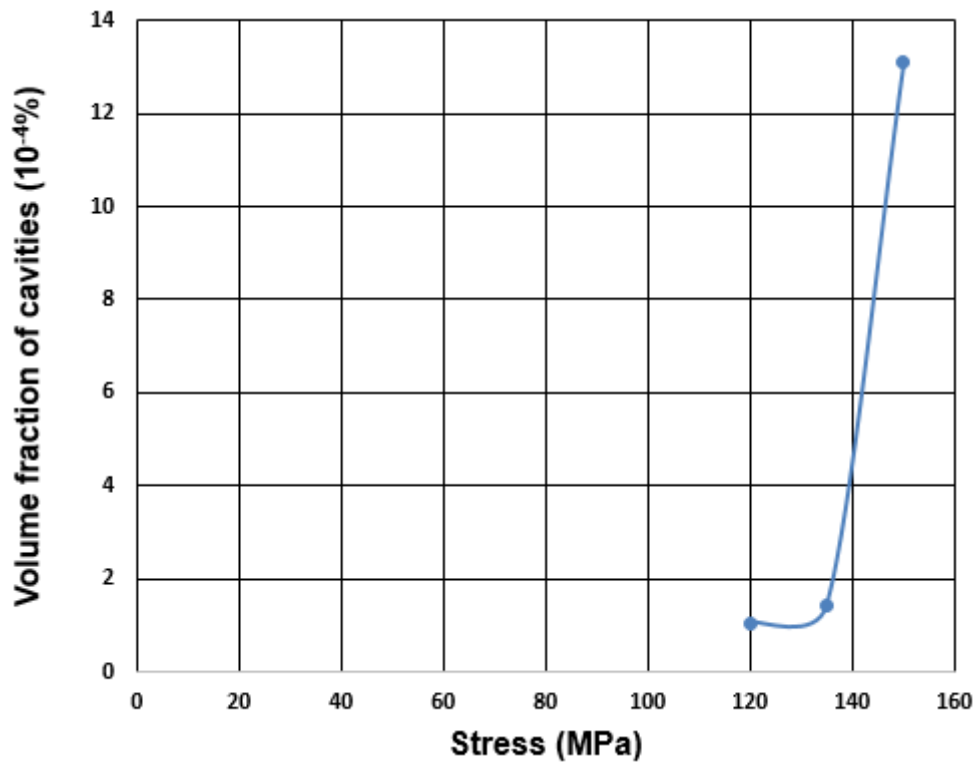
Figure 4. 16: Volume fraction of cavities and stress
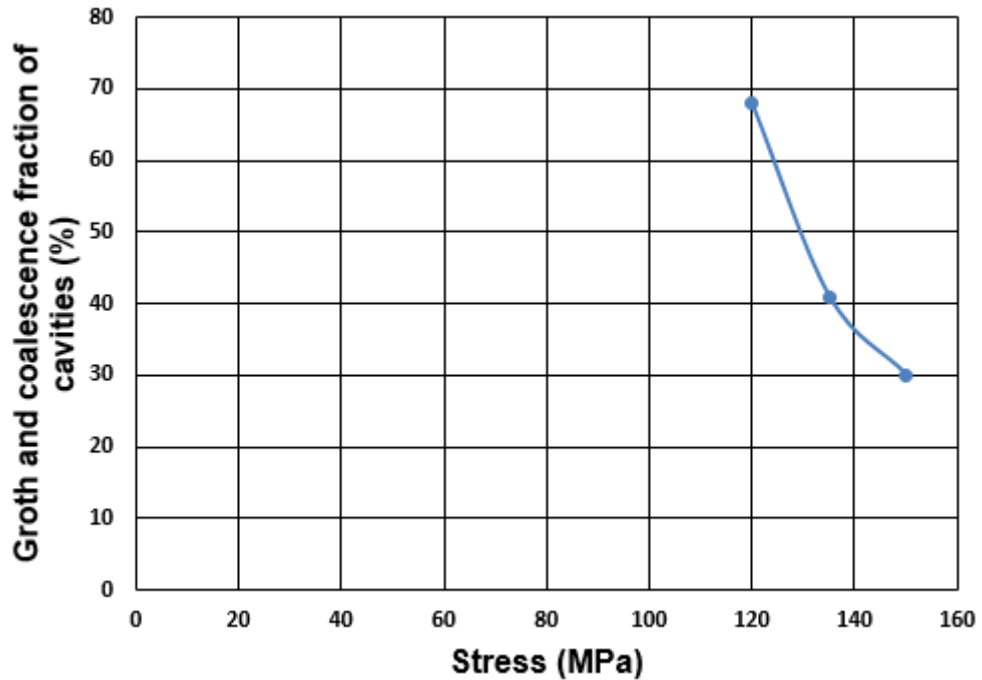
Figure 4. 17: Growth and coalescence fraction of cavities and stress

Figure 4.16 shows that the volume fraction of cavities decreases when the stress is decreasing. The volume fraction of cavities at the stress of 150MPa is dramatically decreased at the stress of 135MPa. There is a smooth decreasing of volume fraction of cavities from stress 135MPa to 120MPa. The volume fraction of cavities at a lower stress level is smaller than the volume fraction of cavities at a high stress level. Gupta et al. (2013) has also reported that the volume fraction of cavities at lower stress level is about 3 times smaller than the volume fraction of cavities at higher stress level. In the other words, the cavity growth in size has less influence on the failure of materials at lower stress levels.

Figure 4.17 shows that the growth and coalescence fraction of cavities increases when the stress is decreasing. There is a significant increasing of cavity growth and coalescence fraction from stress 135MPa to stress 120MPa. In summary, the

cavity nucleation, growth and coalescence has more influence on the fracture of materials than the cavity growth in size (Gupta et al., 2013).

B. Experimental data selection and evaluation of constrained diffusional cavity growth for high chromium alloy steel P91 under 600℃

The constrained diffusional cavity growth mechanism has been introduced in Chapter 2. Theoretically, whether constrained diffusional cavity growth or un-constrained diffusional cavity growth could be determined by comparing the theoretically minimum creep strain rate with the practical value. The diffusional cavity growth is constrained if the experimental minimum creep strain rate is less than the theoretically minimum creep strain rate.

The material parameters for high chromium alloy steel P91 at the transition stress of 80MPa under 600℃ are summarized in Table 4.14.

Table 4. 14: Material parameters for high chromium alloy steel P91 at the stress of 80MPa under 600℃

Constants	q'	Ω	k	δD_b
Values	12.5	1.21*10⁻²⁹m^3	1.38*10⁻²³ J/K	$3.56 * 10^{-21} m^3/s$
Constants	d	T	$q(\omega)$	λ
Values	$0.35 * 10^{-6} m$	873K	1	$1 * 10^{-6}$

The constants $\alpha_v, k, R, \delta D_b, \Omega, q(\omega)$ are obtained from Riedel's book, appendix A.1 (1987). The parameters d and λ are obtained from Shrestha et al (2013).

- Theoretical minimum creep strain rate for high chromium alloy steel P91 at the stress of 80MPa under 600℃ can be obtained by

$$\dot{\varepsilon}_e^\infty = \frac{2q'\Omega\delta D_b\sigma_e^\infty}{q(\omega)kT\lambda^2 d} \approx 2.97281 * 10^{-8} \ (s^{-1}) \tag{4.13}$$

$$\dot{\varepsilon}_e^\infty = A(\sigma_e^\infty)^n \approx 1.01827 * 10^{-8} \ (s^{-1}) \tag{4.14}$$

where stress exponent $n \approx 4$.

- Experimental minimum creep strain rate for high chromium alloy steel P91 at the stress of 80MPa under 600℃ was reported by Panait (Panait et al., 2010a; Panait et al., 2010b). The experimental minimum creep strain rate is

$$\dot{\varepsilon} = 1.8 \times 10^{-7} \ (h^{-1}) \approx 3.06 \times 10^{-11} (\ s^{-1}) \tag{4.15}$$

Therefore, the diffusional cavity growth for high chromium alloy steel P91 at the stress of 80MPa under 600℃ is constrained. However, the constrained cavity growth model combined with the power law function could not accurately predict the lifetime for 9%Cr alloy steels. The creep strain rate has been underestimated by the constrained cavity growth model (Ogata et al., 2010b, 2011).

4.7.4 Constitutive equations for cavitation damage effect

In conclusion, the brittle rupture for 9-12%Cr alloy steels at the transition stress range is caused by the cavitation damage. The cavitation damage mechanism is argued as continuous cavities nucleation assisted by the constrained diffusional cavities growth at the transition stress range for 9-12%Cr alloy steels under different stresses and temperatures. However, the continuous cavities nucleation,

growth and coalescence mechanism has significant influence on the fracture of 9-12%Cr alloy steels.

The continuous cavities nucleation rate is argued as strain-controlled. According to Dyson's cavitation damage theory, the cavitation damage rate is

$$\dot{\omega} = \frac{K_N}{\varepsilon_{fu}}\dot{\varepsilon} = C\dot{\varepsilon} \qquad (4.\ 16)$$

where K_N has an upper limit of $\approx \frac{1}{3}$, ε_{fu} is uniaxial strain at fracture, cavitated area $\omega = \frac{1}{3}$ at failure for uni-axial, cavitated area $\omega = 1$ at failure for multi-axial stress state.

The material constant C is related to the failure criterion ($C = 1/3\varepsilon_R$ at uni-axial stress). However, the constant C had not been discussed in Dyson's theory (Dyson, 2000). Perrin and Hayhurst (1996a) had argued that the material constant C may be determined from the experimental failure strain rate by

$$C = C_0 \exp(-\frac{Q_c}{RT}) \qquad (4.\ 17)$$

where C_0 is the constant of proportionality, Q_c is the activation energy.

4.8 Experimental data selection and evaluation of failure criteria

The influence of hydrostatic stress on the rupture of materials is controversial. Some researchers argued that the hydrostatic stress has no effect on the fracture of materials. The rupture lifetime of materials at the multi-axial stress condition is (Sket et al., 2010)

$$t_f = M(\alpha\sigma_1 + \beta\sigma_h + \gamma\sigma_e)^{-x} \tag{4. 18}$$

where M and x are temperature dependent constants, σ_1 is the maximum principal stress with $\sigma_1 > \sigma_2 > \sigma_3$, σ_e is the von Mises stress (equivalent stress), σ_h is the hydrostatic stress, $\alpha, \beta, and\ \gamma$ are material parameters. These parameters indicate the contribution of each stress to the final rupture with the relations $(\alpha + \beta + \gamma = 1)$.

If the hydrostatic stress has no effect on the rupture of materials, the hydrostatic stress can be ignored (β=0). The rupture lifetime of materials becomes

$$t_f = M(\alpha\sigma_1 + (1 - \alpha)\sigma_e)^{-x} \tag{4. 19}$$

This expression of rupture lifetime indicates that the contribution of the maximum principal stress and the equivalent stress to the fracture of materials at multi-axial stress states condition.

However, some researchers argued that the hydrostatic stress has contribution to the fracture of materials at multi-axial stress condition. Sawada (2010) has reported that the multi-axiality of stress state is defined by the Von Mises stress and the hydrostatic stress for high chromium alloy steel E911 under 600℃ after a long-term creep test. The hydrostatic stress is

$$\sigma_h = \frac{\sigma_1 + \sigma_2 + \sigma_3}{3} \tag{4. 20}$$

The ratio of equivalent stress and hydrostatic stress is

$$q = \frac{1}{\sqrt{3}} \frac{\sigma_v}{\sigma_h} \tag{4. 21}$$

where $q = 2$ (Sawada et al., 2010).

In the current research, at multi-axial stress state condition, the failure criterion is identified by the ratio of maximum principal stress and the equivalent stress for 9-12%Cr alloy steels in the current research. Uni-axial is the special case when the maximum principal stress equals the effective stress equals $\sigma_1 = \sigma_e$. The current researcher argues that the hydrostatic stress could be ignored because the hydrostatic stress only has influence on the volume changes. The hydrostatic stress does not cause plastic deformation. If assume $\sigma_v = 1$, then $\sigma_h = 0.3$, and the maximum stress $\sigma_1 + \sigma_2 + \sigma_3 = 0.9$. The combination of Von Mises stress and the maximum principal stress have significant contributions to the final rupture stress at multi-axial stress state. This point of view has been supported by many researchers (Hyde et al., 2010a, 2010b; Liu & Murakami, 1998; Tabuchi & Hongo, 2009).

Therefore, the rupture stress is written as

$$\sigma_r = \alpha\sigma_1 + (1 - \alpha)\sigma_e \qquad (4.22)$$

where α is a material parameter. α is related to the multi-axial stress state behavior of the materials. α is obtained by determining the time to failure of notched bar specimens. $\alpha = 0.3$ for Mod.91Cr-Mo steel under 600°C at multi-axial stress state (Tabuchi & Hongo, 2009), $\alpha = 0.215$ for high chromium alloy steel P91 parent materials under 650°C (Hyde et al., 2010b).

The expression of the cavitation damage rate at multi-axial stress state is suggested as (Perrin & Hayhurst, 1996a)

$$\dot{\omega} = C\dot{\varepsilon}_e \left(\frac{\sigma_1}{\sigma_e}\right)^v \qquad (4.\ 23)$$

where C is the proportionality constant, the stress index v defines the multi-axial stress rupture criterion of materials. v is a material constant which is related to tri-axial stress sate sensitivity of the materials. The stress index v can be determined from the FE modelling of the notched bar creep rupture tests. $v = 2.8$ for high chromium alloy steel P91 (Hyde et al., 2006a).

Chapter 5

Proposed constitutive equations for high chromium alloy steel P91 at the transition stress range under 600℃

5.1 Key findings of selected experimental data for high chromium alloy steel P91 at the transition stress range under 600℃

To improve the constitutive equations for high chromium alloy steel P91 at the transition stress range under 600℃, chapter 4 mainly summarizes 7 aspects of experimental data selection and evaluation. The key findings of the selected experimental data are

1. The classification of stress ranges for high chromium alloy steel P91 under 600℃, as shown in Table 4.2.

2. The brittle rupture assisted by the N-H diffusion creep deformation is argued as the creep deformation and rupture mechanism for high chromium alloy steel P91 at the transition stress range under 600℃, as discussed in section 4.3.

3. The power law function is argued to be used in the proposed constitutive equations to describe the relation between creep strain rate and stress, as discussed in section 4.4.

4. The isotropic hardening effect and dimensionless damage variable H are used in the proposed constitutive equations to describe the strain hardening effect in the primary creep stage, as discussed in section 4.5.

5. The particle coarsening effect and dimensionless variable D_p are used in the proposed constitutive equations to describe the particle coarsening effect in the secondary creep stage, as discussed in section 4.6.

6. The continuous cavity nucleation (in numbers) with constrained cavity growth (in size) mechanism is argued as the cavitation damage mechanism for high chromium alloy steel P91 at the transition stress range under $600°C$. However, the continuous cavity nucleation, growth and coalescence has more significant influence on the fracture of materials than the cavity growth. The creep strain rate has been underestimated by the constrained cavity growth model combined with the power law function, as discussed in the section 4.7.

7. The failure criterion is identified by the ratio of maximum principal stress and the equivalent stress for 9-12%Cr alloy steels at multi-axial stress state. At uni-axial situation, the maximum principal stress equals the equivalent stress.

5.2 Formation of proposed constitutive equations for high chromium alloy steel P91 at the transition stress range under 600°C

Based on these 7 key findings and KRH constitutive equations, the proposed constitutive equations at uni-axil and multi-axial stress sate are

Uni-axial form

$$
\left[
\begin{array}{l}
\dot{\varepsilon} = A_1 \left(\frac{\sigma(1-H)}{(1-D_p)(1-\omega)} \right)^n \\[2mm]
\dot{H} = \frac{h}{\sigma} \left(1 - \frac{H}{H^*} \right) \dot{\varepsilon} \\[2mm]
\dot{D}_p = \frac{K_p}{3} \left(1 - D_p \right)^4 \\[2mm]
\dot{\omega} = C_1 \dot{\varepsilon}
\end{array}
\right.
\tag{5.1}
$$

Multi-axial form

$$
\left[
\begin{array}{l}
\dot{\varepsilon}_{ij} = \frac{2S_{ij}}{3\sigma_e} A_2 \left(\frac{\sigma_e(1-H)}{(1-D_p)(1-\omega)} \right)^n \\[2mm]
\dot{H} = \frac{h}{\sigma_e} \left(1 - \frac{H}{H^*} \right) \dot{\varepsilon} \\[2mm]
\dot{D}_p = \frac{K_p}{3} \left(1 - D_p \right)^4 \\[2mm]
\dot{\omega} = C_2 N \dot{\varepsilon}_e \left(\frac{\sigma_1}{\sigma_e} \right)^v
\end{array}
\right.
\tag{5.2}
$$

where $N = 1$, $\sigma_1 > 0$ (tensile); $N = 0$, $\sigma_1 < 0$ (compressive). $A1$ and $A2$ are material parameters which relate to the temperature, grain size, activation energy, atomic volume. h, H^*, K_p are material constants, which are determined by fitting a number of uni-axial strain rate curves obtained from creep tests at a given temperature to the uni-axial strain time relationship. v is the index of multi-axial stress state of materials, which can be determined from the FE modelling of the notched bar creep rupture tests. $C1$ and $C2$ relate to the cavity nucleation rate, might also accelerate by the large participates coarsening at tertiary creep

stage. The damage variable H ($0 < H < H^* < 1$) indicates the strain hardening effect during primary creep stage. The damage variable D_p ($0 < D_p < 1$) indicates the evolution of the spacing of the carbide precipitates. The damage variable ω represents the inter-granular cavitation damage. The value of the damage variable ω indicates the cavitated area fraction of cavitation damage at failure, which in uni-axial case $\omega \cong \frac{1}{3}$; in multi-axial stress state case, $\omega \cong 1$ (Hyde et al., 2006a). S_{ij} is deviatoric stress.

The material parameters $A1$ and $A2$ relate to the temperature, grain size, activation energy, atomic volume at uni-axial condition and multi-axial stress state condition, respectively. For example, the material parameter $A1$ can be obtained from

$$A_1 = \frac{\alpha_v \sigma \Omega D_v}{kTd^2} \tag{5.3}$$

$$D_v = D_{v0} \exp\left(-\frac{Q_v}{RT}\right) \tag{5.4}$$

The material parameters $C1$ and $C2$ relate to the cavity nucleation rate, but, it might also be accelerated by the coarsening effect (large precipitates, cavities, sub-grain) at tertiary creep stage. For example, the parameter $C1$ might be determined by (Perrin & Hayhurst, 1996a)

$$C1 = C_0 \exp\left(-\frac{Q_c}{RT}\right) \tag{5.5}$$

156

However, the value of material parameter $C1$ might be much larger at the lower stress levels. The coarsening of large precipitates, sub-grain and cavities might accelerate the fracture of materials.

5.3 Comparison of the proposed constitutive equations with KRH constitutive equations

The uni-axial form of KRH constitutive equations are (Hyde et al., 2006a)

$$\begin{bmatrix} \dot{\varepsilon} = A\sinh(\frac{B\sigma(1-H)}{(1-\varphi)(1-\omega)}) \\ \dot{H} = \frac{h}{\sigma}\left(1 - \frac{H}{H^*}\right)\dot{\varepsilon}_c \\ \dot{\varphi} = \frac{K_C}{3}(1-\varphi)^4 \\ \dot{\omega} = D\dot{\varepsilon}_c \end{bmatrix} \qquad (5.6)$$

The material constant A is related to the activation energy for volume diffusion Q_A

$$A = A_0 B\exp(-\frac{Q_A}{RT}) \qquad (5.7)$$

A_0 is the constant of proportionality. The constant B is temperature dependence and also is related to the kinetics of dislocation motion. The constant B might have the expression as

$$B = B_0\exp(-\frac{Q_B}{RT}) \qquad (5.8)$$

B_0 is the constant of proportionality. Q_B is the activation energy which relates to the kinetics of dislocation motion.

The multi-axial from of KRH constitutive equations are (Evans & Wilshire, 1993; Hyde et al., 2006a)

$$\begin{cases} \dot{\varepsilon}_{ij} = \frac{3}{2} \frac{S_{ij}}{\sigma_{eq}} A \sinh(\frac{B\sigma(1-H)}{(1-\omega_2)(1-\varphi)}) \\ \dot{H} = \frac{h}{\sigma_{eq}} \left(1 - \frac{H}{H^*}\right) \dot{\varepsilon}_c \\ \dot{\varphi} = \frac{K_C}{3}(1-\varphi)^4 \\ \dot{\omega}_2 = DN\dot{\varepsilon}_c(\frac{\sigma_1}{\sigma_{eq}})^\nu \end{cases} \qquad (5.9)$$

where $N = 1, \sigma_1 > 0\ (tensile); N = 0, \sigma_1 < 0\ (compressive)$. A, B, h, H^*, K_c and D are material constants, which are determined by fitting a number of uni-axial strain rate curves obtained from creep tests at a given temperature to the uni-axial strain time relationship. ν is the index of multi-axial stress state of materials, which can be determined from the FE modelling of the notched bar creep rupture tests. The damage variable H $(0 < H < H^*)$ indicates the strain hardening effect during primary creep stage. The value of H increases from 0 until the maximum value H^* from primary creep stage to secondary creep stage. The damage variable φ indicates the evolution of the spacing of the carbide precipitates. The damage variable φ varies from 0 to 1 $(0 < \varphi < 1)$. The damage variable ω_2 represents the inter-granular cavitation damage. The value of the damage variable ω_2 indicates the cavitated area fraction of cavitation damage at failure, which in uni-axial case $\omega_2 \cong \frac{1}{3}$; in multi-axial stress state case, $\omega_2 \cong 1$ (Hyde et al., 2006a).

Firstly, the constitutive equations in the current research is proposed based on the KRH constitutive equations. Within the continuum damage mechanics, the

constitutive equations combined with the microstructural degradation is argued as the most effective way to predict the lifetime of materials. The microstructural degradation of strain hardening, particle coarsening and cavitation damage are considered in both KRH constitutive equations and the proposed constitutive equations.

Secondly, the current research aims to improve the KRH constitutive equations for high chromium alloy steel P91 at the transition stress range. In KRH constitutive equations, the hyperbolic law function does not consider the creep deformation and damage mechanism at different stress ranges. However, in the current model, the power law function could consider the different creep deformation and damage mechanism at different stress ranges with different stress exponent. For high chromium alloy steel P91 under $600°C$, the stress exponent $n \approx 1$ at the low stress range, $n \approx 4$ at the transition stress range, and $n > 10$ at the high stress range.

Thirdly, the strain hardening effect and particle coarsening effect at different stress ranges are inevitable. The dimensionless damage variables H and D_p (φ in KRH constitutive equations) are used in both KRH constitutive equations and the proposed constitutive equations to describe the strain hardening effect and particle coarsening effect.

However, the cavitation damage is different at different stress ranges. The ductile rupture is identified at the high stress range. The brittle rupture is identified at the transition stress range. A high density but small size of cavities are observed at the transition stress range. The continuous cavity nucleation, growth and

coalescence finally lead to the fracture of materials. However, the premature failure at the transition stress range is argued by the coarsening effect. The coarsening of large precipitates, sub-grain and cavities might accelerate the fracture of material.

Lastly, the most important aspect is the definition and determination of material parameters. For example, the material parameters $A1, A2$ and C in the proposed constitutive equations model. The material parameters A, B and D in the KRH constitutive equations. The failure criteria in both KRH constitutive equations and the proposed constitutive equations at multi-axial stress sate are identified by the ratio of the maximum principal stress and the equivalent stress for high chromium steels. The time to fracture in both KRH constitutive equations and the proposed constitutive equations is determined by the cavitated area fraction at failure, which is $\omega_2 \cong \frac{1}{3}$ in uni-axial case, $\omega_2 \cong 1$ in multi-axial stress state case.

Chapter 6

Validations and discussions

6.1 Introduction

Case study method is used in the current research to validate the feasibility of the proposed constitutive equations for high chromium alloy steel P91 at the transition stress under 600℃. In the uni-axial situation, the validation method is to check the predicted creep strain and creep strain rate curves by comparing with the experimental data of creep strain and creep strain rate.

Firstly, case study 1 is the comparison of the predicted results for high chromium alloy steel P91 at the stresses of 80MPa and 70MPa under 600℃ with the experimental data. The experimental lifetime of high chromium alloy steel P91 at the stress of 80MPa under 600℃ is about 113,431 hours in uni-axial situation. The experimental lifetime of high chromium alloy steel P91 at the stress of 70MPa under 600℃ is about 80,000 hours in uni-axial situation. At the multi-axial stress state, the validation method is considered in the future work due to the inadequate experimental data of material parameters for high chromium alloy steel P91 under 600℃.

Secondly, case study 2 is the comparison of the predicted results by the proposed constitutive equations and the KRH constitutive equations for high chromium alloy steel P91 at the stress of 80MPa under 600℃.

6.2 Validations of the proposed constitutive equations for high chromium alloy steel P91 at the stresses of 70MPa and 80MPa under 600℃

6.2.1 Selection of material parameters for high chromium alloy steel P91 under 600℃

The material parameters for high chromium alloy steel P91 at the stress of 80MPa under 600℃ are summarized in Table 6.1. The material parameters for high chromium alloy steel P91 under 625℃ and 650℃ are summarized in Table 6.2.

Table 6. 1: The material constants for high chromium alloy steel P91 at the stress of 80MPa under 600℃

Constants	A	K_p	C	n	h	H^*
Values	2.5×10^{-16}	2.7×10^{-4}	6.5	4	9000	0.203

Table 6. 2: Materials constants for high chromium steels P91 under 650℃ (Bar 257) and 625℃ (A-369 FP91) (Hyde et al., 2006a)

Constants	h	H^*	K_p	D
650℃	10000	0.35	4.998×10^{-4}	2
625℃	9000	0.203	2.7×10^{-4}	6.2

The proportional material parameter A is related to the activation energy, grain size, temperature, and atomic volume at a given temperature in the proposed constitutive equations. The proportional material parameter A can be determined by equation 4.5 in the current research. The material parameter C is related to the cavity nucleation rate, and might accelerate by the coarsening rate before

fracture. The material constants h, H^*, K_p and C can be determined by fitting a number of uni-axial strain rate curves obtained from creep tests at a given temperature to the uni-axial strain time relationship. The stress exponent n can be determined by plotting the creep strain rate as a function of stress at a given temperature.

In the current research, the values of material parameters h, H^*, K_p are selected from the previous research for high chromium alloy steel A-369 FP91 under 625 ℃ (Hyde et al., 2006a). The experimental values of these material parameters for high chromium alloy steel P91 under 600℃ are not available so far based on the literature review study (updated until July in 2014). According to Table 4.2, the stress changes under 600℃ vary from 70MPa to100MPa and the stress changes under 625℃ vary from 50 to 90MPa for high chromium alloy steel T91. The stress of 80MPa belongs to the transition stress range for high chromium alloy steel T91 under 600℃ and 625℃. Table 6.2 shows that the material parameters for high chromium alloy steel P91 under 625℃ and 650℃. There is a small difference of these material parameters between 625℃ and 650℃. Therefore, the current researcher assumes that the minor difference of these values of material parameters at different temperatures could be ignored. The material parameters for high chromium alloy steel P91 under 625℃ are selected for the high chromium alloy steel P91 under 600℃.

However, the current research argues that the value of material parameter C is related to the cavity nucleation rate, and might accelerate by the coarsening rate before fracture. The value of material parameter C under 600℃ should higher

than the value of 6.2 under 625℃ (no discussion of determination of material parameter D in Dyson's work). The value of material parameter $C = 6.5$ is assumed here.

6.2.2 Comparison of the predicted results with experimental results
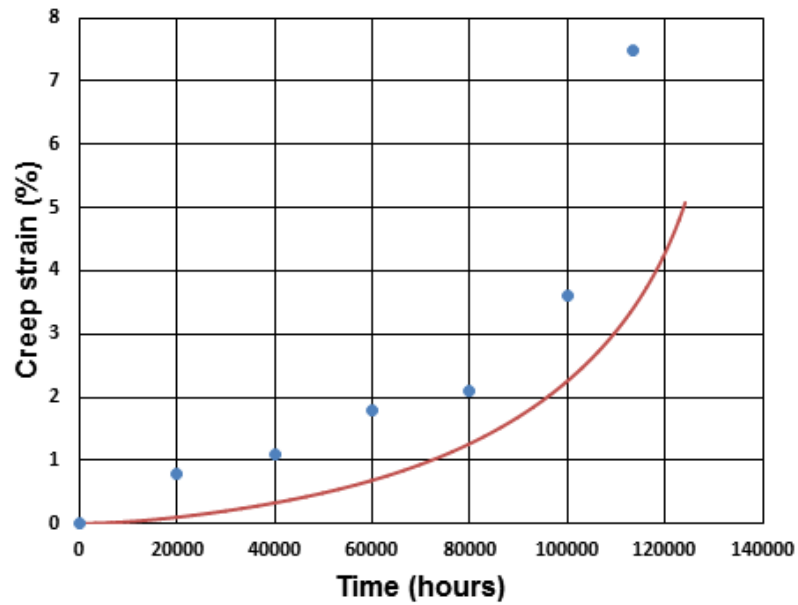
Figure 6. 1: Predicted creep strain curve for high chromium alloy steel P91 at the stress of 80MPa under 600℃ (dots are experimental values, data from (Panait et al., 2010b)
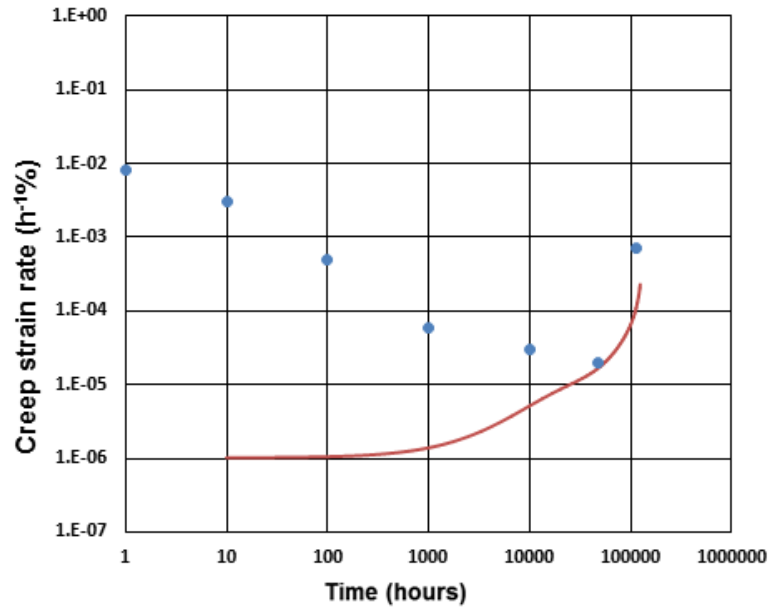
Figure 6. 2: Predicted creep strain rate curve for high chromium alloy steel P91 at the stress of 80MPa under 600℃ (dots are experimental values, data from (Panait et al., 2010b)
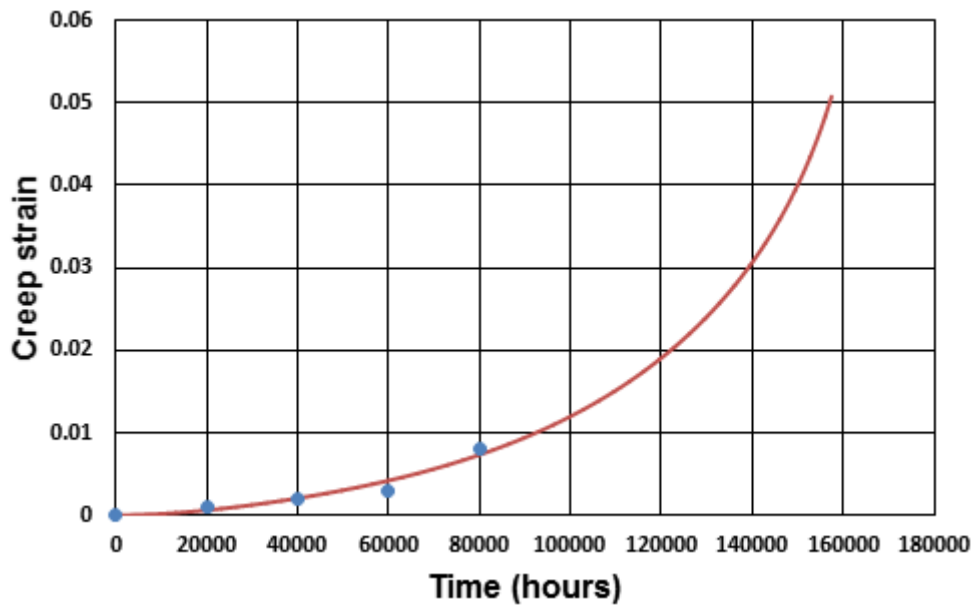
Figure 6. 3: Predicted creep strain curve for high chromium alloy steel P91 at the stress of 70MPa under 600℃ (dots are experimental values, data from (Sawada et al., 2011)
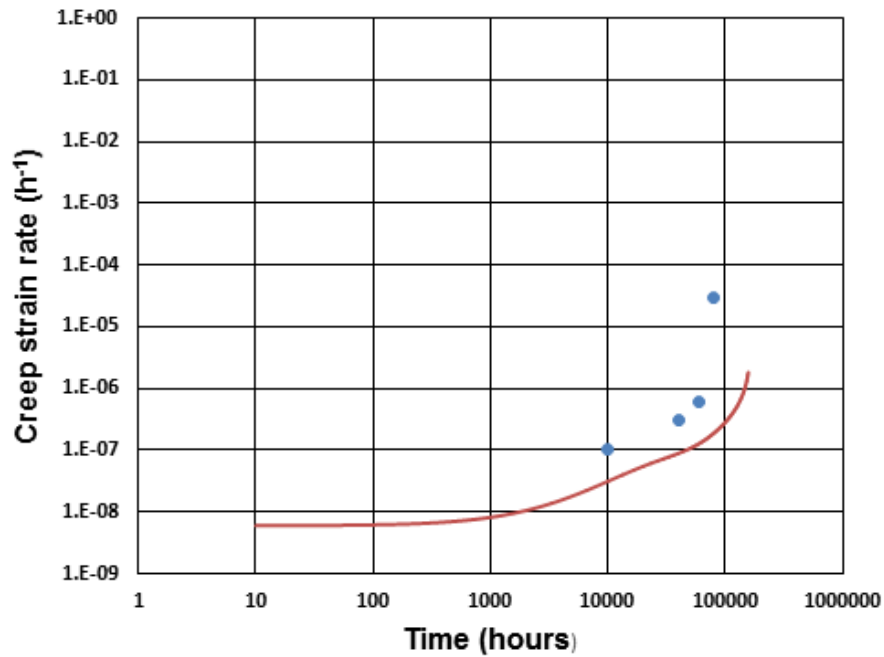
Figure 6. 4: Predicted creep strain rate curve for high chromium alloy steel P91 at the stress of 70MPa under 600℃ (dots are experimental values, data from (Sawada et al., 2011)

6.2.3 Discussion 1

Figure 6.1 and Figure 6.2 represent the comparison between the predicted results and the experimental values (dots) for high chromium alloy steel P91 at the stress of 80MPa under 600℃. It can be seen that the predicted creep strain and strain rate is smaller than the experimental values. Here are several reasons could be considered for underestimating the creep strain and strain rate for high chromium alloy steel P91 at the stress of 80MPa under 600℃. Firstly, the selection of material parameters for high chromium alloy steel P91 at the stress of 80MPa under 600℃. The influence of temperature on the selection of material parameters should be investigated, especially for the material parameter A which is related to the temperature.

166

Secondly, the cavitation damage parameter C might have significant influence on the fracture of materials and the creep strain rate. At the transition stress range, the premature failure is argued by the microstructural degradation, especially the coarsening of large precipitates, sub-grain and cavities. If the cavitated area fraction $\omega = 1/3$ in uni-axil situation, the predicted lifetime for high chromium alloy steel P91 at the stress of 80MPa under 600℃ is 124,115 hours. The experimental lifetime for high chromium alloy steel P91 at the stress of 80MPa under 600℃ is 113,431 hours (Panait et al., 2010a; Panait et al., 2010b). The lifetime error is about 9.4%. Even the lifetime error is about 9.4%, however, the proposed constitutive equations could not accurately predict the creep behaviors for high chromium alloy steel P91 at the transition stress range under 600℃.

Figure 6.3 and Figure 6.4 represent the comparison between the predicted results and the experimental values (dots) for high chromium alloy steel P91 at the stress of 70MPa under 600℃. As discussed before, for high chromium alloy steel P91 under 600℃, the transition stress range varies from 70MPa to 110MPa with a stress exponent $n \approx 4$. The stress of 70MPa and stress 110MPa are the boundary stresses. The creep deformation and damage mechanism is more complicated at the critical stresses. It has been argued that both diffusion and dislocation creep deformation could contribute to the creep deformation mechanism together. The proposed constitutive equations only could describe the creep behaviors at the primary creep stage, as shown in Figure 6.3. The creep strain rate has been underestimated by the proposed constitutive equations model, as shown in Figure 6.4. The proposed constitutive equations are invalid at the stress of 70MPa.

6.2.4 Comparison of the proposed constitutive equations with KRH constitutive equations for high chromium alloy steel P91 at the stress of 80MPa under 600℃
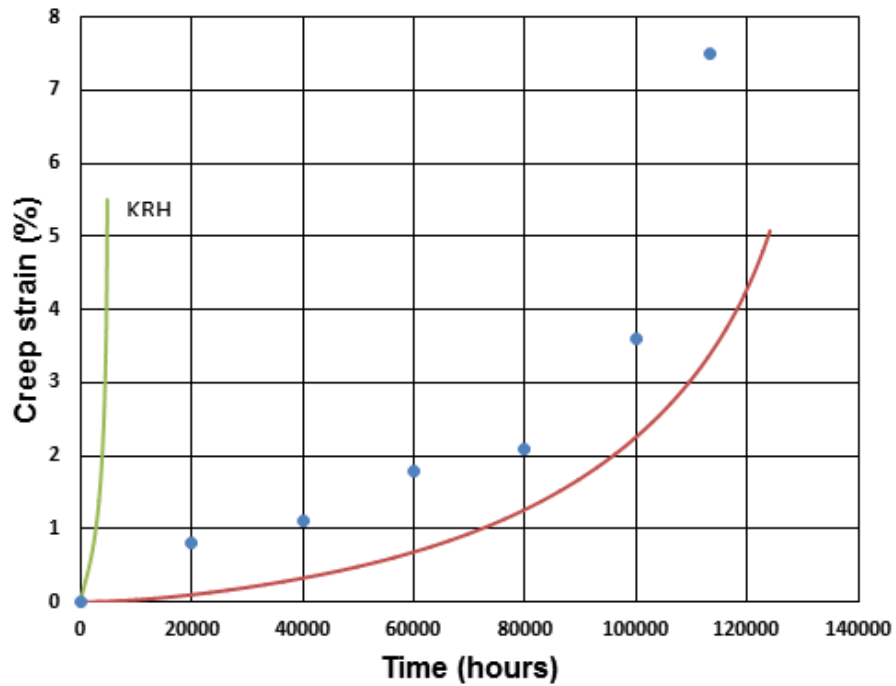
Figure 6. 5: Predicted creep strain curves by the proposed constitutive equations and KRH constitutive equations for high chromium alloy steel P91 at the stress of 80MPa under 600℃
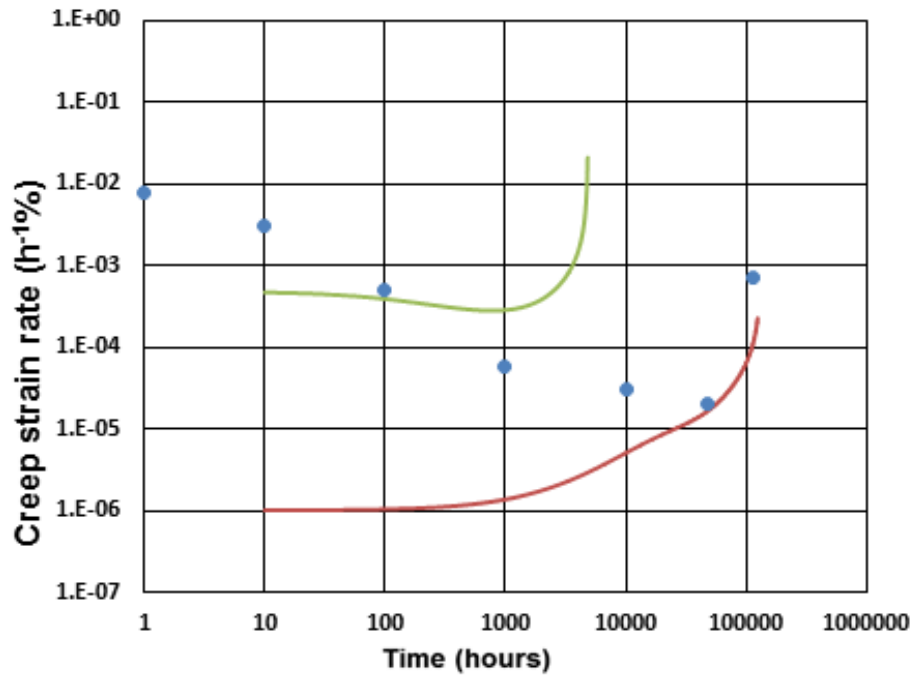
Figure 6. 6: Predicted creep strain rate curves by the proposed constitutive equations and KRH constitutive equations for high chromium alloy steel P91 at the stress of 80MPa under 600℃

6.2.5 Discussion 2

Figures 6.5 and 6.6 represent the comparison of the proposed constitutive equations with the KRH constitutive equations for high chromium alloy steel P91 at the stress of 80MPa under 600℃. Comparing with the experimental lifetime for high chromium alloy steel P91 at the stress of 80MPa under 600℃, the lifetime error is about 9.4% by the proposed constitutive equations. The lifetime error is about 70% by the KRH constitutive equations. However, both the proposed constitutive equations and the KRH constitutive equations could not accurately describe the creep behaviours of materials, especially the creep strain rate. The possible reasons are 1) the selection of material parameters, 2) the influence of

169

coarsening effect on the failure of materials, 3) the influence of temperature on the failure of materials.

The experimental lifetime for high chromium alloy steel P91 under 600℃ at the stress of 80MPa is about 113,431 hours (Panait et al., 2010a; Panait et al., 2010b). The experimental lifetime for high chromium alloy steel P91 under 600℃ at the stress of 70MPa is about 80,000 hours (Sawada et al., 2011). At the same given conditions, the lifetime at the stress of 70MPa is supposed longer than the stress of 80MPa. Within the transition stress range, the premature failure of materials is argued by the microstructural degradation, like MX precipitates, M23C6 carbides, Lave phases and cavities (Sawada et al., 2011). The current researcher argues that the selection of material parameter C should be re-determined by more experimental data, especially the coarsening effect of large precipitates, sub-grain and cavities at the tertiary creep stage.

In addition, the proposed constitutive equations is invalid at the high stress range for high chromium alloy steel P91 under 600℃. Firstly, the creep deformation mechanism changes at different stress ranges. The material parameters are different at different stress ranges, especially for the material parameters A and C in the proposed constitutive equations in the current research. Secondly, the cavitation damage mechanism changes at different stress ranges.

The current proposed constitutive equations have the limitation on creep deformation mechanism. The diffusion creep deformation has only been considered in the proposed constitutive equations model, even the dislocation creep deformation occurs throughout the whole creep damage process. If the

experimental data at the high stress ranges are available, the power law function could be used to describe the creep behaviors at different stress ranges separately with different stress exponents.

Chapter 7

Conclusions

7.1 Key conclusions

The key conclusions of the current research are summarized as below according to the previous chapters. Firstly, the classification of the stress ranges for high chromium alloy steel P91 under 600℃ is summarized in Table 4.2. The literature review in the current research shows that the majority of the previous researches mainly focus on the investigations of the high stress range for high chromium alloy steel P91 combined with the constitutive equations models. Several researches have only investigated the influence of the microstructural degradation on the fracture of materials. Only few researches have investigated the influence of microstructural degradation on the fracture of materials combined with the constitutive equations. However, for high chromium alloy steel P91 under 600℃, the applied stresses in the previous researches are higher than the transition stress range.

Secondly, the power law function with the stress exponent is applied in the current constitutive equations for high chromium alloy steel P91 under 600℃. The power law function with different stress exponents could separately describe the creep deformation mechanism at different stress ranges.

Thirdly, the brittle fracture assisted by the diffusion creep deformation is identified as the creep deformation and damage mechanism for high chromium alloy steel

172

P91 at the transition stress range under 600℃. The brittle fracture is caused by the cavitation damage mechanism. The continuous cavity nucleation with the constrained diffusional cavity growth is argued as the cavitation damage mechanism for high chromium alloy steel P91 at the transition stress range under 600℃. However, the continuous cavity nucleation has more significant influence on the fracture of materials than the constrained diffusional cavity growth mechanism. The high density but with small size of cavities was observed by previous researches for high chromium alloy steel P91 at the transition stress range under 600℃. The cavity growth in size has less influence on the fracture of materials. The cavitated area fraction at fracture is argued as the failure measurement of materials.

Fourthly, the validation of the proposed constitutive equations in the current research shows that the predicted lifetime error for high chromium alloy steel P91 at the stress of 80MPa under 600℃ is about 9.4%. However, the proposed constitutive equations could not accurately predict the creep behaviours of the creep strain rate. The considered reason for that is the selection of material parameters for high chromium alloy steel P91 at the transition stress range under 600℃. The material parameters for high chromium alloy steel P91 under 625℃ are selected in the current research, due to the lack of experimental material parameters for high chromium alloy steel P91 under 600℃. The influence of temperature should be considered in the further research. Moreover, the experimental data also shows that there is a premature failure for high chromium alloy steel P91 at the stress of 70MPa under 600℃. This premature failure is argued by the microstructural degradation, especially because of the coarsening

173

of large precipitates, sub-grain and cavities which finally leads to the failure. In addition, the creep deformation mechanism is argued by both diffusion creep deformation and dislocation creep deformation at the boundary critical stress of 70MPa for high chromium alloy steel P91 under 600℃.

Finally, the limitations of the current research have also been considered. Firstly, the limitation of the proposed constitutive equations to a wider stress levels and temperatures. The applicability of the proposed constitutive equations is only valid for high chromium alloy steel P91 at the stress of 80MPa under 600℃. Secondly, the limitation of predicting the creep behaviours, such as the creep strain rate. The selection of material parameters for high chromium alloy steel under 600℃ should be improved.

7.2 Further work

After the current research has been done, the author suggests several things could be undertaken or improved in the future:

1) Investigate how the microstructure degradation (such as coarsening of large precipitates, sub-grain and cavities) affects the lifetime of materials combine with constitutive equations

2) Determine the material parameters at a wider stress and temperature ranges

3) Expand the feasibility of the constitutive equations to a wider stress and temperature ranges

4) Expand the uniaxial constitutive equations to multi-axial stress states situation

5) Obtain more experimental data on the cavitation damage evolution and cavitated area fraction at fracture

6) Synchrotron micro-tomography and serial sectioning techniques might be one technique to obtain the experimental data, as this technique has been applied into the 12%Cr ferritic steel at the stress range 90MPa-185MPa under 600^0C (Eggeler et al., 1989; Wu & Sandström, 1995).

References

[1] Abd El-Azim, M. E., Ibrahim, O. H., & El-Desoky, O. E. (2013). Long term creep behaviour of welded joints of P91 steel at 650°C. *Materials Science and Engineering: A, 560*(0), 678-684. doi: 10.1016/j.msea.2012.10.013

[2] Abe, F. (2012). Creep modeling and creep life estimation of Gr. 91. *International journal of materials research, 103*(6), 765-773.

[3] Academic Resource Center. Creep deformation in materials Retrieved 28/09, 2014, from http://www.iit.edu/arc/workshops/pdfs/MaterialsCreep.pdf

[4] Allen, D. J., Harvey, B., & Brett, S. J. (2007). "FOURCRACK"—An investigation of the creep performance of advanced high alloy steel welds. *International Journal of Pressure Vessels and Piping, 84*(1-2), 104-113. doi: 10.1016/j.ijpvp.2006.09.010

[5] Armaki, H. G., Chen, R., Maruyama, K., & Igarashi, M. (2010). Premature creep failure in strength enhanced high Cr ferritic steels caused by static recovery of tempered martensite lath structures. *Materials Science and Engineering: A, 527*(24), 6581-6588.

[6] Bailey, D. (1997). Ductile Fracture Retrieved 28/07, 2014, from http://www.sv.vt.edu/classes/MSE2094_NoteBook/97ClassProj/exper/bailey/www/bailey.html

[7]   Ballard, J. (1997). Brittle Fracture Retrieved 24/06, 2014, from

http://www.sv.vt.edu/classes/MSE2094_NoteBook/97ClassProj/exper/ballard/www/ballard.html

[8]   Bendick, W., Cipolla, L., Gabrel, J., & Hald, J. (2010). New ECCC assessment of creep rupture strength for steel grade X10CrMoVNb9-1 (Grade 91). *International Journal of Pressure Vessels and Piping, 87*(6), 304-309.

[9]   Berkeley Engineering And Research. (2008). Refinery and power plants Retrieved 10/03, 2015, from

http://www.bearinc.com/projects/refinerypowerplants.html

[10] Besson, J., Leclercq, S., Gaffard, V., & Gourgues-Lorenzon, A. F. (2009). Analysis of creep lifetime of a ASME Grade 91 welded pipe. *Engineering Fracture Mechanics, 76*(10), 1460-1473. doi: 10.1016/j.engfracmech.2008.12.007

[11] Betten, J. (2005). *Creep mechanics* (2 ed.). Berlin; New York: Springer.

[12] Charles Sturt University. (2015). Crack theory and the failure materials Retrieved 01/09, 2015, from

http://hsc.csu.edu.au/engineering_studies/application/civil/3032/Crack_theory.html

[13] Chen, I.-W. (1983a). Cavity growth on a sliding grain boundary. *Metallurgical Transactions A, 14*(11), 2289-2293.

[14] Chen, I.-W. (1983b). Mechanisms of cavity growth in creep. *Scripta Metallurgica, 17*(1), 17-22.

[15] Chen, Y. X., Yan, W., Hu, P., Shan, Y. Y., & Yang, K. (2011). CDM modeling of creep behaviour of T/P91 steel under high stresses *Acta Metallurgica Sinica, 47*(11). doi: 10.3724/SP.J.1037.2011.00309

[16] Chen, Y. X., Yan, W., Wang, W., Shan, Y. Y., & Yang, K. (2012). Constitutive equations of the minimum creep rate for 9% Cr heat resistant steels. *Materials Science and Engineering: A, 534*, 649-653. doi: 10.1016/j.msea.2011.12.022

[17] Czyrska-Filemonowicz, A., Zieliń„ska-Lipiec, A., & Ennis, P. J. (2006). Modified 9% Cr steels for advanced power generation: microstructure and properties. *Journal of Achievements in Materials and Manufacturing Engineering, 19*(2), 43-48.

[18] Dunand, D., Han, B., & Jansen, A. (1999). Monkman-grant analysis of creep fracture in dispersion-strengthened and particulate-reinforced aluminum. *METALLURGICAL AND MATERIALS TRANSACTIONS A, 30*(3), 829-838.

[19] Dyson, B. F. (1988). Creep and fracture of metals : mechanisms and mechanics. *Revue de Physique Appliquée, 23*(4), 605-613. doi: 10.1051/rphysap:01988002304060500

[20] Dyson, B. F. (2000). Use of CDM in materials modeling and component creep life prediction. *Journal of pressure vessel technology, 122*(3), 281-296.

[21] Eggeler, G., Earthman, J., Nilsvang, N., & Ilschner, B. (1989). Microstructural study of creep rupture in a 12% chromium ferritic steel. *Acta Metallurgica, 37*(1), 49-60.

[22] Eggeler, G., Ramteke, A., Coleman, M., Chew, B., Peter, G., Burblies, A., . . . Mohrmann, R. (1994). Analysis of creep in a welded 'P91'pressure vessel. *International Journal of Pressure Vessels and Piping, 60*(3), 237-257.

[23] European Creep Collaborative Committee. (2001-2005). Advanced Creep Retrieved 01/09, 2015, from http://www.ommi.co.uk/etd/eccc/advancedcreep/com.html

[24] European Technology Development. (2014). European Creep Collaborative Committee (ECCC). Retrieved 01/09, 2014, from http://www.etd-consulting.com/eccc/

[25] Evans, R. W., & Wilshire, B. (1993). *Introduction to creep*: Institute of Materials London.

[26] Fumitoshi, S., Nobuhiko, N., Masahiro, K., Masashi, O., & Akira, S. (2009). Regenerative heat treatment technology for on-site life extension of high energy pipe welds degraded by creep damage *Mitsubishi Heavy Industries Technical Review, 46*(2), 48-53.

[27] Gaffard, V., Besson, J., & Gourgues-Lorenzon, A. F. (2004). Creep failure model of a 9cr1Mo-NbV(P91) steel integrating multiple deformation and damage.

[28] Gaffard, V., Besson, J., & Gourgues-Lorenzon, A. F. (2008). Modelling high temperature creep flow, damage and fracture behaviour of 9Cr1MoNbV steel weldments. *Materials at High Temperatures, 25*(3), 159-167.

[29] Gaffard, V., Gourgues-Lorenzon, A. F., & Besson, J. (2005). High temperature creep flow and damage properties of 9Cr1MoNbV steels: Base metal and weldment. *Nuclear Engineering and Design, 235*(24), 2547-2562. doi: 10.1016/j.nucengdes.2005.07.001

[30] Gao, k. (2014). Review: mechanisms in creep and anelastic recovery of face-contered cubic alloys

[31] Ghauri, P., & Gronhaug, K. (2010). Research Methods in Business Studies: A Practical Guide (pp. 288): Financial Times/ Prentice Hall; 4 edition.

[32] Ghauri, P. N., & Grønhaug, K. (2005). *Research methods in business studies: A practical guide*: Pearson Education.

[33] Gorash, Y. (2008). *Development of a creep-damage model for non-isothermal long-term strength analysis of high-temperature components operating in a wide stress range.* (PhD), Martin Luther University of Halle-Winttenberg, Halle Germany.

[34] Gupta, C., Toda, H., Schlacher, C., Adachi, Y., Mayr, P., Sommitsch, C., . . . Kobayashi, M. (2013). Study of creep cavitation behavior in tempered martensitic steel using synchrotron micro-tomography and serial sectioning

techniques. *Materials Science and Engineering: A, 564*(0), 525-538. doi: 10.1016/j.msea.2012.12.002

[35] Haney, E. M., Dalle, F., Sauzay, M., Vincent, L., Tournié, I., Allais, L., & Fournier, B. (2009). Macroscopic results of long-term creep on a modified 9Cr–1Mo steel (T91). *Materials Science and Engineering: A, 510-511*, 99-103. doi: 10.1016/j.msea.2008.04.099

[36] Hayhurst, R. J., Mustata, R., & Hayhurst, D. R. (2005). Creep constitutive equations for parent, Type IV, R-HAZ, CG-HAZ and weld material in the range 565–640°C for Cr–Mo–V weldments. *International Journal of Pressure Vessels and Piping, 82*(2), 137-144. doi: 10.1016/j.ijpvp.2004.07.014

[37] Hayhurst, R. J., Vakili-Tahami, F., & Hayhurst, D. R. (2009). Verification of 3-D parallel CDM software for the analysis of creep failure in the HAZ region of Cr–Mo–V crosswelds. *International Journal of Pressure Vessels and Piping, 86*(8), 475-485. doi: 10.1016/j.ijpvp.2009.04.015

[38] Holdsworth, S. R., Askins, M., Baker, A., Gariboldi, E., Holmström, S., Klenk, A., . . . Spigarelli, S. (2008). Factors influencing creep model equation selection. *International Journal of Pressure Vessels and Piping, 85*(1-2), 80-88. doi: 10.1016/j.ijpvp.2007.06.009

[39] Holdsworth, S. R., & Merckling, G. (2003). ECCC Developments in the Assessment of Creep-Rupture Properties.   Retrieved 07/08, 2014, from http://www.ommi.co.uk/etd/eccc/advancedcreep/SRHGMpap1.pdf

[40] Hosseini, E., Holdsworth, S. R., & Mazza, E. (2012). Creep constitutive model considerations for high temperature finite element numerical simulations.

[41] Hyde, T. H., Becker, A. A., Sun, W., & Williams, J. A. (2006a). Finite-element creep damage analyses of P91 pipes. *International Journal of Pressure Vessels and Piping, 83*(11-12), 853-863. doi: 10.1016/j.ijpvp.2006.08.013

[42] Hyde, T. H., Becker, A. A., Sun, W., Yaghi, A., Williams, J. A., & Concari, S. (2006b). *Determination of creep properties for P91 weldment materials at 625ºC.* Paper presented at the Proceedings of the 5th International Conference on Mechanics and materials in design (Eds JFS Gomes, and SA Meguid), Porto, Portugal.

[43] Hyde, T. H., Saber, M., & Sun, W. (2010a). Creep crack growth data and prediction for a P91 weld at 650°C. *International Journal of Pressure Vessels and Piping, 87*(12), 721-729. doi: 10.1016/j.ijpvp.2010.09.002

[44] Hyde, T. H., Saber, M., & Sun, W. (2010b). Testing and modelling of creep crack growth in compact tension specimens from a P91 weld at 650°C. *Engineering Fracture Mechanics, 77*(15), 2946-2957. doi: 10.1016/j.engfracmech.2010.03.043

[45] Hyde, T. H., & Sun, W. (2006). Creep failure behaviour of a circumferential P91 pipe weldment with an anisotropic weld metal subjected to internal pressure and end load. *Proceedings of the Institution of Mechanical Engineers, Part L: Journal of Materials Design and Applications, 220*(3), 147-162.

[46] Hyde, T. H., Sun, W., Becker, A. A., & Williams, J. A. (2004). Creep properties and failure assessment of new and fully repaired P91 pipe welds at 923 K. *Proceedings of the Institution of Mechanical Engineers, Part L: Journal of Materials Design and Applications, 218*(3), 211-222. doi: 10.1177/146442070421800305

[47] IFM. (2009). TWI holds survey on P91 and P92 grade steel component failures. 2011

[48] Ion, J. C., Barbosa, A., Ashby, M. F., Dyson, B. F., & McLean, M. (1986). The modelling of creep for engineering design-1 (Vol. A115).

[49] Johnzactruba, & Lamar, S. (2011). P91-The workhorse of the power industry Retrieved 25/03, 2014, from http://www.brighthubengineering.com/power-plants/64886-the-workhorse-of-the-power-industry-p91/

[50] Kachanov, L. M. (1986). *Introduction to continuum damage mechanics* (Vol. 10): Springer Science & Business Media.

[51] Kalck, C., Fournier, B., Barcelo, F., Forest, L., Dalle, F., Giroux, P. F., . . . Gourgues-Lorenzon, A. F. (2010). High temperature creep properties and microstructural examinations of P92 welds. *Materials for advanced power engineering 2010*, 424-434.

[52] Kassner, M. E., & Hayes, T. A. (2003). Creep cavitation in metals. *International Journal of Plasticity, 19*(10), 1715-1748. doi: 10.1016/S0749-6419(02)00111-0

[53] Kassner, M. E., & Perez-Prado, M. T. (2004). *Fundamentals of creep in metals and alloys*: Elsevier.

[54] Key to Metals AG. (2010). Total Material: 9-12% Chromium Steels: Part One Retrieved 02/06, 2015, from

http://www.keytometals.com/page.aspx?ID=CheckArticle&site=KTS&NM=272

[55] Key to Metals AG. (2010). Total Materia: 9-12% Chromium Steels: Part Two Retrieved 02/06, 2015, from

http://www.keytometals.com/page.aspx?ID=CheckArticle&site=KTS&NM=275

[56] Kimura, K., Kushima, H., & Abe, F. (2002). *Degradation and assessment of long-term creep strength of high Cr ferritic creep resistant steels.* Paper presented at the Proc. Inter. Conf. Advances in Life Assessment and Optimization of Fossil Power Plant.

[57] Kimura, K., Toda, Y., Kushima, H., & Sawada, K. (2010). Creep strength of high chromium steel with ferrite matrix. *ECCC Second International Creep Conference, 87*(6), 282-288. doi: 10.1016/j.ijpvp.2010.03.016

[58] Kloc, L., & Sklenička, V. (2004). Confirmation of low stress creep regime in 9% chromium steel by stress change creep experiments. *Materials Science and Engineering: A, 387-389*, 633-638. doi: 10.1016/j.msea.2003.12.078

[59] Krajcinovic, D. (1996). *Damage mechanics* (Vol. 41): Elsevier

[60] Li, Y., Hongo, H., Tabuchi, M., Takahashi, Y., & Monma, Y. (2009). Evaluation of creep damage in heat affected zone of thick welded joint for Mod.9Cr–1Mo

steel. *International Journal of Pressure Vessels and Piping, 86*(9), 585-592. doi: 10.1016/j.ijpvp.2009.04.008

[61] Lim, R., Sauzay, M., Dalle, F., Tournie, I., Bonnaillie, P., & Gourgues-Lorenzon, A. F. (2011). Modelling and experimental study of the tertiary creep stage of Grade 91 steel. *International Journal of Fracture, 169*(2), 213-228.

[62] Liu, Y., & Murakami, S. (1998). Damage localization of conventional creep damage models and proposition of a new model for creep damage analysis. *JSME international journal. Series A, Solid mechanics and material engineering, 41*(1), 57-65.

[63] Magnusson, H., & Sandström, R. (2007). *Modelling of the influence of Laves phase on the creep properties in 9% Cr steels.* Paper presented at the ASME 2007 Pressure Vessels and Piping Conference.

[64] Massé, T., & Lejeail, Y. (2012). Creep behaviour and failure modelling of modified 9Cr1Mo steel. *Nuclear Engineering and Design, 246*, 220-232. doi: 10.1016/j.nucengdes.2012.02.006

[65] Massé, T., & Lejeail, Y. (2013). Creep mechanical behaviour of modified 9Cr1Mo steel weldments: Experimental analysis and modelling. *Nuclear Engineering and Design, 254*, 97-110. doi: 10.1016/j.nucengdes.2012.09.007

[66] Materials & Welding. (2007). Heat Resistant Martensitic Steel P91 Retrieved 04/07, 2014, from http://materials-welding.blogspot.co.uk/2007/09/heat-resistant-martensitic-steel-p91.html

[67] Mathers, G. (2014). Creep and creep testing Retrieved 23/01, 2014, from http://www.twi-global.com/technical-knowledge/job-knowledge/creep-and-creep-testing-081/

[68] Merckling, G. (2005). *Creep & Fracture in High Temperature Components: Design & Life Assessment Issues*: DEStech Publications, Inc.

[69] Murakami, S. (2012). *Continuum damage mechanics: a continuum mechanics approach to the analysis of damage and fracture* (Vol. 185): Springer.

[70] Nagode, A., Ule, B., Jenko, M., & Kosec, L. (2007). A constitutive creep equation for 9Cr-1 Mo-0.2 V (P91-type) steel under constant load and constant stress. *STEEL RESEARCH INTERNATIONAL, 78*(8), 638-642.

[71] National research institute for metals. (1996). *Data sheet on the elevated temperature properties of 9Cr-1Mo-V-Nb steel tubes for boilers and heat exchangers and 9Cr-1Mo-V-Nb steel plates for boilers and pressure vessels*.

[72] Naumenko, K. (2006). Modeling of high-temperature creep for structural analysis applications. *Habilitationschrift, Mathematisch-Naturwissenschaftlich-Technische Fakultät, Martin-Luther-Universität Halle-Wittenberg, 16*, 17-63.

[73] Naumenko, K., & Altenbach, H. (2007). *Modeling of creep for structural analysis*: Springer Science & Business Media.

[74] Naumenko, K., & Kostenko, Y. (2009). Structural analysis of a power plant component using a stress-range-dependent creep-damage constitutive model.

Materials Science and Engineering: A, 510-511, 169-174. doi: 10.1016/j.msea.2008.04.096

[75] Ogata, T., Sakai, T., & Yaguchi, M. (2009a). Damage characterization of a P91 steel weldment under uniaxial and multiaxial creep. *Materials Science and Engineering: A, 510-511*, 238-243. doi: 10.1016/j.msea.2008.04.124

[76] Ogata, T., Sakai, T., & Yaguchi, M. (2009b). Uniaxial Creep Rupture Property of Mod. 9 Cr-1 Mo Steel Weld Joint and Proposal of Creep Damage Evaluation Method. *Journal of the Society of Materials Science, Japan, 58*(2), 94-100.

[77] Ogata, T., Sakai, T., & Yaguchi, M. (2010a, 2007). *Creep damage evolution and life assessment of P91 weld joint.* Paper presented at the Proceeding of the third international conference on integrity of high temperature welds, April.

[78] Ogata, T., Sakai, T., & Yaguchi, M. (2010b). Damage assessment method of P91 steel welded tube under internal pressure creep based on void growth simulation. *International Journal of Pressure Vessels and Piping, 87*(11), 611-616. doi: 10.1016/j.ijpvp.2010.08.009

[79] Ogata, T., Sakai, T., & Yaguchi, M. (2010c). Damage evolution and life prediction of a P91 longitudinal welded tube under internal pressure creep. *Journal of pressure vessel technology, 132*(5).

[80] Ogata, T., Sakai, T., & Yaguchi, M. (2011). Modelling of creep damage in high temperature component life assessment. *Materials at High Temperatures, 28*(2), 147-154.

[81] Panait, C. G., Bendick, W., Fuchsmann, A., Gourgues-Lorenzon, A. F., & Besson, J. (2010a). Study of the microstructure of the Grade 91 steel after more than 100,000 h of creep exposure at 600℃. *International Journal of Pressure Vessels and Piping, 87*(6), 326-335. doi: 10.1016/j.ijpvp.2010.03.017

[82] Panait, C. G., Zielińska-Lipiec, A., Koziel, T., Czyrska-Filemonowicz, A., Gourgues-Lorenzon, A. F., & Bendick, W. (2010b). Evolution of dislocation density, size of subgrains and MX-type precipitates in a P91 steel during creep and during thermal ageing at 600C for more than 100,000h. *Materials Science and Engineering: A, 527*(16-17), 4062-4069. doi: 10.1016/j.msea.2010.03.010

[83] Parker, J. (2013). In-service behavior of creep strength enhanced ferritic steels Grade 91 and Grade 92 – Part 1 parent metal. *International Journal of Pressure Vessels and Piping, 101*, 30-36. doi: 10.1016/j.ijpvp.2012.10.001

[84] Perrin, I., & Hayhurst, D. (1996a). Creep constitutive equations for a 0.5 Cr– 0.5 Mo–0.25 V ferritic steel in the temperature range 600–675 C. *The Journal of Strain Analysis for Engineering Design, 31*(4), 299-314.

[85] Perrin, I. J., & Hayhurst, D. R. (1996b). A method for the transformation of creep constitutive equations. *International Journal of Pressure Vessels and Piping, 68*(3), 299-309.

[86] Petry, C., & Gariboldi, E. (2010). *Materials at High Temperatures, 27*(1), 1-10.

[87] Pétry, C., & Lindet, G. (2009). Modelling creep behaviour and failure of 9Cr–0.5Mo–1.8W–VNb steel. *International Journal of Pressure Vessels and Piping, 86*(8), 486-494. doi: 10.1016/j.ijpvp.2009.03.006

[88] Picard, D., & Fafard, M. (2011). Three-Dimensional Constitutive Viscoelastic Model for Isotropic Materials.   Retrieved 28/03, 2013, from http://www.intechopen.com/books/thermodynamics-physical-chemistry-of-aqueous-systems/three-dimensional-constitutive-viscoelastic-model-for-isotropic-materials

[89] Rauch, M., Maile, K., & Ringel, M. (2004). *Numerical calculation and experimental validation of damage development in 9Cr steels.* Paper presented at the Proc. of 30th-MPA-"Seminar in conjunction with the 9th German-Japanese Seminar, Stuttgart.

[90] Rice, J. R. (1974). *Continuum mechanics and thermodynamics of plasticy in relation to microscale deformation mechanisms* US, Providence, R.I.: Brown University

[91] Riedel, H. (1987). *Fracture at high temperatures*: Springer-Verlag Berlin.

[92] Rouse, J. P., Sun, W., Hyde, T. H., & Morris, A. (2013). Comparative assessment of several creep damage models for use in life prediction. *International Journal of Pressure Vessels and Piping, 108-109*, 81-87. doi: 10.1016/j.ijpvp.2013.04.012

[93] Saha, P. K. (2003). Comparing materials for high-temperature steam piping Retrieved 15/02, 2015, from http://www.thefabricator.com/article/tubepipefabrication/comparing-materials-for-high-temperature-steam-piping

[94] Sawada, K., Bauer, M., Kauffmann, F., Mayr, P., & Klenk, A. (2010). Microstructural change of 9% Cr-welded joints after long-term creep. *Materials Science and Engineering: A, 527*(6), 1417-1426. doi: 10.1016/j.msea.2009.10.044

[95] Sawada, K., Kushima, H., Tabuchi, M., & Kimura, K. (2011). Microstructural degradation of Gr.91 steel during creep under low stress. *Materials Science and Engineering: A, 528*(16-17), 5511-5518. doi: 10.1016/j.msea.2011.03.073

[96] Sheridan, N. (Producer). (2010, 25/03). Writing a methodology chapter Retrieved from https://www.youtube.com/watch?v=zQFSNB-0sfQ

[97] Shibli, A., & Starr, F. (2007). Some aspects of plant and research experience in the use of new high strength martensitic steel P91. *International Journal of Pressure Vessels and Piping, 84*(1), 114-122.

[98] Shrestha, T., Basirat, M., Charit, I., Potirniche, G. P., & Rink, K. K. (2013). Creep rupture behavior of Grade 91 steel. *Materials Science and Engineering: A, 565*, 382-391. doi: 10.1016/j.msea.2012.12.031

[99] Shrestha, T., Basirat, M., Charit, I., Potirniche, G. P., Rink, K. K., & Sahaym, U. (2012). Creep deformation mechanisms in modified 9Cr–1Mo steel. *Journal of Nuclear Materials, 423*(1-3), 110-119. doi: 10.1016/j.jnucmat.2012.01.005

[100]Shu, G., Zhao, Y., Xue, F., Zhang, L., & Zhang, G. (2010). Experiment Research and Numerical Simulation of Creep Damage for P91 Steel. *Proceedings of the CSEE, 23*, 019.

[101]Sket, F., Dzieciol, K., Borbely, A., Kaysser-Pyzalla, A. R., Maile, K., & Scheck, R. (2010). Microtomographic investigation of damage in E911 steel after long term creep. *Special Topic Section: Local and Near Surface Structure from Diffraction, 528*(1), 103-111. doi: 10.1016/j.msea.2010.07.029

[102]Sklenicka, V. (2003). Long-term creep behavior of 9–12%Cr power plant steels. *Materials Characterization, 51*(1), 35-48. doi: 10.1016/j.matchar.2003.09.012

[103]Sklenička, V. Microstructural mechanisms in high creep of creep-resistant materials Retrieved 1/09, 2015, from http://konference.tanger.cz/data/metal2000/sbornik/papers/710.pdf

[104]Spigarelli, S. (2013). Microstructure-based assessment of creep rupture strength in 9Cr steels. *International Journal of Pressure Vessels and Piping, 101*, 64-71. doi: 10.1016/j.ijpvp.2012.10.005

[105]Sundararajan, G. (1989). The Monkman-Grant Relationship. *Materials Science and Engineering: A, 112*, 205-214.

[106] Tabuchi, M., & Hongo, H. (2009). *Creep Damage Behavior of Welded Joints for High Cr Steels.* Paper presented at the Proc. of 3rd Symposium on heat resistant steels and alloys for high efficiency USC power plants, Japan.

[107] The British Library Board. Qualitative and Quantitative research Retrieved 27/08, 2015, from http://www.bl.uk/bipc/resmark/qualquantresearch/qualquantresearch.html

[108] ThyssenKrupp. (2011). Material data sheet P91/T91.   Retrieved 02/06, 2013, from http://www.s-k-h.com/media/de/Service/Werkstoffblaetter_englisch/Kesselrohre_ASTM/P91_T91_engl.pdf

[109] Tu, S. D. (2005). *High temperature creep of structural integrity*. China

[110] TWI. (2014). What is creep damage, and how is it detected? .   Retrieved 18/03, 2014, from http://www.twi-global.com/technical-knowledge/faqs/material-faqs/faq-what-is-creep-damage-and-how-is-it-detected/

[111] TWI. (2015). What is the Larson-Miller parameter? .   Retrieved 18/03, 2014, from http://www.twi-global.com/technical-knowledge/faqs/material-faqs/faq-what-is-the-larson-miller-parameter/

[112] Ule, B., & Nagode, A. (2007). A model based creep equation for 9Cr–1Mo–0·2V (P91 type) steel. *Materials Science and Technology, 23*(11), 1367-1374. doi: 10.1179/174328407x161187

[113]University of Cambridge. Creep rate equation.   Retrieved 27/08, 2015, from

http://www.doitpoms.ac.uk/tlplib/creep/rate_equation.php

[114]University of Cambridge. (2014). Creep mechanisms Retrieved 01/09, 2015,

from http://www.doitpoms.ac.uk/tlplib/creep/mechanisms.php

[115]University of New South Wales Australia. (2014). Crack theory.   Retrieved

11/08, 2014, from

http://www.hsctut.materials.unsw.edu.au/Crack%20Theory/cracktheory1a.htm

[116]Vivier, F., Gourgues-Lorenzon, A. F., & Besson, J. (2010). Creep rupture of a

9Cr1MoNbV steel at 500°C: Base metal and welded joint. *Nuclear Engineering*

and Design, 240(10), 2704-2709. doi: 10.1016/j.nucengdes.2010.06.031

[117]Vivier, F., Panait, C. G., Gourgues-Lorenzon, A. F., & Besson, J. (2008, 2013).

Microstructure evolution in base metal and welded joint of Grade 91

martensitic steels after creep at 500-600 C. Paper presented at the ECF17,

Brno

[118]Vöse, M., Otto, F., Fedelich, B., & Eggeler, G. (2014). Micromechanical

investigations and modelling of a Copper–Antimony-Alloy under creep

conditions. *Mechanics of Materials, 69*(1), 41-62. doi:

10.1016/j.mechmat.2013.09.013

[119]Wadsworth, J., Ruano, O. A., & Sherby, O. D. (1998). *Deformation by grain*

boundary sliding and slip creep versus diffusional creep Paper presented at

the The minerals, metals and materials (TMS) 1999 annual meeting San Diego, CA.

[120]Watanabe, T., Tabuchi, M., Yamazaki, M., Hongo, H., & Tanabe, T. (2006). Creep damage evaluation of 9Cr–1Mo–V–Nb steel welded joints showing Type IV fracture. *International Journal of Pressure Vessels and Piping, 83*(1), 63-71. doi: 10.1016/j.ijpvp.2005.09.004

[121]Wu, R., & Sandström, R. (1995). Creep cavity nucleation and growth in 12Cr–Mo–V steel. *Materials Science and Technology, 11*(6), 579-588.

[122]Xu, Q. (2000). *The development of creep damage constitutive equations under multi-axial states of stress.* Paper presented at the European Conference on Advances in Mechanical Behaviour, Plasticity and Damage.

[123]Xu, Q. (2001). Creep damage constitutive equations for multi-axial states of stress for 0.5 Cr0. 5Mo0. 25V ferritic steel at 590 C. *Theoretical and Applied Fracture Mechanics, 36*(2), 99-107.

[124]Xu, Q. (2004). The development of validation methodology of multi-axial creep damage constitutive equations and its application to 0.5Cr0.5Mo0.25V ferritic steel at 590°C. *Nuclear Engineering and Design, 228*(1-3), 97-106. doi: 10.1016/j.nucengdes.2003.06.021

[125]Xu, Q. (2007). *The development and application of creep continuum damage mechanics*

[126]Xu, Q., & Barrans, S. (2003). The Development of multi-axial creep damage constitutive equations for 0.5 Cr0. 5Mo0. 25V ferritic steel at 590. DEG. C. *JSME International Journal Series A, 46*(1), 51-59.

[127]Xu, Q., Wright, M., & Xu, Q. H. (2011). *The development and validation of multi-axial creep damage constitutive equations for P91.* Paper presented at the Automation and Computing (ICAC), 2011 17th International Conference on.

[128]Yao, H.-T., Xuan, F.-Z., Wang, Z., & Tu, S.-T. (2007). A review of creep analysis and design under multi-axial stress states. *Nuclear Engineering and Design, 237*(18), 1969-1986. doi: 10.1016/j.nucengdes.2007.02.003

[129]Yin, Y. F., & Faulkner, R. G. (2006). Continuum damage mechanics modelling based on simulations of microstructural evolution kinetics. *Materials Science and Technology, 22*(8), 929-936. doi: 10.1179/174328406x102426

[130]Zhang, F., & Zhou, W. (2009). *Materials performance*: Shanghai jiaotong university